haematologica
Journal of the Ferrata Storti Foundation

NSUN2-FOSB reciprocity facilitates leukemogenesis in an m^{5}C-dependent manner by increasing BCL2L1 expression

by Bin Zhou, Yigang Yuan, Yue Cai, Jingying Zhou, Liuzhi Shi, Yaqian Qin, Chen Meng, Shixin Zhang, Shirui Yu, Xinyao Chen, Xiaofei He, Shanshan Wu, Min Li, Xuanyu Yu, Yifen Shi, Chongyun Xing, Chiqi Chen, Meng Zhao and Shenmeng Gao

Received: September 25, 2025.
Accepted: February 27, 2026.

Citation: Bin Zhou, Yigang Yuan, Yue Cai, Jingying Zhou, Liuzhi Shi, Yaqian Qin, Chen Meng, Shixin Zhang, Shirui Yu, Xinyao Chen, Xiaofei He, Shanshan Wu, Min Li, Xuanyu Yu, Yifen Shi, Chongyun Xing, Chiqi Chen, Meng Zhao and Shenmeng Gao. NSUN2-FOSB reciprocity facilitates leukemogenesis in an m^{5}C-dependent manner by increasing BCL2L1 expression.
Haematologica. 2026 Mar 12. doi: 10.3324/haematol.2025.289250 [Epub ahead of print]

NSUN2-FOSB reciprocity facilitates leukemogenesis in an m^{5}C-dependent manner by increasing BCL2L1 expression

Bin Zhou[1, *], Yigang Yuan[1, *], Yue Cai[2, *], Jingying Zhou[3, *], Liuzhi Shi[4], Yaqian Qin[1], Chen Meng[1], Shixin Zhang[1], Shirui Yu[1], Xinyao Chen[1], Xiaofei He[1], Shanshan Wu[1], Min Li[1], Xuanyu Yu[1], Yifen Shi[5], Chongyun Xing[5], Chiqi Chen[6, #], Meng Zhao[7, #], Shenmeng Gao[1, 8, #]

[1]Medical Research Center, The First Affiliated Hospital of Wenzhou Medical University, 1 Xuefubei Street, Ouhai District, Wenzhou, Zhejiang Province, China

[2]Department of Clinical Medicine, Wenzhou Medical University, Chashan District, Wenzhou, Zhejiang Province, China

[3]Department of Pediatrics, Ningbo First Hospital, Ningbo, Zhejiang, China. 59 Liuting Road, Ningbo, 315000, Zhejiang Province, China

[4]Department of Clinical Laboratory, The First Affiliated Hospital of Wenzhou Medical University, 1 Xuefubei Street, Ouhai District, Wenzhou, Zhejiang Province, China

[5]Department of Hematology, The First Affiliated Hospital of Wenzhou Medical University, 1 Xuefubei Street, Ouhai District, Wenzhou, Zhejiang Province, China

[6]Key Laboratory of Cell Differentiation and Apoptosis of Chinese Ministry of Education, Faculty of Basic Medicine, Shanghai Jiao Tong University School of Medicine, Shanghai, China.

[7]Key Laboratory of Stem Cells and Tissue Engineering (Ministry of Education), Zhongshan School of Medicine, Sun Yat-sen University, Guangzhou, Guangdong Province, China.

[8]The Key Laboratory of Pediatric Hematology and Oncology Diseases of Wenzhou, the Second Affiliated Hospital and Yuying Children's Hospital of Wenzhou Medical University, Wenzhou, Zhejiang, China

*These authors contributed equally to this work

#Correspondence to:

Dr. Chiqi Chen, E-mail: chenchiqi@sjtu.edu.cn, Hongqiao International Institute of Medicine, Shanghai Tongren Hospital, Key Laboratory of Cell Differentiation and Apoptosis of Chinese Ministry of Education, Faculty of Basic Medicine, Shanghai Jiao Tong University School of Medicine, Shanghai 200025, China.

Tel: +86-021-63846590; Fax: +86-021-63846590

Dr. Meng Zhao, E-mail: zhaom38@mail.sysu.edu.cn, Key Laboratory of Stem Cells and Tissue Engineering (Ministry of Education), Zhongshan School of Medicine, Sun Yat-sen University, Guangzhou, Guangdong Province, China.

Tel: +86-020-84036491; Fax: +86-020-84036491

Dr. Shenmeng Gao, E-mail: gaoshenmeng77@wzhospital.cn, Medical Research Center, The First Affiliated Hospital of Wenzhou Medical University, 1 Xuefubei Street, Ouhai District, Wenzhou, 325000, Zhejiang Province, China.

Tel: +86-577-55578080; Fax: +86-577-55578080

Running heads: NSUN2-FOSB reciprocity facilitates leukemogenesis

Data-sharing statement

All datasets generated or analyzed during this study have been included in this manuscript. The data are available from the corresponding author on reasonable request.

Disclosures

The authors declare that they have no competing interests.

Contributions

Z.B., Y.Y.G., C.Y., and Z.J.Y. were responsible for writing the protocol and report, conducting the search, and screening potentially eligible studies. L.M., M.C., W.S.S., and Q.Y.Q. performed the experiments and analyzed data. Z.S.X., Y.S.R., C.X.Y., and X.C.Y. contributed to the design of the review protocol, writing the report, arbitrating potentially eligible studies, providing human specimens, and data analysis. H.X.F., S.L.Z., S.Y.F., and Y.X.Y. performed AML model *in vivo*. C.C.Q., Z.M., and G.S.M. designed the experiments and wrote the manuscript.

Funding

This research was supported by Zhejiang Provincial Natural Science Foundation of China (LY23H080003), the National Key Research and Development Program of China (2022YFA1103300), the National Natural Science Foundation of China (81971991; 82300194; 82370180; 82325002), Discipline Cluster of Oncology of Wenzhou Medical University of China (z2-2023021), and Zhejiang Provincial Medical and Health Science and Technology Project (2025KY1314).

Word count: 3991; Figures: 8; Tables: 0; supplementary file: 1

Abstract

NOP2/Sun RNA methyltransferase family member 2 (NSUN2) catalyzes 5-methylcytosine (m^5C) modifications on RNA to regulate mRNA stability. However, its roles in normal hematopoiesis and leukemogenesis remain poorly understood. Here, we show that NSUN2 is markedly upregulated in primary AML patient samples compared with normal hematopoietic cells. NSUN2 knockdown (KD) impaired AML cell proliferation, induced apoptosis, and reduced colony formation. Genetic ablation of Nsun2 in an MLL-AF9 (MA9)-transformed murine AML model substantially impaired leukemia stem cell (LSC) self-renewal and prolonged overall survival (OS), while sparing normal hematopoiesis, highlighting NSUN2 as a potential therapeutic target. Notably, wild-type NSUN2, but not catalytically inactive mutants, restored LSC function and leukemogenesis in NSUN2-deficient AML cells, indicating that these effects are m□C-dependent. Mechanistically, NSUN2 stabilized FosB proto-oncogene (FOSB) mRNA via m□C modification at nucleotide 3656 in the 3′-UTR, thereby upregulating FOSB expression. In turn, FOSB transcriptionally activated NSUN2, forming a feedforward regulatory loop. Furthermore, FOSB promoted expression of the anti-apoptotic regulator B-cell lymphoma-2-like protein 1 (BCL2L1) by directly binding to its promoter. In conclusion, these findings uncover a novel NSUN2-FOSB-BCL2L1 axis that drives AML leukemogenesis in an m^5C-dependent manner, suggesting the therapeutic potential for targeting this pathway.

Keywords: NSUN2, FOSB, 5-methylcytosine, BCL2L1

Introduction

Chemical modifications on RNA, including N□-methyladenosine (m□A) and 5-methylcytosine (m□C), play critical roles in regulating gene expression at the posttranscriptional level.[1] m□C modification occurs on multiple types of eukaryotic RNA, including ribosomal RNA, transfer RNA, and messenger RNA (mRNA), and has been increasingly recognized on mRNA, where it modulates RNA stability and translation efficiency.[2] For example, m^5C modification of *p16* mRNA enhances its stability.[3] Thus, dysregulated m^5C modulation of mRNA has critical implications for processes such as tumorigenesis, protein synthesis, and cell proliferation.[4] AML is a fatal hematologic malignancy characterized by blocked differentiation and impaired cell death, driven by clonal expansion of hematopoietic stem and progenitor cells (HSPCs).[5] Emerging evidence indicates that aberrant m□C modification contributes to AML initiation and progression.[6]

NSUN2 is a methyltransferase that catalyzes m^5C modifications of various RNAs, including tRNA, mRNA, and ribosome RNA.[7] Elevated NSUN2 expression promotes tumor proliferation, metastasis, and progression through m□C-mediated stabilization of target mRNAs.[8] For instance, NSUN2 enhances esophageal squamous cell carcinoma progression by stabilizing *GRB2* mRNA via m□C modification.[9] Recent studies suggest that NSUN2 also supports proliferation and survival in AML.[6, 10] However, its precise role in normal hematopoiesis and leukemogenesis remains unclear.

In this study, we demonstrate that NSUN2 KD impairs AML survival and LSC self-renewal while sparing normal hematopoiesis. Mechanistically, NSUN2 methylates *FOSB* mRNA, and FOSB reciprocally regulates NSUN2 expression, establishing an NSUN2-FOSB regulatory circuit.

Furthermore, FOSB increases BCL2L1 expression by directly binding to its promoter. Our findings reveal the therapeutic potential of targeting the NSUN2-FOSB-BCL2L1 axis in AML.

Methods

Leukemic cell lines, primary AML samples, and normal hematopoietic cells

Human leukemic cell lines were obtained from ATCC (Manassas, VA, USA) and cultured in RPMI 1640 medium (Invitrogen, Carlsbad, CA, USA) supplemented with 10% fetal bovine serum (Invitrogen) in a humidified incubator with 5% CO_2 at 37 °C. Human bone marrow (BM) mononuclear cells were isolated from *de novo* AML patients using density gradient centrifugation (Invitrogen). Primary $CD34^+$ cells from AML patients were isolated by the EasySep™ human CD34 positive selection kit (StemCell Technologies, Vancouver, BC, Canada). Normal $CD34^+$ cells isolated from healthy donors were used as normal controls (NCs). All procedures involving human participants adhered to the ethical standards set by the Ethics Committee of the First Affiliated Hospital of Wenzhou Medical University (KY2022-R110) and to the Helsinki Declaration of 1975, as revised in 2000. The clinical characteristics of AML patients are summarized in Table S1.

Methylated RNA immunoprecipitation (MeRIP)

Details of MeRIP are provided in the supplemental methods. qPCR was performed using m^5C- or m^6A-IPed RNA or input RNA with primers (Table S2).

Limiting dilution assays (LDA)

Nsun2-depleted or WT GFP^+ cells were isolated from MA9-induced secondary BMT recipients. Three doses of donor cells (Table S3) were transplanted into lethally irradiated mice (n = 6 for each group). Recipient survival was monitored for 6 months after BMT. The LSC frequency was

evaluated using the extreme limiting dilution assay (ELDA) software.[11]

Data availability

All RNA-seq data are publicly available on the Gene Expression Omnibus under accession numbers GSE 252880, GSE 253074, and GSE 308401.

Other procedures

CCK-8, apoptosis assay, m^5C blot, and other experiments, please see Supplemental Methods.

Statistical analysis

Data from at least three independent experiments *in vitro* were expressed as Mean ± SD. Mann-Whitney-Wilcoxon was used to compare differences in two independent subgroups in clinical samples. Generally, a two-tailed Student's t-test was used to compare differences between two groups. A one-way ANOVA followed by Tukey's test was performed to compare three or more groups. Kaplan-Meier survival curves were generated to analyze OS, and *P* values were calculated using the log-rank test. Fisher's exact tests were applied to compare categorical variables. All statistical analyses were conducted using GraphPad Prism 9.0 (GraphPad Software Inc., USA). Differences were considered significant when $P < 0.05$.

Results

NSUN2 expression is elevated in AML cells compared with normal controls (NC)

To investigate NSUN2 expression in AML, we measured *NSUN2* levels in 102 *de novo* AML patients (Table S1) and 18 healthy volunteers as NC. *NSUN2* expression was significantly higher in AML patients than NC (Figure 1A), and *NSUN2* level was elevated in AML cells with specific chromosomal translocations (Figure 1B) and FAB subtypes (Figure 1C) compared with NC. *NSUN2* expression was also higher in 12 $CD34^+$ AML cells than in 7 $CD34^+$ NC samples (Figure

1D). To further validate these findings, we analyzed public datasets. *NSUN2* expression was consistently higher in AML cells than NC according to the BloodSpot (Figure S1A, B),[12] GSE 114868 (Figure S1C),[13] and the Beat AML database (Figure S1D). Also, *NSUN2* expression was elevated in both $CD34^-$ and $CD34^+$ AML cells than $CD34^+$ NC in the GSE30029 (Figure S1E).[14] Furthermore, NSUN2 protein level was higher in six primary AML than two NC samples (Figure 1E), and its level was also elevated in six $CD34^+$ AML than two $CD34^+$ NC samples (Figure 1E). Similarly, the mean fluorescence intensity (MFI) of NSUN2 was markedly higher in two primary AML than in the two NC samples (Figure 1F).

We next assessed whether NSUN2 expression correlates with patient outcome. The Therapeutically Applicable Research to Generate Effective Treatments (TARGET) AML database revealed that AML patients with higher *NSUN2* levels had shorter OS ($P < 0.05$, Figure S2A). However, NSUN2 expression above the median did not predict poor prognosis in TCGA database (Figure S2B). Only AML patients with NSUN2 expression above the upper quartile had inferior survival (Figure S2C).

NSUN2 facilitates the survival of AML cells

To investigate the functional role of NSUN2 in AML, we decreased NSUN2 expression using two shRNAs (Figure 2A, B). NSUN2 KD markedly reduced cell proliferation (Figure 2C), induced G0 cell cycle arrest (Figure S3A), impaired colony formation (Figure S3B), and increased apoptosis (Figure 2D). PARP, a substrate of caspase-3, was prominently cleaved in *NSUN2*-KD cells (Figure S3C, D). Because apoptosis is often initiated via mitochondrial pathways, we examined mitochondrial function[15]. NSUN2 KD decreased mitochondrial membrane potential (MMP) in AML cells (Figure S3E) and reduced mitochondrial mass compared with sh-NC control (Figure

S3F). Transmission electron microscopy (TEM) revealed that NSUN2 KD caused irregular mitochondrial swelling, disrupted and blurred cristae, and reduced cristae density in MOLM-13 cells (Figure 2E). Furthermore, MOLM-13 cells with or without NSUN2 KD were xenografted in NSG mice. NSUN2 KD substantially reduced the leukemic burden as evidenced by decreased human $CD45^+$ (hCD45) cells in peripheral blood (PB) (Figure S4A) and extended OS in NSG mice (Figure S4B). Since NSUN2 is the main enzyme catalyzing m^5C modification,[2] we measured the global m^5C level. NSUN2 KD reduced global m^5C levels, as shown by m^5C blot (Figure S4C) and ELISA assay (Figure S4D).

We further evaluated the effects of NSUN2 KD in primary AML patient samples. KD efficiency is shown in Figure S5A. In three independent specimens, NSUN2 KD reduced colony formation (Figure S5B), induced apoptosis (Figure S5C), and prolonged OS in NSG mice (Figure S5D-F).

NSUN2 positively regulates FOSB expression and facilitates leukemogenesis in an m^5C-dependent manner

To identify the specific m^5C sites regulated by NSUN2, we performed methylated RNA immunoprecipitation sequencing (MeRIP-seq) and RNA-seq to analyze the differentially methylated genes (DMGs) and differentially expressed genes (DEGs) in NSUN2-KD versus sh-NC cells. m^5C sites were predominantly enriched in the coding sequence (CDS) than 5'UTR and 3'UTR (Figure S6A-C). Cell growth and regulation of cell growth were enriched in NSUN2-KD compared to sh-NC cells by Kyoto Encyclopedia of Genes and Genomes (KEGG) analysis (Figure S6D). Because NSUN2-mediated m^5C modification enhances gene expression,[16] we analyzed the shared downregulated DMGs and DEGs. Only 20 such genes were identified in the Venn diagram (absolute log2-fold change > 0.5, $P < 0.05$, Figure S6E). Among these, we

measured 12 genes associated with cell proliferation and found that *SEMA3A*, *RYR1*, *FHAD1*, and *FOSB* were consistently decreased in *NSUN2*-KD than sh-NC cells (Figure S6F). We prioritized FOSB for further study given its role as a member of the activator protein-1 (AP-1) family and its critical function in cell survival.[17] Consistently, *NSUN2* KD reduced FOSB transcript and protein expressions (Figure 3A, B), whereas NSUN2 OE increased them (Figure S7A-C).

To investigate whether NSUN2 facilitates leukemogenesis and increases FOSB expression in an m^5C catalytic activity-dependent manner, we reintroduced wild-type (WT) NSUN2 or two enzyme-dead mutants (C271A or C321A) into NSUN2-KD AML cells.[18] WT NSUN2, but not its mutants, restored the reduction in FOSB expression (Figure 3C), the decrease in colony (Figure 3D, E), and the increase in apoptosis (Figure S7D, E) induced by NSUN2 KD.

NSUN2 maintains *FOSB* mRNA stability via 3'UTR methylation

We next examined whether NSUN2 regulates *FOSB* mRNA stability. NSUN2 KD markedly shortened the half-life of *FOSB* mRNA (Figure 4A) without affecting pre-*FOSB* transcript levels (Figure S8A), indicating post-transcriptional regulation. To map the m^5C-modified sites on *FOSB* mRNA, we constructed pGL-3-based vectors containing FOSB 5'UTR, CDS, or individual 3′UTR fragments (Figure 4B). NSUN2 KD reduced Luc activity driven by the 3′UTR-3 fragment, but not by other regions (Figure 4C). Conversely, NSUN2 OE increased activity of 3′UTR-3 (Figure 4D), and this effect required intact catalytic activity, as WT but not mutant NSUN2 enhanced reporter activity (Figure 4E). Parallel effects were observed at the Luc mRNA level (Figure S8B, C). In MOLM-13 cells expressing sh-NC, 12 of 13 clones (92.3%) were methylated at 3656 of *FOSB* 3′UTR (Figure 4F), compared with only 5 of 13 (38.4%) in sh-NSUN2 cells (Figure 4F). Mutation of C3656 to T (3′UTR-3M, Figure S8D) abolished NSUN2-dependent regulation, as KD or OE of

NSUN2 no longer altered reporter activity (Figure 4C, D, column 7). To exclude contributions from N6-methyladenosine (m^6A), we performed RIP. *FOSB* mRNA was enriched by anti-m^5C but not anti-m^6A antibody, confirming that FOSB undergoes m^5C rather than m^6A modification (Figure S8E).

To determine whether there is a physical interaction between NSUN2 protein and *FOSB* mRNA, a RIP-PCR assay was performed. Anti-NSUN2 but not anti-IgG antibody significantly enriched *FOSB* mRNA, confirming that NSUN2 protein binds to *FOSB* mRNA (Figure S8F, G).

YBX1 KD does not regulate FOSB expression

Given that YBX1 binds to m^5C-modified transcripts and enhances their stability,[19] we tested its involvement. However, YBX1 KD had no effect on FOSB expression (Figure S9A–D), suggesting that FOSB stability is maintained through a YBX1-independent mechanism.

FOSB rescues the anti-leukemic effects induced by NSUN2 KD and FOSB transcriptionally activates NSUN2 expression

To explore whether FOSB mediates oncogenic function of NSUN2, FOSB was overexpressed in AML cells transduced with sh-NSUN2 or sh-NC. OE of FOSB (Line 3 vs. 1, Figure 5A) blocked proliferation defects (Figure 5B) and apoptosis (Figure 5C) induced by NSUN2 KD. Interestingly, OE of FOSB also increased NSUN2 expression (Line 3 vs. 1, Figure 5A). Conversely, FOSB KD markedly reduced NSUN2 transcript and protein levels (Figure 5D, E), induced apoptosis (Figure S10A), and inhibited proliferation (Figure S10B, C). FOSB OE increased NSUN2 expression (Figure S10D-F) and slightly promoted proliferation (Figure S10G, H). In murine $MA9^+$ leukemic cells, Fosb KD reduced Nsun2 expression (Figure S10I, J), decreased GFP^+ leukemic burden in PB (Figure S10K, L), and prolonged OS (Figure S10M).

Given FOSB's role as a transcription factor,[20] we next investigated whether it directly activates NSUN2 transcription. Motif prediction (JASPAR) identified a TGA(C/G)T(C/A)A consensus sequence with three potential binding sites in the NSUN2 promoter (Figure S11A, B).[21] OE of FOSB increased the Luc activity of WT and WT3, but not WT1 or WT2 constructs (Figure S11C). Mutation of the WT3 (Mut3) motif largely abolished this effect (Figure S11C, column 5), indicating that WT3 contains the FOSB-binding motifs. ChIP-PCR confirmed FOSB binding to WT3 but not WT1 or WT2 (Figure S11D). Moreover, ChIP-seq were performed in AML cells OE of Flag-tagged FOSB, which were IPed by anti-IgG or anti-Flag antibody. Anti-Flag antibody had higher occupancy at the *NSUN2* promoter than anti-IgG antibody (Figure S11E).

Consistent with this reciprocal loop, FOSB was elevated in AML compared with NC samples in both our cohort (Figure S12A-C) and TCGA (Figure S12D), and positively correlated with NSUN2 expression in Gene Expression Profiling Interactive Analysis (GEPIA) database (Figure S12E).[22]

FOSB transcriptionally activates the expression of BCL2L1 (BCL-XL)

To identify additional FOSB targets, we performed RNA-seq in MOLM-13 cells with or without FOSB KD. Pathway analysis revealed enrichment of apoptosis-related signatures (Figure S13A). Heatmap analysis showed downregulation of the anti-apoptotic regulator BCL2L1 and upregulation of apoptotic executors in FOSB-KD cells (Figure 6A). KD of FOSB decreased BCL2L1 mRNA and protein levels (Figure 6B). Consistently, NSUN2 KD reduced BCL2L1 mRNA and protein levels (Figure S13B, C). Moreover, OE of FOSB increased BCL2L1 expression (Figure 6C). Functionally, FOSB KD reduced mitochondrial mass (Figure 6D) and MMP level (Figure S13D).

Promoter analysis identified two potential FOSB-binding motifs in *BCL2L1* promoter (Figure S14A). FOSB OE increased Luc activity of WT, WT1, and WT2 constructs, but not Mut1/2 (Figure S14B). ChIP-PCR confirmed FOSB occupancy at both motifs (Figure S14C). ChIP-seq were performed in AML cells OE of Flag-tagged FOSB, which were IPed by anti-IgG or anti-Flag antibody. Anti-Flag antibody presented higher occupancy at the *BCL2L1* promoter than anti-IgG antibody (Figure S14D).

To determine whether BCL2L1 is an essential target of NSUN2-FOSB axis, BCL2L1 was overexpressed in AML cells with or without *NSUN2* KD. OE of BCL2L1 (Figure S15A) partially blocked the decreased viability (Figure S15B, C) and increased apoptosis (Figure S15D) induced by NSUN2 KD. We further overexpressed BCL2L1 in AML cells with or without *FOSB* KD. Similarly, BCL2L1 overexpression (Figure S16A) partially rescued the decrease in viability (Figure S16 B, C) and the increase in apoptosis (Figure S16D) induced by FOSB KD.

To explore whether NSUN2-FOSB-BCL2L1 axis is also operative in AML cells driven by other common genetic lesions, we KD NSUN2 expression in K562 cells bearing BCR-ABL fusion gene[23] and OCI-AML3 cells carrying mutant NPM1.[24] NSUN2 KD decreased FOSB and BCL2L1 protein levels in these two cells (Figure S17A).

Furthermore, we explored whether NSUN2-FOSB axis regulates other BCL-2 family members. NSUN2 and FOSB KD both decreased BCL2 protein level, but had little effect on MCL1 and BAX expressions (Figure S18A, B). However, we did not find FOSB-recognizing motif (TGA(C/G)T(C/A)A) in the *BCL2* promoter by Motif prediction (JASPAR, data not shown). Therefore, FOSB probably indirectly regulates BCL2 expression, and BCL2 downregulation in FOSB-KD cells might be a by-product of apoptosis.

To better understand clinical relevance, we analyzed the correlation between *NSUN2*, *FOSB*, and *BCL2L1* mRNA levels within the same cohort. The positive correlation exists between *NSUN2* vs *FOSB*, *NSUN2* vs *BCL2L1*, and *FOSB* vs *BCL2L1* mRNA levels (Figure S19A-C).

Nsun2 knockout attenuates AML progression and inhibits LSC self-renewal in MA9-induced murine leukemia

To investigate the role of Nsun2 in leukemogenesis, we generated conditional knockout mice ($Nsun2^{fl/fl}$ Cre^{ERT2}, hereafter fl/fl; Figure S20A).[25] Tamoxifen (TAM) injection achieved efficient Nsun2 deletion in BM cells (Δ/Δ; Figure S20B). MA9-transduced BM Lin^- cells from fl/fl mice were transplanted into recipients (Figure S20C), and TAM treatment at days 15–20 after BMT depleted Nsun2 in GFP^+ AML cells (Figure S20D, E). In secondary BMT (Figure S21A), TAM-induced Nsun2 loss (days 10–15) markedly reduced GFP^+ leukemic cells in PB (Figure S21B, C) and BM (Figure 7A, B), decreased spleen and liver weights (Figure S21D, E), and limited leukemic infiltration in the spleen and liver (Figure S21F, G). Proliferation was suppressed, as EdU^+ cells were about 9-fold lower in Δ/Δ than fl/fl samples (Figure S21H). Importantly, Nsun2 deletion significantly reduced LSC activity: L-GMP frequency[26] decreased by > 50% (Figure 7C), and ELDA showed a ~75% reduction in functional LSCs (1 in 48 vs. 1 in 144, $P < 0.05$; Figure 7D; Table S3).[11, 27] Nsun2 deficiency almost eliminated colony formation (Figure 7E), and prolonged OS across primary, secondary, and tertiary transplants (Figure 7F–H). Restoration of WT Nsun2, but not enzymatically inactive mutants (C271A, C321A) (Figure S21I), reversed the extended survival (Figure S21J), indicating that Nsun2's catalytic activity is required for leukemogenesis.

Our results indicate that Nsun2 is essential for AML maintenance. To further investigate the role

of Nsun2 in AML initiation, we injected TAM 3 days after transplantation in secondary BMT. TAM treatment markedly extended OS during AML initiation (Figure S21K).

Nsun2 deletion did not impair BM homing (Figure S22A), and control experiments excluded confounding effects of floxed alleles or Cre^{ERT2} (Figure S22B). In the AML1-ETO9a (A/E9a)-driven M2 AML model, Δ/Δ cells similarly conferred prolonged OS in both primary and secondary BMT (Figure S22C-F), confirming that Nsun2 is broadly required for AML maintenance.

Nsun2 knockout decreases Fosb in murine AML cells and OE of Fosb rescues leukemogenesis

Given that NSUN2 regulates FOSB in human AML, we examined Fosb expression in murine Δ/Δ leukemic cells. Nsun2 deletion reduced Fosb transcript and protein levels (Figure S23A, B). Fosb OE restored Nsun2 expression (Figure S23C) and reversed the OS extension conferred by Nsun2 deletion (Figure S23D). These findings establish Fosb as a critical downstream effector of Nsun2 in murine AML.

Nsun2 depletion does not affect normal hematopoiesis

To investigate the role of NSUN2 in steady-state hematopoiesis, we first performed cell counts in PB in fl/fl and Δ/Δ mice. Four weeks after the last TAM injection, total blood cell counts and lineage distributions were comparable between the two groups (Figure S24A-C). Similarly, total BM cellularity showed no difference (Figure S24D), and the proportions of T, B, and myeloid cells in PB were indistinguishable (Figure S24E). Additionally, Nsun2 depletion did not affect the frequency of EdU^+ cells (Figure S24F). We then explored whether *Nsun2* depletion affects the frequency and function of HSPC. The frequencies of distinct HSPC subsets, including long-term

hematopoietic stem cells (LT-HSCs), were similar between fl/fl and Δ/Δ mice (Figure 8A). Functional assays further demonstrated that Nsun2-deficient LSK (Lin□c-Kit□Sca-1□) cells formed colonies at comparable numbers and distributions relative to controls (Figure 8B). Finally, a competitive repopulation assay confirmed that Nsun2 deletion did not impair self-renewal or lineage output: the proportions of donor-derived total CD45.2□ cells (Figure S24G, H), as well as myeloid (Figure S24I), B (Figure S24J), and T lineages (Figure S24K) in PB, were equivalent between fl/fl and Δ/Δ groups.

We also monitored over a longer term (> 12 months) to rule out potential delayed effects on hematopoietic stem cell function. Total blood cell counts and lineage distributions were comparable between the two groups (Figure S25A-C).

NSUN2 KD sensitizes AML cells to chemotherapy

Finally, we investigated whether *NSUN2* KD enhances the cytotoxicity of chemotherapeutic drugs. NSUN2-KD and sh-NC cells were treated with or without various chemotherapeutic drugs, and cell death was measured by 7-AAD staining. NSUN2 KD potentiated the cytotoxic effects of cytarabine (Ara-C), cladribine (Cla), decitabine (DAC), tucidinostat (Tuc), and homoharringtonine (HHT) in MOLM-13 and MV4-11 cells (Figure S26A-D), suggesting that NSUN2 KD sensitizes AML cells to chemotherapy.

NSUN2 inhibitor MY-1B inhibits FOSB-BCL2L1 axis[10]

Next, we explored whether NSUN2 inhibitor MY-1B phenocopies the genetic KD of NSUN2. MY-1B treatment markedly decreased FOSB and BCL2L1 protein levels (Figure S27A), suggesting that NSUN2 is a therapeutic target. However, two well-known hypomethylation agents, DAC and 5-Azacytidine (AZA), did not regulate NSUN2 protein levels (Figure S27B).

Discussion

Our study uncovers a previously unrecognized mechanism by which m□C RNA modification promotes leukemogenesis, offering both mechanistic insights and therapeutic opportunities. NSUN2 increases FOSB expression by enhancing *FOSB* mRNA stability, while FOSB transcriptionally activates NSUN2, establishing an NSUN2-FOSB reciprocal loop (Figure 8C). In addition, FOSB transcriptionally activates BCL2L1 expression to facilitate cell survival (Figure 8D). Together, these findings identify the NSUN2-FOSB-BCL2L1 axis as a potential therapeutic target in AML.

m□C modification has been implicated in RNA stability, protein translation, and nuclear export, thereby contributing to oncogene activation across multiple tumor types.[7, 28] In AML, overexpression of NSUN2 (WT), but not its mutants, fully rescues leukemogenesis in NSUN2-deficient AML cells, confirming that its oncogenic effect is m□C-dependent. Prior studies have shown that m□C modifications frequently stabilize target mRNAs.[3, 6] For example, m^5C modification on 3'-UTR of *PKM2* mRNA facilitates its stability.[29] Our data extend this paradigm by showing that m□C modification of *FOSB* mRNA similarly promotes its stability. Nevertheless, m□C can also influence translation efficiency or nuclear export,[30] suggesting that its biological consequences may vary with cellular context.

YBX1 has been considered the principal “reader” of m□C-modified transcripts, stabilizing oncogenic mRNAs in several cancers.[19] YBX1 binds to m^5C-modified androgen receptor (*AR*) mRNA and stabilizes it in prostate cancer cells.[31] However, YBX1 recognizes m^6A-modified *BCL2* mRNA in an m^6A but not m^5C-dependent manner in AML cells.[32] In our study, YBX1 can not regulate FOSB expression, indicating that YBX1 is not the reader of m□C-modified FOSB,

and YBX1's binding specificity may depend on transcript context and modification type. Identification of the m□C reader(s) responsible for stabilizing *FOSB* mRNA remains an important avenue for future investigation.

NSUN2 expression itself is subject to transcriptional regulation by multiple factors.[9, 33] Although FOSB has been extensively characterized as an immediate-early gene,[34] its function in AML has been unclear. We show that FOSB KD inhibits cell proliferation and induces apoptosis, establishing FOSB as an unexpected oncogenic driver in AML. This is consistent with the report that FOSB acts as an oncogene in piperlongumine-treated breast cancer cells.[35] Our data further demonstrate that FOSB directly activates *NSUN2* transcription, suggesting that stress-induced FOSB activation may drive persistent upregulation of both FOSB and NSUN2 through a reinforcing positive feedback loop in AML.[17]

We also identified BCL2L1 as a novel transcriptional target of FOSB. BCL2L1 is a critical anti-apoptotic regulator whose inhibition induces apoptosis and mitochondrial dysfunction.[36] Its overexpression contributes to resistance to BCL2 inhibitors in chronic lymphocytic leukemia and resistance to bortezomib in mantle cell lymphoma.[37, 38] BCL2L1 upregulation is also a hallmark of myeloproliferative neoplasm-derived AML, where its inhibition confers therapeutic benefit.[39] Thus, the FOSB-BCL2L1 axis represents an attractive therapeutic vulnerability in AML.

FOSB transcriptionally activates BCL2L1 expression by directly binding to its promoter, and NSUN2 positively regulates BCL2L1 expression. Therefore, it is reasonable that NSUN2 indirectly regulates BCL2L1 expression through FOSB. NSUN2 KD induces apoptosis in AML cells, and induces ferroptosis in AML and tumor cells,[10, 40-42] suggesting a complicated function of NSUN2. In addition, NSUN2 KD sensitizes AML cells to chemotherapy, likely by inducing

apoptosis or ferroptosis. Notably, NSUN2 is dispensable for normal hematopoiesis. Therefore, NSUN2 is a promising therapeutic target in AML.

Considering that NSUN2 is highly expressed in AML cells, it is reasonable that AML cells with high NSUN2 expression rely on m□C modification to maintain rapid proliferation and survival. Therefore, AML cells are more susceptible to the depletion of *NSUN2* compared with normal HSPC cells. Consistent with this, Nsun2 depletion does not affect normal hematopoiesis and the self-renewal ability of HSPCs. However, it is possible that HSPCs rely more on other m□C methyltransferases such as DNMT2 (encoded by tRNA aspartic acid methyltransferase 1), because double knockout of Nsun2 and DNMT2 in mice impairs cellular differentiation, while single knockout has no detectable effects.[4]

Target AML database demonstrates that AML patients with high NSUN2 levels are associated with poor outcomes. However, NSUN2 expression levels alone in AML do not predict prognosis, and the differences in OS were only observed in AML with SRSF2 P95H mutation according to Beat AML database.[43] In contrast, TCGA data revealed a consistent association between high NSUN2 levels and poor prognosis.[6] We speculate that differences among enrolled AML patients account for this discrepancy.

Mechanistically, we mapped an m□C modification site (C3656) within the FOSB 3′UTR that mediates mRNA stabilization. Although KD or OE of NSUN2 did not alter Luc activity of constructs containing the 5′UTR or CDS, low-level modifications at these regions can not be excluded. Moreover, standard bisulfite sequencing can not distinguish m□C from related modifications (hm□C or m□C) and is prone to RNA degradation, potentially leading to underestimation of modification sites. The development of more precise m□C-mapping methods

will be critical to refining our understanding of m□C biology in leukemia.

In conclusion, our study identifies the NSUN2-FOSB positive feedback loop as a driver of leukemogenesis that spares normal hematopoiesis. Disrupting this circuit by inhibiting NSUN2 or blocking the NSUN2-FOSB-BCL2L1 signaling axis offers a promising therapeutic strategy for AML.

References

1. Witkin KL, Hanlon SE, Strasburger JA, et al. RNA editing, epitranscriptomics, and processing in cancer progression. Cancer Biol Ther. 2015;16(1):21-27.
2. Sun Z, Xue S, Xu H, et al. Effects of NSUN2 deficiency on the mRNA 5-methylcytosine modification and gene expression profile in HEK293 cells. Epigenomics. 2019;11(4):439-453.
3. Zhang X, Liu Z, Yi J, et al. The tRNA methyltransferase NSun2 stabilizes p16INK(4) mRNA by methylating the 3'-untranslated region of p16. Nat Commun. 2012;6(3):712.
4. Tuorto F, Liebers R, Musch T, et al. RNA cytosine methylation by Dnmt2 and NSun2 promotes tRNA stability and protein synthesis. Nat Struct Mol Biol. 2012;19(9):900-905.
5. Zhu N, Chen M, Eng R, et al. MLL-AF9- and HOXA9-mediated acute myeloid leukemia stem cell self-renewal requires JMJD1C. J Clin Invest. 2016;126(3):997-1011.
6. Li S, Liu Y, Wu X, et al. The m((5))C methyltransferase NSUN2 promotes progression of acute myeloid leukemia by regulating serine metabolism. Cell Rep. 2025;44(5):115661.
7. Mei L, Shen C, Miao R, et al. RNA methyltransferase NSUN2 promotes gastric cancer cell proliferation by repressing p57(Kip2) by an m(5)C-dependent manner. Cell Death Dis. 2020;11(4):270.
8. Hu Y, Chen C, Lin K, et al. NSUN2 promotes colorectal cancer progression and increases lapatinib sensitivity by enhancing CUL4B/ErbB-STAT3 signalling in a non-m5C manner. Clin Transl Med. 2025;15(4):e70282.
9. Su J, Wu G, Ye Y, et al. NSUN2-mediated RNA 5-methylcytosine promotes esophageal squamous cell carcinoma progression via LIN28B-dependent GRB2 mRNA stabilization. Oncogene. 2021;40(39):5814-5828.
10. Ye W, Zhao Y, Zhou Y, et al. NSUN2-mediated cytosine-5 methylation of FSP1 protects acute myeloid leukemia cells from ferroptosis. Mol Cancer. 2025;24(1):201.
11. Hu Y, Smyth GK. ELDA: extreme limiting dilution analysis for comparing depleted and enriched populations in stem cell and other assays. J Immunol Methods. 2009;347(1-2):70-78.
12. Gislason MH, Demircan GS, Prachar M, et al. BloodSpot 3.0: a database of gene and protein expression data in normal and malignant haematopoiesis. Nucleic Acids Res. 2024;52(D1):D1138-D1142.
13. Huang HH, Chen FY, Chou WC, et al. Long non-coding RNA HOXB-AS3 promotes myeloid cell proliferation and its higher expression is an adverse prognostic marker in patients with acute myeloid leukemia and myelodysplastic syndrome. BMC Cancer. 2019;19(1):617.
14. de Jonge HJ, Woolthuis CM, Vos AZ, et al. Gene expression profiling in the leukemic stem cell-enriched CD34+ fraction identifies target genes that predict prognosis in normal karyotype AML. Leukemia. 2011;25(12):1825-1833.
15. Newmeyer DD, Farschon DM, Reed JC. Cell-free apoptosis in Xenopus egg extracts: inhibition by Bcl-2 and requirement for an organelle fraction enriched in mitochondria. Cell. 1994;79(2):353-364.
16. Yang X, Yang Y, Sun BF, et al. 5-methylcytosine promotes mRNA export - NSUN2 as the methyltransferase and ALYREF as an m(5)C reader. Cell Res. 2017;27(5):606-625.
17. Shahzad MM, Arevalo JM, Armaiz-Pena GN, et al. Stress effects on FosB- and interleukin-8 (IL8)-driven ovarian cancer growth and metastasis. J Biol Chem. 2010;285(46):35462-35470.
18. Xu X, Zhang Y, Zhang J, Zhang X. NSun2 promotes cell migration through methylating autotaxin mRNA. J Biol Chem. 2020;295(52):18134-18147.

19. Chen X, Li A, Sun BF, et al. 5-methylcytosine promotes pathogenesis of bladder cancer through stabilizing mRNAs. Nat Cell Biol. 2019;21(8):978-990.
20. Barrett CS, Millena AC, Khan SA. TGF-beta Effects on Prostate Cancer Cell Migration and Invasion Require FosB. Prostate. 2017;77(1):72-81.
21. Sandelin A, Alkema W, Engstrom P, Wasserman WW, Lenhard B. JASPAR: an open-access database for eukaryotic transcription factor binding profiles. Nucleic Acids Res. 2004;32(Database issue):D91-94.
22. Tang Z, Li C, Kang B, Gao G, Li C, Zhang Z. GEPIA: a web server for cancer and normal gene expression profiling and interactive analyses. Nucleic Acids Res. 2017;45(W1):W98-W102.
23. Karagiannis TC, Wall M, Ververis K, et al. Characterization of K562 cells: uncovering novel chromosomes, assessing transferrin receptor expression, and probing pharmacological therapies. Cell Mol Life Sci. 2023;80(9):248.
24. Quentmeier H, Martelli MP, Dirks WG, et al. Cell line OCI/AML3 bears exon-12 NPM gene mutation-A and cytoplasmic expression of nucleophosmin. Leukemia. 2005;19(10):1760-1767.
25. Feng J, Xu T, He M, et al. NSUN2-mediated m5C modification of HBV RNA positively regulates HBV replication. PLoS Pathog. 2023;19(12):e1011808.
26. Krivtsov AV, Twomey D, Feng Z, et al. Transformation from committed progenitor to leukaemia stem cell initiated by MLL-AF9. Nature. 2006;442(7104):818-822.
27. Sieburg HB, Cho RH, Muller-Sieburg CE. Limiting dilution analysis for estimating the frequency of hematopoietic stem cells: uncertainty and significance. Exp Hematol. 2002;30(12):1436-1443.
28. Zhang X, Zhang Y, Li R, et al. STUB1-mediated ubiquitination and degradation of NSUN2 promotes hepatocyte ferroptosis by decreasing m(5)C methylation of Gpx4 mRNA. Cell Rep. 2024;43(11):114885.
29. Qi Q, Zhong R, Huang Y, et al. The RNA M5C methyltransferase NSUN2 promotes progression of hepatocellular carcinoma by enhancing PKM2-mediated glycolysis. Cell Death Dis. 2025;16(1):82.
30. Jian D, Cheng X, Qi D, et al. Nsun2 controls cardiac homeostasis and hypertrophic response by regulating PRKACA expression. Theranostics. 2025;15(6):2393-2412.
31. Zhu W, Wan F, Xu W, et al. Positive epigenetic regulation loop between AR and NSUN2 promotes prostate cancer progression. Clin Transl Med. 2022;12(9):e1028.
32. Feng M, Xie X, Han G, et al. YBX1 is required for maintaining myeloid leukemia cell survival by regulating BCL2 stability in an m6A-dependent manner. Blood. 2021;138(1):71-85.
33. Frye M, Watt FM. The RNA methyltransferase Misu (NSun2) mediates Myc-induced proliferation and is upregulated in tumors. Curr Biol. 2006;16(10):971-981.
34. Wang H, Zhang W, Liu J, et al. NF-kappaB and FosB mediate inflammation and oxidative stress in the blast lung injury of rats exposed to shock waves. Acta Biochim Biophys Sin (Shanghai). 2021;53(3):283-293.
35. Park JA, Na HH, Jin HO, Kim KC. Increased Expression of FosB through Reactive Oxygen Species Accumulation Functions as Pro-Apoptotic Protein in Piperlongumine Treated MCF7 Breast Cancer Cells. Mol Cells. 2019;42(12):884-892.
36. Chiou JT, Wu YY, Lee YC, Chang LS. BCL2L1 inhibitor A-1331852 inhibits MCL1 transcription and triggers apoptosis in acute myeloid leukemia cells. Biochem Pharmacol. 2023;215:115738.
37. Luanpitpong S, Janan M, Yosudjai J, Poohadsuan J, Chanvorachote P, Issaragrisil S. Bcl-2 Family Members Bcl-xL and Bax Cooperatively Contribute to Bortezomib Resistance in Mantle Cell Lymphoma. Int J Mol Sci. 2022;23(22):14474.

38. Ghia EM, Rassenti LZ, Choi MY, et al. High expression level of ROR1 and ROR1-signaling associates with venetoclax resistance in chronic lymphocytic leukemia. Leukemia. 2022;36(6):1609-1618.
39. Wang Z, Skwarska A, Poigaialwar G, et al. Efficacy of a novel BCL-xL degrader, DT2216, in preclinical models of JAK2-mutated post-MPN AML. Blood. 2025;146(3):341-355.
40. Tong R, Li Y, Wang J, et al. NSUN2 Knockdown Promotes the Ferroptosis of Colorectal Cancer Cells Via m5C Modification of SLC7A11 mRNA. Biochem Genet. 2025;64(1):524-537.
41. Chen SJ, Zhang J, Zhou T, et al. Epigenetically upregulated NSUN2 confers ferroptosis resistance in endometrial cancer via m(5)C modification of SLC7A11 mRNA. Redox Biol. 2024;69:102975.
42. Chen Y, Jiang Z, Zhang C, et al. 5-Methylcytosine transferase NSUN2 drives NRF2-mediated ferroptosis resistance in non-small cell lung cancer. J Biol Chem. 2024;300(4):106793.
43. Ma HL, Bizet M, Soares Da Costa C, et al. SRSF2 plays an unexpected role as reader of m(5)C on mRNA, linking epitranscriptomics to cancer. Mol Cell. 2023;83(23):4239-4254.e10.

Figure legend

Figure 1. NSUN2 expressions are higher in primary AML samples compared with normal controls (NC). (A) The transcript expressions of *NSUN2* were measured by qRT-PCR in bone marrow (BM) cells from 102 untreated AML patients in-house and 18 healthy volunteers as NC. (B and C) NSUN2 expression in the same AML cohort, stratified by chromosomal translocation (B) and FAB subtype (C), compared with NC. NK: normal karyotype; CK: complex karyotype. (D) *NSUN2* expressions were measured by qRT-PCR in 12 $CD34^+$ AML cells versus 7 normal $CD34^+$ hematopoietic stem and progenitor cells (HSPCs). (E) NSUN2 protein levels were measured in two NC and six AML samples, and NSUN2 protein levels were measured in two $CD34^+$ NC and six $CD34^+$ AML samples. (F) NSUN2 expressions were determined in two NC and two primary AML samples by immunofluorescence (IF) assay. Bar scales represent 10 μm. Data are expressed as the mean ± SD. n = 3 or more independent biological replicates. **P* < 0.05; ***P* < 0.01; ****P* < 0.001 compared with NC; ns = not significant.

Figure 2. NSUN2 knockdown (KD) impairs survival and induces apoptosis in AML cell lines. (A and B) NSUN2 protein and transcript levels were measured in MOLM-13 and MV4-11 cells after transduction with sh-NSUN2 or sh-NC for 48 h, followed by puromycin (1 μg/mL) treatment for an additional 48 h. (C) CCK-8 assay was performed in AML cells at the indicated times after transduction with sh-NSUN2 or sh-NC for 48 h. (D) Apoptosis was measured in AML cells after transduction with sh-NSUN2 or sh-NC for 48 h, followed by puromycin (1 μg/mL) treatment for an additional 48 h. Annexin V/7-AAD staining was used to assess early and late apoptosis. The representative plots (left) and statistical analysis of Annexin V^+/7-AAD^+ + Annexin V^+/7-AAD^-

cells (right) are shown. (E) Representative transmission electron microscopy images for mitochondria (left) and quantitation of mitochondrial cristae (right) are shown in MOLM-13 cells transduced with sh-NSUN2 (NS2) or sh-NC (n = 20/per group). Bar scales represent 500 nm. n = 3 or more independent technical replicates. ***$P < 0.001$ versus sh-NC.

Figure 3. NSUN2 positively regulates FOSB expression and promotes leukemogenesis in an m^{5}C-dependent manner. (A and B) NSUN2 and FOSB transcript and protein levels were measured in leukemic cells transduced with sh-NSUN2 or sh-NC. (C–E) AML cells transduced with sh-NC were overexpressed with Vec, and AML cells transduced with sh-NSUN2#3 (3'-UTR) were overexpressed with Vec, wild-type (WT) NSUN2, or its two catalytically inactive mutants (C271A or C321A). Cells were analyzed for NSUN2 and FOSB protein levels (C) and colony formation analysis (2×10^3/dish for each group) (D and E). n = 3 or more independent biological replicates. *$P < 0.05$; **$P < 0.01$; ***$P < 0.001$; ns = not significant.

Figure 4. NSUN2 stabilizes *FOSB* mRNA by methylating its 3'UTR. (A) The half-lives of *FOSB* mRNA were measured in AML cells transduced with sh-NSUN2 or sh-NC for 48 h, followed by actinomycin D (Act. D, 2 μM) treatment for the indicated times. (B) Schematic presentation of different fragments of *FOSB* mRNA used in the luciferase (Luc) reporter assays. (C and D) Blank pGL3 (Vec) and pGL3 vectors carrying the indicated *FOSB* mRNA sequences were transfected into 293T cells, followed by KD of NSUN2 (C) or overexpression (OE) of NSUN2 (D). Relative Luc activity (Firefly/Renilla) was measured in each cell lysate 48 h after transfection. (E) 293T cells were transfected with blank vector (NC), wild-type (WT) NSUN2, or

its two mutants, together with pGL3-*FOSB*-3'UTR-3. Luc activity was measured in each cell lysate. (F) Bisulfite sequencing of FOSB-3'UTR-3 in MOLM-13 cells with or without NSUN2 KD. Methylation frequency was calculated as methylation/(methylation + unmethylation) (left). The arrow indicates base C (position 3656), which was not converted to T after bisulfite treatment, indicating m^5C modification. Representative sequences show m^5C modification at C3656 (right). n = 3 or more independent biological replicates. **P* < 0.05; ***P* < 0.01; ****P* < 0.001 compared with sh-NC. ns = not significant.

Figure 5. OE of FOSB rescues NSUN2 KD-induced anti-leukemia effects, and FOSB activates NSUN2 expression. (A–C) Leukemic cells were transduced with sh-NC or sh-NSUN2 for 48 h and overexpressed with blank vector (Vec) or vector overexpressing FOSB for another 48 h. NSUN2 and FOSB protein levels (A), cell proliferation (B), and apoptosis (C) were measured. (D and E) The transcript and protein levels of FOSB and NSUN2 were measured in AML cells transduced with sh-FOSB or sh-NC for 48 h, followed by puromycin (1 μg/mL) treatment for an additional 48 h. n = 3 or more independent biological replicates. **P* < 0.05; ***P* < 0.01; ****P* < 0.001. ns = not significant.

Figure 6. FOSB activates BCL2L1 expression and affects mitochondrial function. (A) MOLM-13 cells transduced with sh-NC or sh-FOSB#1 (sh-FOSB) were subjected for RNA-seq. Apoptosis-associated genes including BCL2L1 were visualized by heatmap assay. (B) BCL2L1 transcript and protein levels were measured in MOLM-13 and MV4-11 cells after sh-FOSB or sh-NC transduction for 48 h, followed by puromycin (1 μg/mL) treatment for an additional 48 h.

(C) BCL2L1 transcript and protein levels were measured in AML cells, which were overexpressed with FOSB or blank control (Vec) for 48 h. (D) The mitochondria were stained by MitoTracker Red CMXRos in red in AML cells after transduction with sh-FOSB or sh-NC. Mitochondrial mass was analyzed by MFI of MitoTracker staining. The representative images (left) and statistical analysis of MFI of MitoTracker staining (right, n = 50 per group) are shown. Bar = 50 nm. n = 3 or more independent biological replicates. ***$P < 0.001$ versus sh-NC cells.

Figure 7. Nsun2 facilitates leukemia stem cell (LSC) survival and self-renewal in a murine AML model. (A) The frequency of GFP^+ cells was measured in BM from fl/fl (n = 4) and Δ/Δ (n = 4) leukemic mice. The representative flow cytometry plots (left) and statistical analysis (right) are shown. (B) Representative images of BM smears from fl/fl (n = 3) and Δ/Δ (n = 3) mice (left). Statistical analysis of the average percentage of leukemic cells in BM is shown (right). Scale bar =10 μm. (C) LSC frequency was measured in BM GFP^+ cells from fl/fl (n = 4) and Δ/Δ (n = 4) leukemic mice. (D) Extreme limiting dilution assay (ELDA) was conducted in secondary BMT mice (fl/fl, n = 6; Δ/Δ, n = 6). (E) GFP^+ fl/fl (1000 cells per dish) or Δ/Δ cells (1000 cells per dish) were sorted from BM for colony assay. The representative images of colony (left) and statistical analysis of colony number (right). A two-tailed Student's t-test was used to compare differences between two groups. (F–H) OS was calculated in the primary (F), secondary (G), and tertiary BMT (H). Kaplan-Meier survival curves were generated to analyze OS time. n = 3 or more independent biological replicates. *$P < 0.05$; ***$P < 0.001$. ns = not significant.

Figure 8. *Nsun2* depletion does not affect normal hematopoiesis. Six-week-old *Nsun2*$^{fl/fl}$

Cre^{ERT2} mice were treated with TAM to deplete *Nsun2* expression (Δ/Δ) or corn oil as a vehicle control (fl/fl). Mice were sacrificed one month after the last TAM injection. (A) Representative plots showing the gating strategy for different cell populations: LK ($Lin^-cKit^+Sca\text{-}1^-$), LSK ($Lin^-cKit^+Sca\text{-}1^+$), GMP ($Lin^-cKit^+Sca\text{-}1^-CD34^+CD16/32^+$), MEP ($Lin^-cKit^+Sca\text{-}1^-CD34^-CD16/32^+$), CMP ($Lin^-cKit^+Sca\text{-}1^-CD34^+CD16/32^-$), MPP ($Lin^-cKit^+Sca\text{-}1^+CD34^+CD135^+$), LT-HSC ($Lin^-cKit^+Sca\text{-}1^+CD34^-CD135^-$), ST-HSC ($Lin^-cKit^+Sca\text{-}1^+CD34^+CD135^-$), and L-MPP ($Lin^-cKit^+Sca\text{-}1^+CD135^+$) from fl/fl (n = 4) and Δ/Δ mice (n = 4). (B) BM $Lin^-c\text{-}Kit^+$ $Sca\text{-}1^+$ cells were isolated from fl/fl and Δ/Δ mice and were plated in methylcellulose medium for colony formation (1000 cells/dish). Representative images, statistical analysis of colony number, and classification of burst-forming unit-erythroid (BFU-E), colony-forming unit-granulocyte, erythroid, macrophage, and megakaryocyte (CFU-GEMM), colony-forming unit-granulocyte (CFU-G), colony-forming unit-macrophage (CFU-M), and colony-forming unit-granulocyte and macrophage (CFU-GM). ns = not significant. (C and D) The schematic diagram showing how NSUN2-FOSB regulatory loop facilitates leukemogenesis. NSUN2 increases FOSB expression by enhancing *FOSB* mRNA stability through accumulating m^5C modifications at *FOSB* 3'-UTR. In turn, FOSB promotes NSUN2 expression by binding to the *NSUN2* promoter, forming NSUN2-FOSB regulatory loop (C). FOSB increases the expression BCL2L1 through binding to *BCL2L1* promoter. NSUN2-FOSB regulatory loop enhances the survival and inhibits apoptosis by upregulating BCL2L1 (D).

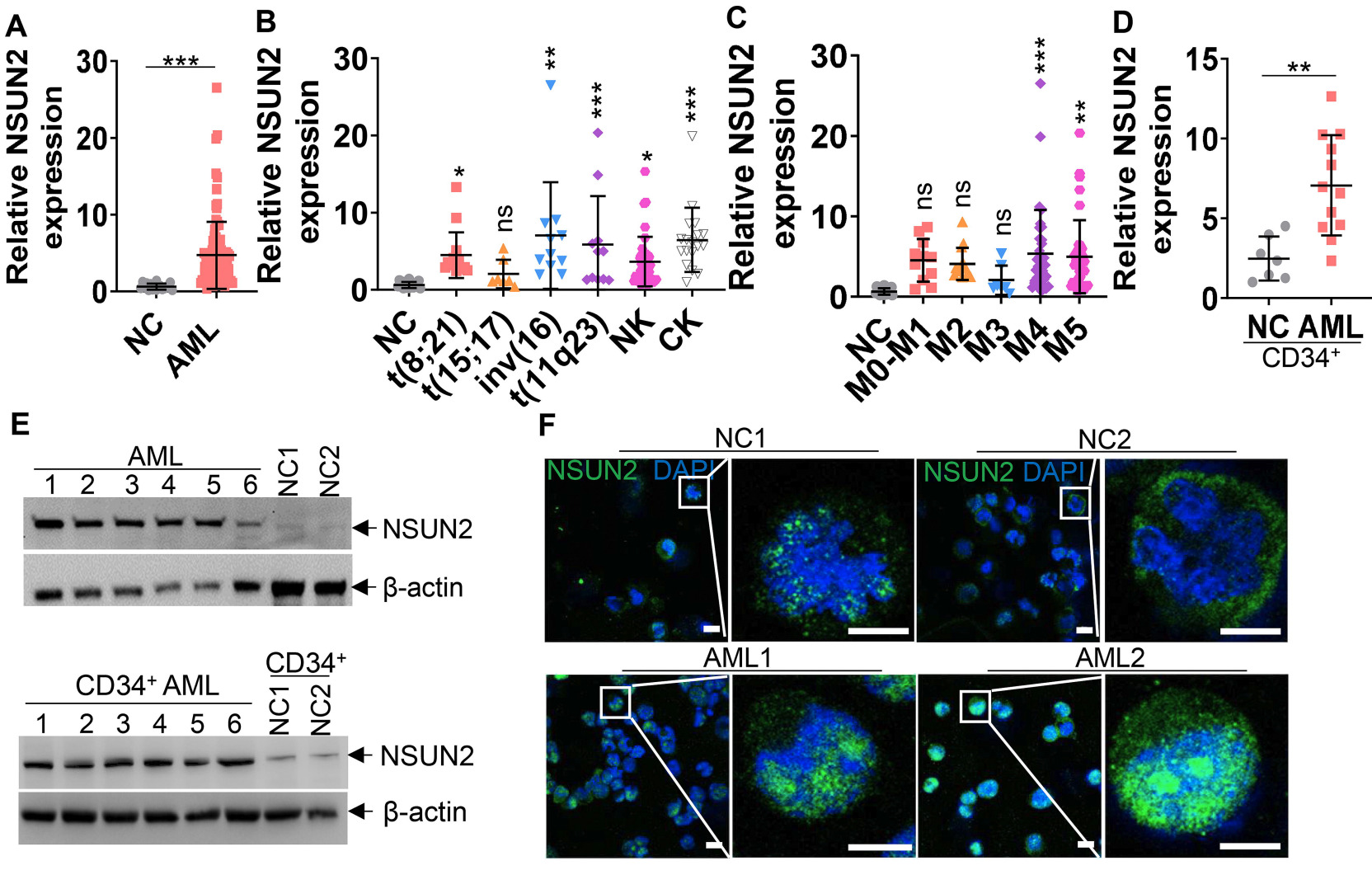
A
Relative NSUN2 expression
30
20
10
0
***
NC
AML
B
Relative NSUN2 expression
30
20
10
0
*
ns
**
***
*
***
NC
t(8;21)
t(15;17)
inv(16)
t(11q23)
NK
CK
C
Relative NSUN2 expression
30
20
10
0
ns
ns
ns
***
**
NC
M0-M1
M2
M3
M4
M5
D
Relative NSUN2 expression
15
10
5
0
**
NC AML
CD34+
E
AML
1 2 3 4 5 6
NC1
NC2
NSUN2
β-actin
CD34+ AML
1 2 3 4 5 6
CD34+
NC1
NC2
NSUN2
β-actin
F
NC1
NC2
NSUN2 DAPI
NSUN2 DAPI
AML1
AML2

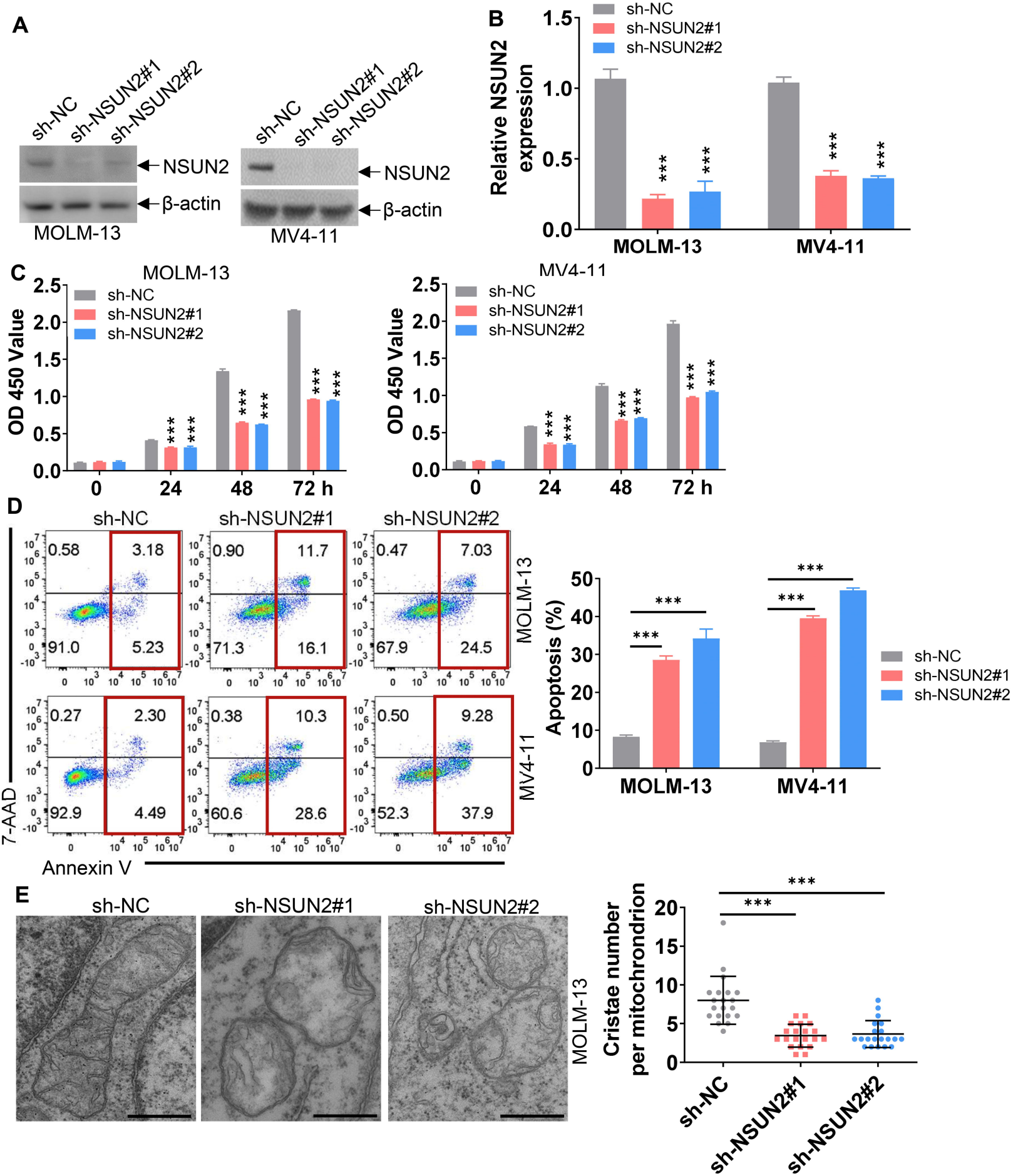
A
sh-NC
sh-NSUN2#1
sh-NSUN2#2
NSUN2
β-actin
MOLM-13
MV4-11
B
Relative NSUN2 expression
sh-NC
sh-NSUN2#1
sh-NSUN2#2
MOLM-13
MV4-11
C
MOLM-13
MV4-11
OD 450 Value
0
24
48
72 h
D
sh-NC
sh-NSUN2#1
sh-NSUN2#2
0.58
3.18
91.0
5.23
0.90
11.7
71.3
16.1
0.47
7.03
67.9
24.5
0.27
2.30
92.9
4.49
0.38
10.3
60.6
28.6
0.50
9.28
52.3
37.9
MOLM-13
MV4-11
7-AAD
Annexin V
Apoptosis (%)
E
sh-NC
sh-NSUN2#1
sh-NSUN2#2
MOLM-13
Cristae number per mitochrondrion

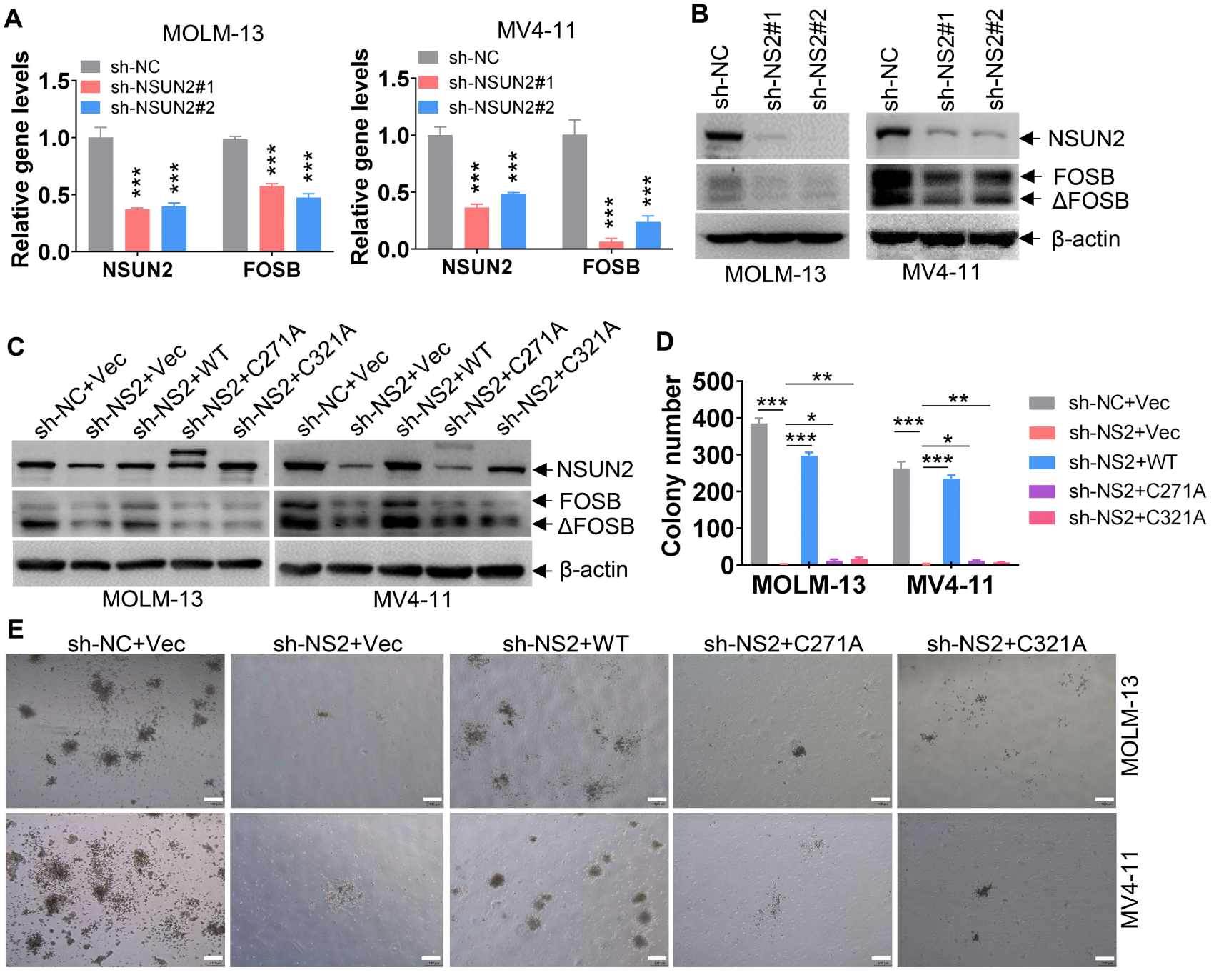
A
MOLM-13
MV4-11
sh-NC
sh-NSUN2#1
sh-NSUN2#2
Relative gene levels
1.5
1.0
0.5
0.0
***
NSUN2
FOSB
B
sh-NC
sh-NS2#1
sh-NS2#2
NSUN2
FOSB
ΔFOSB
β-actin
MOLM-13
MV4-11
C
sh-NC+Vec
sh-NS2+Vec
sh-NS2+WT
sh-NS2+C271A
sh-NS2+C321A
NSUN2
FOSB
ΔFOSB
β-actin
MOLM-13
MV4-11
D
Colony number
500
400
300
200
100
0
**
*
***
MOLM-13
MV4-11
sh-NC+Vec
sh-NS2+Vec
sh-NS2+WT
sh-NS2+C271A
sh-NS2+C321A
E
sh-NC+Vec
sh-NS2+Vec
sh-NS2+WT
sh-NS2+C271A
sh-NS2+C321A
MOLM-13
MV4-11

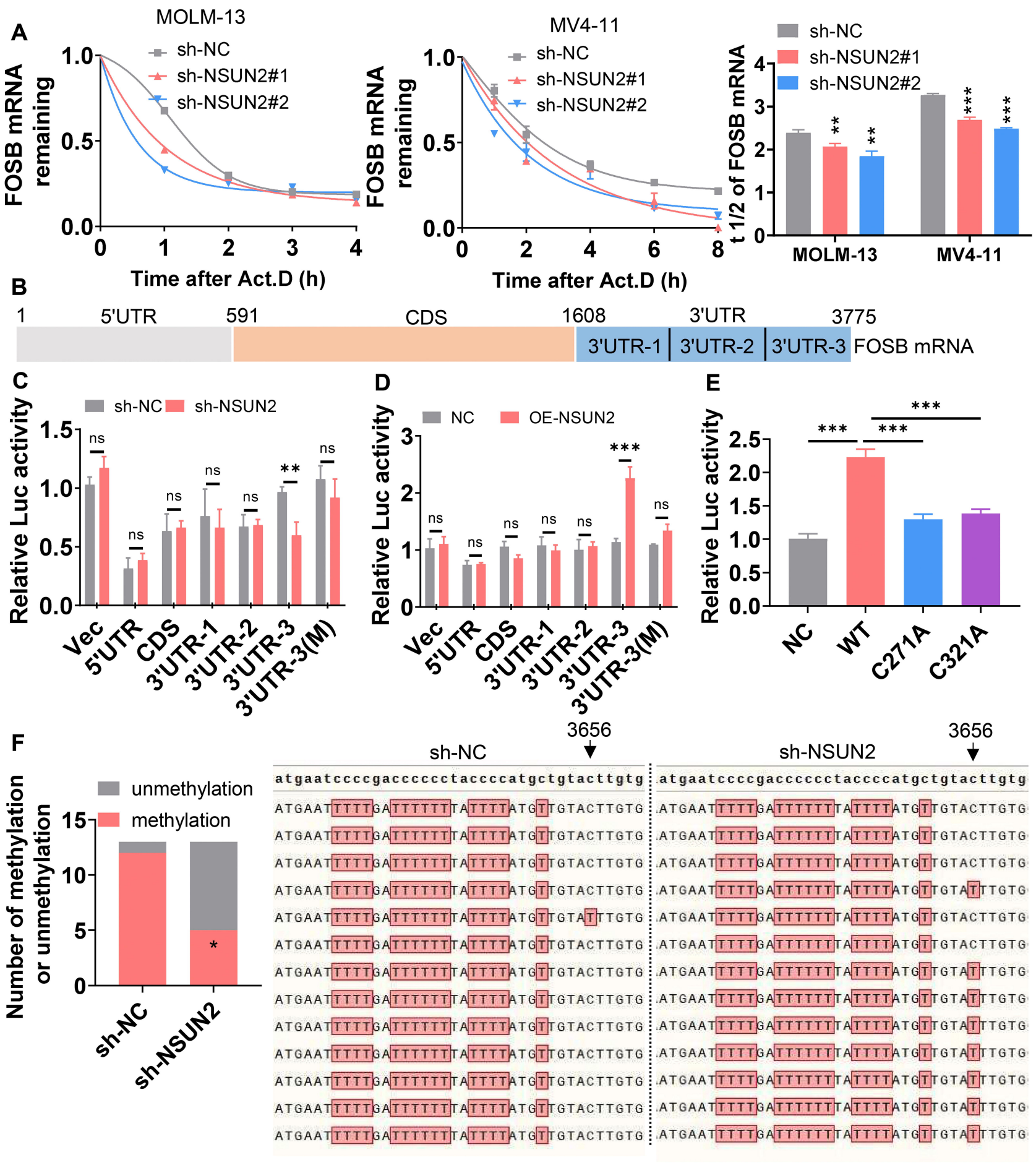
A
MOLM-13
sh-NC
sh-NSUN2#1
sh-NSUN2#2
FOSB mRNA remaining
Time after Act.D (h)
MV4-11
t 1/2 of FOSB mRNA
B
1
5'UTR
591
CDS
1608
3'UTR
3775
3'UTR-1
3'UTR-2
3'UTR-3
FOSB mRNA
C
Relative Luc activity
Vec
5'UTR
CDS
3'UTR-1
3'UTR-2
3'UTR-3
3'UTR-3(M)
D
NC
OE-NSUN2
E
NC
WT
C271A
C321A
F
unmethylation
methylation
Number of methylation or unmethylation
3656
atgaatccccgacccccctaccccatgctgtacttgtg

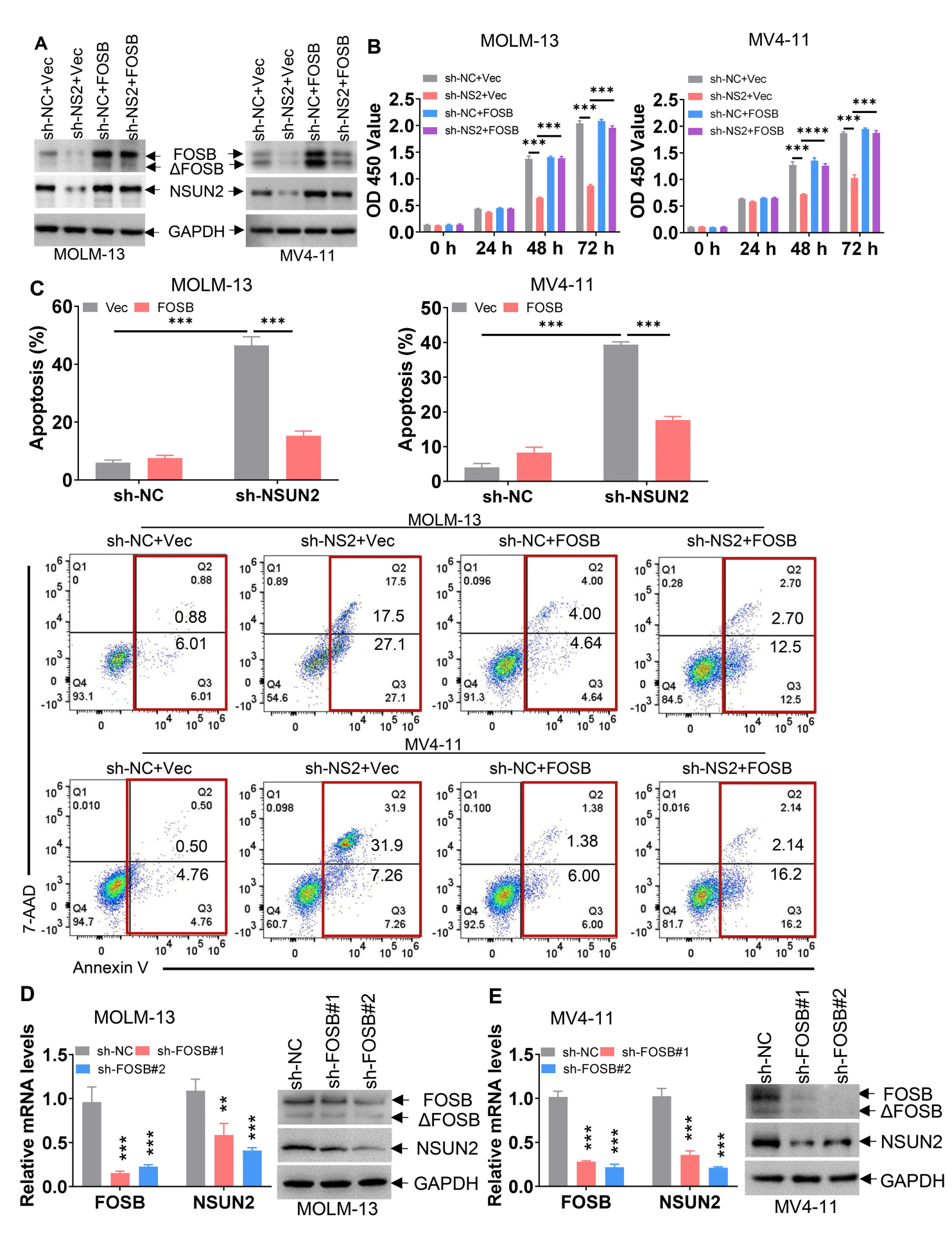
A
sh-NC+Vec
sh-NS2+Vec
sh-NC+FOSB
sh-NS2+FOSB
FOSB
ΔFOSB
NSUN2
GAPDH
MOLM-13
MV4-11
B
MOLM-13
MV4-11
sh-NC+Vec
sh-NS2+Vec
sh-NC+FOSB
sh-NS2+FOSB
OD 450 Value
0 h
24 h
48 h
72 h
C
MOLM-13
MV4-11
Vec
FOSB
Apoptosis (%)
sh-NC
sh-NSUN2
MOLM-13
sh-NC+Vec
sh-NS2+Vec
sh-NC+FOSB
sh-NS2+FOSB
MV4-11
7-AAD
Annexin V
D
MOLM-13
sh-NC
sh-FOSB#1
sh-FOSB#2
Relative mRNA levels
FOSB
NSUN2
GAPDH
E
MV4-11

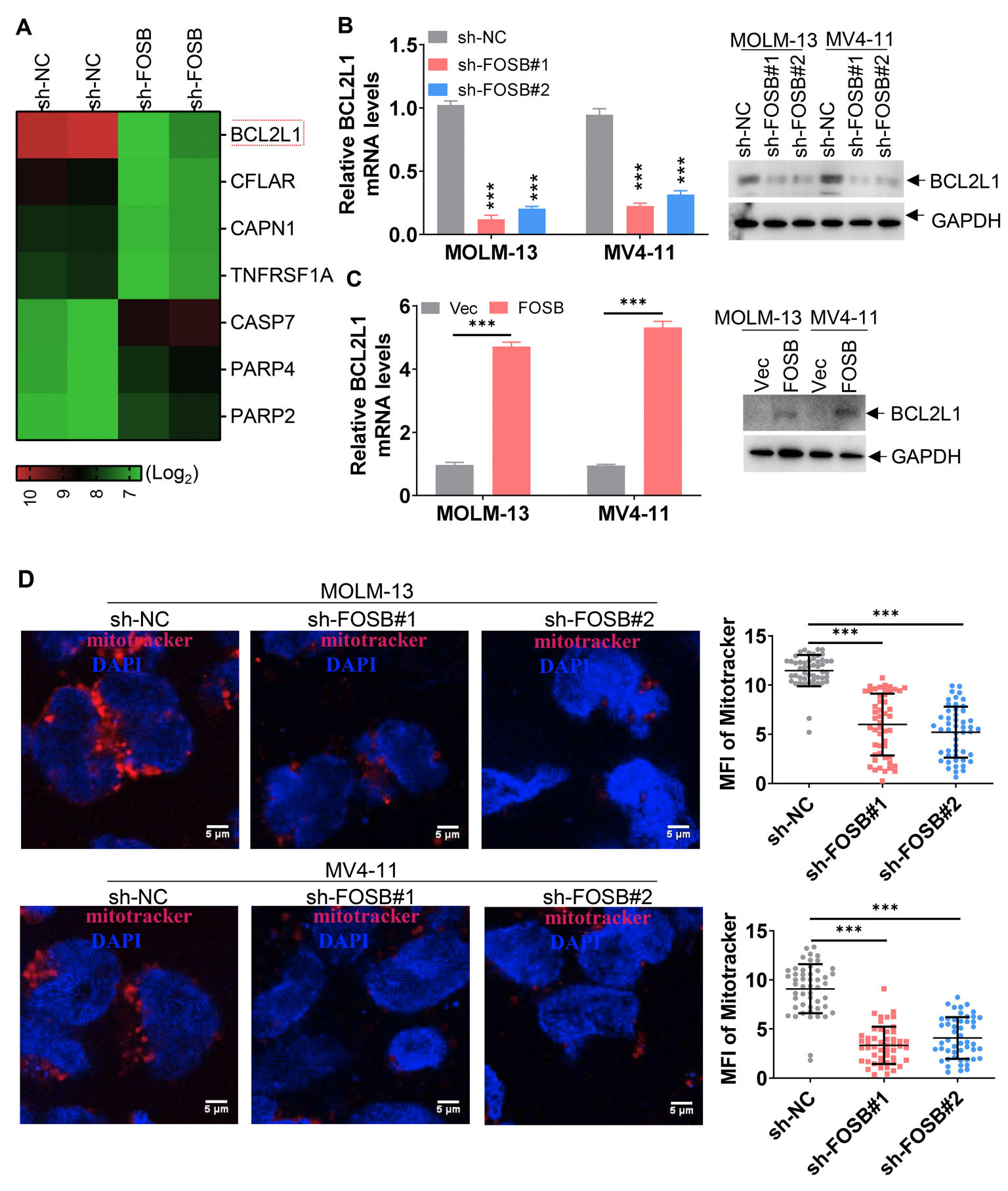
A
sh-NC
sh-NC
sh-FOSB
sh-FOSB
BCL2L1
CFLAR
CAPN1
TNFRSF1A
CASP7
PARP4
PARP2
(Log2)
10
9
8
7
B
sh-NC
sh-FOSB#1
sh-FOSB#2
Relative BCL2L1 mRNA levels
1.5
1.0
0.5
0.0
***
***
***
***
MOLM-13
MV4-11
MOLM-13
MV4-11
sh-NC
sh-FOSB#1
sh-FOSB#2
sh-NC
sh-FOSB#1
sh-FOSB#2
BCL2L1
GAPDH
C
Vec
FOSB
Relative BCL2L1 mRNA levels
6
4
2
0
***
***
MOLM-13
MV4-11
MOLM-13
MV4-11
Vec
FOSB
Vec
FOSB
BCL2L1
GAPDH
D
MOLM-13
sh-NC
sh-FOSB#1
sh-FOSB#2
mitotracker
DAPI
5 μm
MFI of Mitotracker
15
10
5
0
***
***
sh-NC
sh-FOSB#1
sh-FOSB#2
MV4-11
sh-NC
sh-FOSB#1
sh-FOSB#2
mitotracker
DAPI
5 μm
MFI of Mitotracker
15
10
5
0
***
***
sh-NC
sh-FOSB#1
sh-FOSB#2

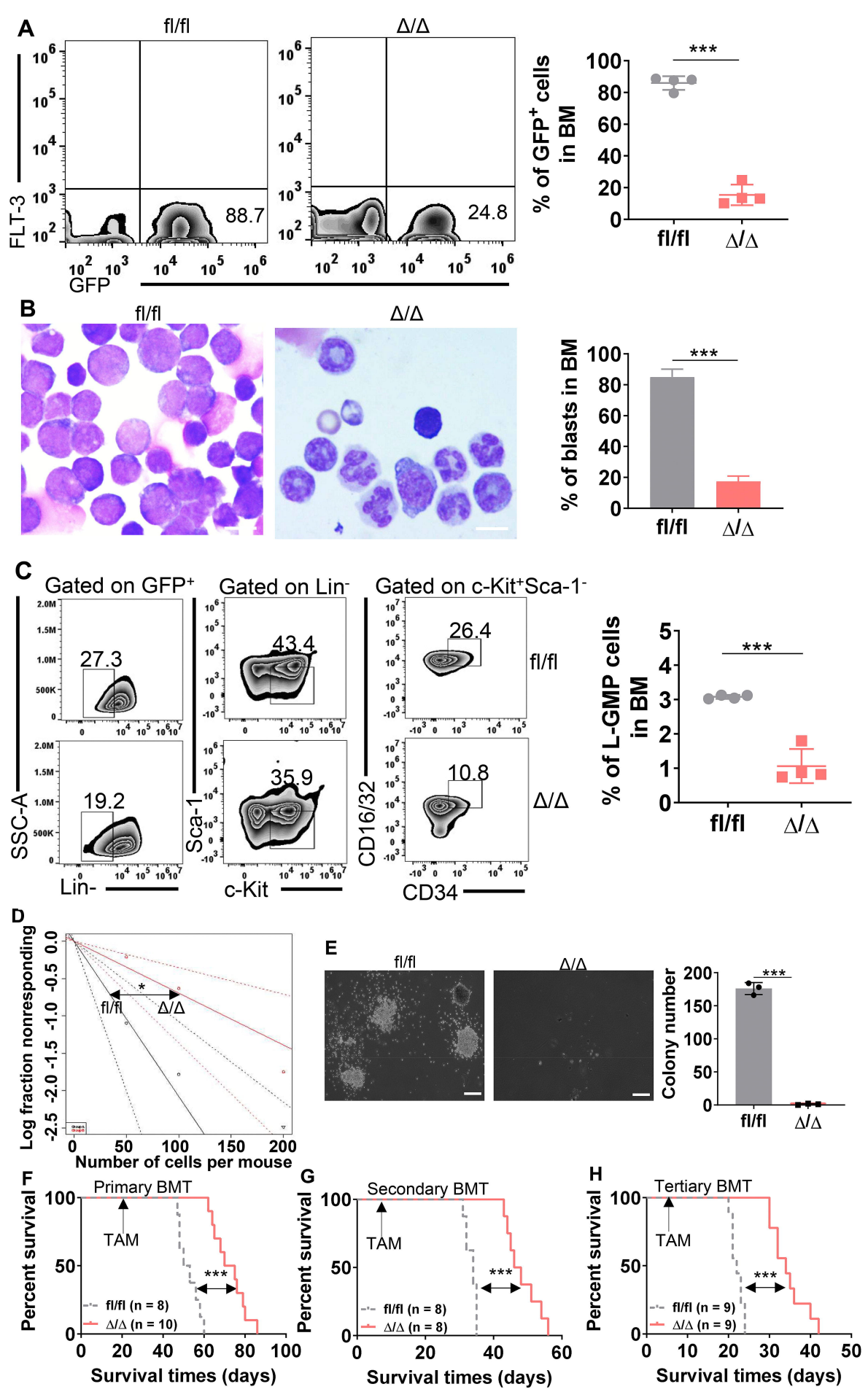
A
fl/fl
Δ/Δ
FLT-3
GFP
88.7
24.8
% of GFP+ cells in BM
***
fl/fl
Δ/Δ
B
fl/fl
Δ/Δ
% of blasts in BM
***
C
Gated on GFP+
Gated on Lin-
Gated on c-Kit+Sca-1-
27.3
19.2
43.4
35.9
26.4
10.8
SSC-A
Lin-
Sca-1
c-Kit
CD16/32
CD34
% of L-GMP cells in BM
***
D
Log fraction nonresponding
Number of cells per mouse
*
E
Colony number
***
F
Primary BMT
TAM
***
fl/fl (n = 8)
Δ/Δ (n = 10)
Percent survival
Survival times (days)
G
Secondary BMT
fl/fl (n = 8)
Δ/Δ (n = 8)
H
Tertiary BMT
fl/fl (n = 9)
Δ/Δ (n = 9)

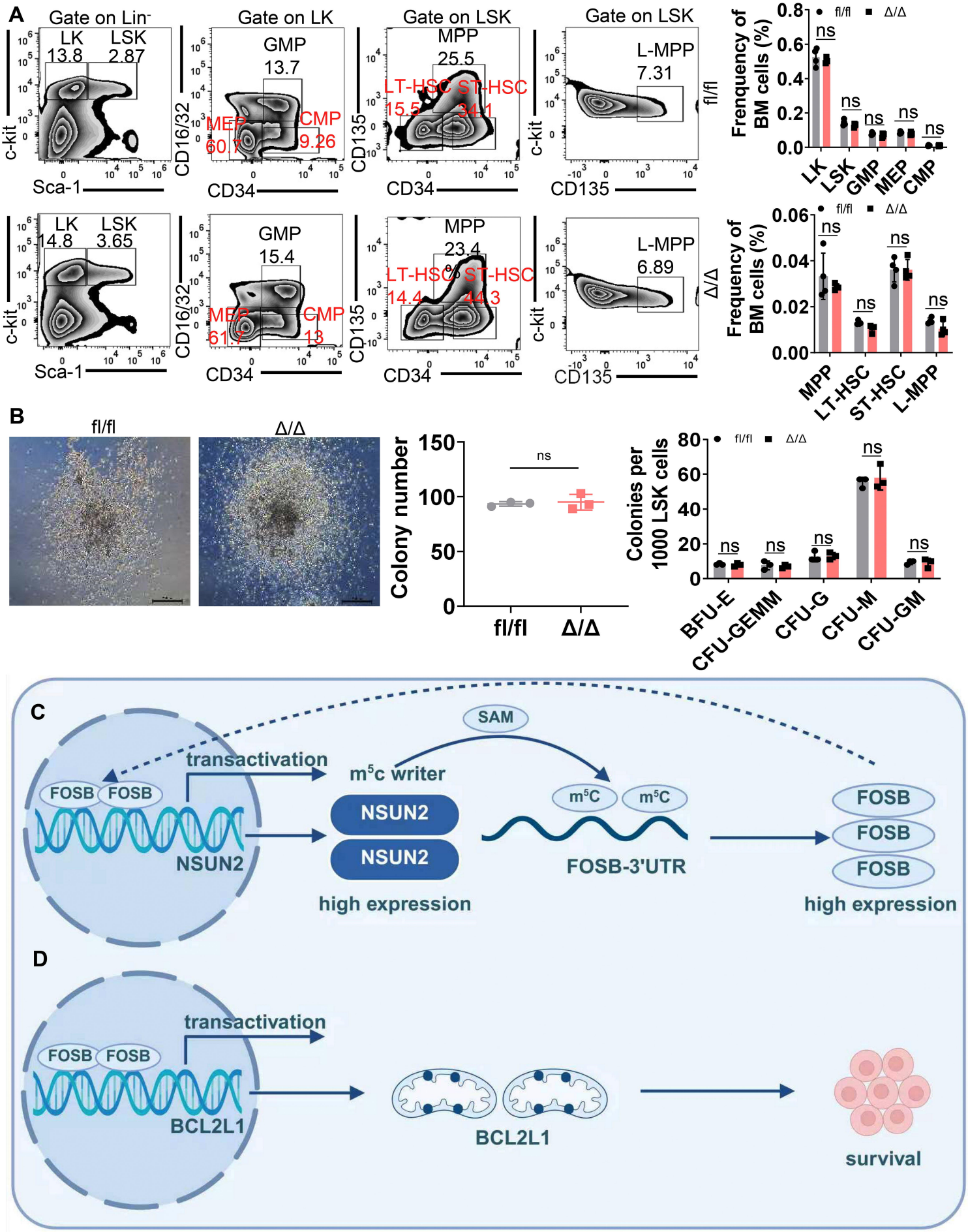
A
Gate on Lin-
LK
13.8
LSK
2.87
c-kit
Sca-1
Gate on LK
GMP
13.7
MEP
60.7
CMP
9.26
CD16/32
CD34
Gate on LSK
MPP
25.5
LT-HSC
15.5
ST-HSC
34.1
CD135
CD34
Gate on LSK
L-MPP
7.31
c-kit
CD135
fl/fl
Frenquency of BM cells (%)
ns
LK
LSK
GMP
MEP
CMP
LK
14.8
LSK
3.65
GMP
15.4
MEP
61.7
CMP
13
MPP
23.4
LT-HSC
14.4
ST-HSC
44.3
L-MPP
6.89
Δ/Δ
Frequency of BM cells (%)
MPP
LT-HSC
ST-HSC
L-MPP
B
fl/fl
Δ/Δ
Colony number
150
100
50
0
ns
fl/fl
Δ/Δ
Colonies per 1000 LSK cells
80
60
40
20
0
BFU-E
CFU-GEMM
CFU-G
CFU-M
CFU-GM
C
SAM
transactivation
m5c writer
FOSB
FOSB
NSUN2
NSUN2
NSUN2
high expression
m5C
m5C
FOSB-3'UTR
FOSB
FOSB
FOSB
high expression
D
transactivation
FOSB
FOSB
BCL2L1
BCL2L1
survival

Supplemental methods

Reagents

Cytarabine **(**Ara-c, TargetMol, Boston, MA, USA), Cladribine (Cla, TargetMol), homoharringtonine (HHT, TargetMol), decitabine (DAC, TargetMol), 5-Azacytidine (AZA, TargetMol), puromycin **(**TargetMol), MY-1B **(**TargetMol), and tucidinostat (Tuc, TargetMol) were dissolved in dimethyl sulfoxide (DMSO) and deposited at -86 °C until use.

Western blot

Western blot analysis was performed according to standard procedures. Briefly, cells were washed twice with ice-cold PBS, and total protein lysates were extracted by RIPA buffer containing protease and phosphatase inhibitors (Thermo Scientific, Waltham, MA, USA). After incubation on ice for 30 min, cell lysates were centrifuged at 12,000×g for 15 min. The supernatants were collected, and protein concentration was measured using a BCA assay (Thermo Scientific). Equal amounts of proteins were loaded, separated by 8-12% SDS-PAGE, and transferred to polyvinylidene fluoride membranes. Membranes were blocked with 5% non-fat milk at room temperature for 2 h and subsequently incubated with primary antibodies at 4℃ overnight. After washing five times with 1×TBST, membranes were incubated with horseradish peroxidase-conjugated secondary antibody. Signals were detected using chemiluminescent reagents (Thermo Scientific), and images were captured digitally using a ChemiDoc MP (Bio-Rad, Richmond, CA, USA). The following antibodies were used: NSUN2 (1:5000, ab259941, Abcam, Cambridge, MA, USA); FOSB (1:2000, ab11959, Abcam); YBX1 (1:2000, ab76149, Abcam); cleaved poly (ADP-ribose) polymerase (PARP, 1:2000, #5625S, Cell Signaling Technology, Beverly, MA, USA); BCL2L1 (1:2000, #2764**,** Cell Signaling Technology); BAX (1:2000, ab32503, Abcam), MCL1 (1:2000, #4572, Cell Signaling Technology),

BCL2 (1:5000, #15071, Cell Signaling Technology), β-actin (1:10000, ab6276, Abcam), and GAPDH (1:10000, ab8245, Abcam) were used as endogenous controls.

RNA extraction and quantitative real-time PCR (qRT-PCR)

Total RNA was extracted by TRIzol (Invitrogen) according to the manufacturer's instructions. Normal and leukemic cells were lysed in TRIzol and incubated at room temperature for 15 min. Chloroform was thoroughly mixed with the TRIzol solution. After centrifugation, the aqueous phase was carefully extracted and mixed with an equal volume of isopropanol. Total RNA was precipitated and washed with 75% ethanol. RNA concentration and quality were analyzed by measuring the absorbance at 260 nm using a spectrophotometer (DS-11, DeNovix, Wilmington, DE, USA). RNA was used as a template for cDNA synthesis using the Primescript^{TM} RT Master Mix (RRO36A, Takara Bio, Tokyo, Japan). qRT-PCR was performed using cDNA as a template by TB Green Premix Ex Taq^{TM} (RR820A, Takara Bio) on the ABI 7500 real-time PCR system (Applied Biosystems, Carlsbad, CA, USA). Human GAPDH and murine β-actin were used as endogenous controls for human and murine samples, respectively. Each sample was run in triplicate, and relative expression was calculated by the $2^{-\Delta\Delta CT}$ method. All primer sequences are listed in Table S2.

Apoptosis assay

Apoptosis was measured using Annexin V/7-AAD staining (BD PharMingen, San Diego, CA, USA). Briefly, leukemic cells plated at 2×10^5 cells/mL in six-well plates were collected, washed with 1×binding buffer, and treated in 100 μL of 1×binding buffer containing 5.0 μL of Annexin V-APC and 5.0 μL of 7-AAD for 15 min at room temperature, protected from light. Cells were then resuspended in 400 μL of 1×binding buffer, and apoptotic cells were analyzed by flow cytometry (CytoFLEX LX, Beckman-Coulter, Brea, CA, USA) within 30 min after staining. The percentage

of apoptotic cells was calculated as Annexin $V^+/7\text{-}AAD^+$ (late apoptosis) + Annexin $V^+/7\text{-}AAD^-$ (early apoptosis).

CCK-8 assay

Leukemic cells (100 μL, 1×10^5 cells/mL) were seeded in 96-well plates. After adding 10 μL of CCK-8 solution (Dojindo, Kumamoto, Japan), cells were incubated for 2–4 h. Absorbance was measured at 450 nm using an MRX II microplate reader (Dynex, Chantilly, VA, USA).

Cell death assay by 7-AAD staining

Leukemic cells (2×10^5 cells/mL) in 12-well plates were collected and washed with 1×PBS buffer, followed by treatment in 100 μL of 1×staining buffer containing 5.0 μL 7-AAD (0.1 mM, Beyotime Biotechnology, Nanjing, Jiangsu, China) for 15 min at room temperature. Cell death ($7\text{-}AAD^+$) was analyzed by flow cytometry (CytoFLEX LX, Beckman-Coulter).

Immunofluorescence (IF) assay

Cells were collected and plated onto slides, followed by fixation with 4% paraformaldehyde for 30 min. Permeabilization was achieved with absolute alcohol for 15 min. After blocking with 5% non-fat milk at room temperature for 2 h, cells were washed and incubated overnight with primary antibodies against NSUN2 (1:200, ab259941, Abcam). After washing, cells were incubated with a secondary antibody conjugated to FITC or PE. Cellular DNA was stained with 4,6-diamidino-2-phenylindole (DAPI, Beyotime Biotechnology), and fluorescence signals were detected by a laser scanning confocal microscope (Leica Stellaris 5, Leica Microsystems Inc., Deerfield, IL, USA).

mRNA half-life (t1/2) measurement

AML cells were transduced with sh-NSUN2 or sh-NC. After 48 h of transduction, AML cells were treated with 2 μM actinomycin D (ActD, TargetMol) at various time points. Total RNA was

extracted and analyzed by qRT-PCR to determine *FOSB* mRNA expression. The half-life of *FOSB* mRNA was calculated using GraphPad Prism.

Global m^{5}C RNA methylation levels assay

Global m^{5}C RNA methylation levels were measured using the MethylFlash™ m^{5}C RNA Methylation ELISA Easy Kit (EpiGentek, Farmingdale, NY, USA) following the manufacturer's instructions. Briefly, 200 ng of global RNA was extracted from leukemic cells, and DNase I was used to remove DNA. RNA samples (200 ng in 2–8 μL of RNase-free water) were mixed with 200 μL of binding solution and added to assay wells. Six different m^{5}C concentrations (0.05%, 0.1%, 0.2%, 0.5%, 1.0%, and 2.0%) were prepared by diluting the positive control containing 2% m^{5}C and added to assay wells. After an incubation for 90 min, the binding solution was removed, and each well was washed three times with 150 μL of diluted wash buffer. Then, 50 μL of m^{5}C detection complex solution was added to each well and incubated for 50 min at room temperature. Finally, 50 μL of the fluorescence development solution was added, and the incubation continued for 4 min at room temperature in the dark. Relative fluorescence units (RFU) were measured at 530ex/590em nm using the SpectraMax iD5 microplate reader (Molecular Devices, San Jose, CA, USA). To calculate the percentage of m^{5}C RNA, a standard curve was generated by plotting RFU values against the positive control at each concentration. Subsequently, linear regression was applied to determine the optimal slope (RFU/1%) and the most linear portion of the standard curve (including at least four concentration points). The percentage of m^{5}C in total RNA was calculated using the formula = (Sample (RFU)-negative control (RFU))/(slope*200).

m^{5}C blot assay

Total RNA was extracted by TRIzol, denatured in RNA incubation buffer at 95 °C for 3 min, and

immediately cooled on ice. The denatured samples were spotted onto an Amersham Hybond-N^+ membrane (GE Healthcare) and crosslinked by UV exposure (254 nm for 5 min). The membrane was washed with 1×standard saline citrate (SSC) buffer and blocked with 5% non-fat milk in 1×PBST for 1 h. The membrane was incubated overnight with an anti-m^5C antibody (1:1000, 28692S, CST) at 4 °C. After washing, the membrane was incubated with an HRP-conjugated secondary antibody for 1 h at room temperature. Finally, the membrane was washed with 1×SSC buffer for 5 min and stained with 0.02% methylene blue for internal control. Images were digitally acquired (ChemiDoc MP, USA).

Flow cytometry

Murine BM mononuclear cells were obtained by crushing femurs, tibias, and iliac bones using a pestle and mortar in staining buffer (PBS with 2% FBS), and BM cells were filtered through a 70 μm cell strainer (BD PharMingen). Peripheral blood (PB) was collected from the tail vein of the mice in EDTA-treated tubes (BD PharMingen). Before staining, red blood cells were lysed by ammonium chloride solution (BD PharMingen). BM cells from transplanted mice were harvested and stained with various antibodies diluted in staining buffer (PBS with 2% FBS) for 30 min. Murine antibodies used for the L-GMP assay included: Lineage (Lin) cocktail was prepared from biotinylated antibodies (Mac-1 and Gr-1 for myeloid cells, B220 for B cells, CD3e for T cells, Ter-119 for erythroid lineage); Streptavidin-APC-R700 (565144, BD Horizon); c-Kit-PE (553355, BD PharMingen); Sca-1-PE-Cy7 (558162, BD PharMingen); CD34-APC (560230, BD PharMingen); CD16/CD32-BV510 (101333, Biolegend); Mac-1-PE-Cy7 (552850, BD PharMingen); For HSPCs: Streptavidin-APC-R700 (565144, BD Horizon); c-Kit-PE (553355, BD PharMingen), Sca-1-PE-Cy7 (558162, BD PharMingen); CD34-APC (560230, BD PharMingen); CD135-BV421 (566292,

BD PharMingen). For blood Lin analysis: Mac-1-PE-Cy7 (552850, BD PharMingen); Gr-1-APC (553129, BD PharMingen); CD3e-BB700 (145-2C11, BD PharMingen); B220-FITC (561877, BD PharMingen). For competitive repopulation assay: CD45.2-PE (560695, BD PharMingen); CD45.1-APC-R700 (565814, BD PharMingen). Flow cytometric analysis was performed using the CytoFLEX LX (Beckman-Coulter, Brea, CA, USA), and cell sorting was conducted on the FACS Aria II (Becton Dickinson, Mountainview, CA, USA). Data were analyzed using the FlowJo software 10.0 (Becton Dickinson).

Engraftment of NOD/SCID-IL2Rγ mice (NSG)

Male 10-week-old NSG mice (Shanghai Model Organisms Center, Shanghai, China) were intraperitoneally injected with busulfan (30 mg/kg, Sigma) 24 h before transplantation. A total of 1×10^6 AML cells were transplanted via tail vein injection into the NSG mice. NSG mice assignment is random. OS time was monitored from the first day of the experiment until the death.

Cell cycle analysis

Leukemic cells (2×10^6) were incubated for 30 min at room temperature in 1×PBS buffer supplemented with propidium iodide (0.04 mg/mL, Invitrogen) and RNase (100 μg/mL, Invitrogen). Cells were analyzed by flow cytometry, and FlowJo software v10.0 (Becton, Dickinson) was used to determine the distribution of cells across the cell cycle phases.

Mitochondrial membrane potential (MMP) assay

The fluorescent carbocyanine dye (JC-1) labeling mitochondria with high membrane potential was used to assess MMP. JC-1 staining buffer was prepared by mixing the JC-1 probe and 1×buffer (Beyotime Biotechnology, Nanjing, Jiangsu, China). AML cells (about 5×10^5) were collected and incubated with JC-1 staining buffer for 20 min in a humidified atmosphere. JC-1 with red

(490ex/530em nm) representing MMP level was measured by flow cytometry.

Transmission electron microscope (TEM) assay

Leukemia cells, with or without NSUN2 knockdown, were fixed by immersion in glutaraldehyde solution, rinsed with cold 1× PBS buffer (pH 7.4), and fixed with an osmium acid solution. Increasing concentrations of acetone were used for dehydration. Finally, AML samples were embedded and polymerized for ultrathin sectioning. TEM (Hitachi H-7500, Japan) was used to examine mitochondrial morphology. The number of cristae per mitochondrion was calculated.

Competitive repopulation assay

Six-week-old *Nsun2*$^{fl/fl}$ Cre^{ERT2} mice were intraperitoneally injected daily with tamoxifen (75 mg/kg, TAM, Sigma–Aldrich, St. Louis, MO, USA) for six days to deplete *Nsun2* expression (referred to as Δ/Δ) or with corn oil as a vehicle control (referred to as fl/fl). Mice were sacrificed one month after the final TAM injection. For competitive repopulation, BM cells from fl/fl or Δ/Δ CD45.2^{+} cells (2×10^{6}) mixed with an equal number of CD45.1^{+} cells from B6.SJL mice were transplanted into lethally irradiated B6.SJL mice (CD45.1^{+}, 6–8 weeks). PB samples from recipient mice were collected monthly for four months to analyze the chimerism of CD45.2/CD45.2+CD45.1 populations.

Bisulfite sequencing

Total RNA was extracted using TRIzol reagent (Invitrogen) from MOLM-13 cells transduced with sh-NSUN2 or sh-NC. RNA was treated with the conversion solution from the RNA Bisulfite Conversion Kit (Epigentek Group Inc., San Diego, CA, USA) and incubated at 65 °C for 5 min, followed by 60 °C for 90 min. After desalting with F-Spin columns, samples were desulfonated by a desulphonation solution and a 90% ethanol mixture for 30 min at room temperature. The converted

RNA was used for cDNA synthesis, followed by PCR amplification. PCR products were inserted into the pUC18 vector and transformed into competent Escherichia coli (DH5α, Vazyme Biotech, Nanjing, Jiangsu, China). The plasmid was extracted from a single clone and sequenced. Methylated cytosines were identified by retaining cytosines as methylated. However, unmethylated cytosines that were converted to uracil and read as thymidine were considered unmethylated.

Wright-Giemsa stain

Murine PB smears and BM cytospins were stained using Wright-Giemsa stain according to standard protocols for morphological analysis.[1] BM mononuclear cells (5×10^5/mL) suspended in 100 μL of staining buffer were collected and centrifuged onto slides. Meanwhile, approximately 3 μL of PB was plated on slides. After the slides were air-dried, Wright-Giemsa staining buffer (1.0 mL) was applied for 4 min. Morphological analysis was performed by an optical microscope after the slides were washed and thoroughly dried.

Hematoxylin and eosin (H&E) stain

Spleen and liver tissues from mice were fixed in formalin and embedded in paraffin. Tissue samples were dehydrated and stained with H&E according to standard protocols.[1]

Virus production and cell infection

These procedures were performed as previously documented[2]. Briefly, HEK293T cells (4×10^6) were plated in 10 cm dishes one day prior to transfection. For retrovirus or lentivirus production, individual expression vectors with packaging plasmids (VSVG and Gappol for retroviruses, PSPA2 and MD2G for lentiviruses) were transfected into 293T cells using polyethylenimine (PEI, Sigma-Aldrich). Viruses were harvested from the supernatant and filtered through a low protein-binding polysulfone filter (0.45 μm, Millipore) 48 and 72 h after the transfection. Leukemic cells were

suspended in viral supernatant with 8 μg/mL polybrene (Sigma-Aldrich) and centrifuged at 2,000×g for 2 h. GFP^+ cells were sorted by flow cytometry for the subsequent analysis. Alternatively, puromycin (1 μg/mL) was added to the medium for 2 to 4 days to select positive clones based on transfection efficiency.

Chromatin immunoprecipitation (ChIP) assay

The enrichment of FOSB binding to the *NSUN2* or *BCL2L1* gene promoter was assessed by ChIP-quantitative real-time PCR assay (qRT-PCR) or ChIP-Seq. Briefly, AML cells were cross-linked with 1% formaldehyde for 10 min. Nuclear extracts were prepared, and chromatin was sonicated to generate DNA fragments of 200 to 1000 bp. DNA-protein complexes were immunoprecipitated using specific antibodies against FOSB or non-relevant mouse immunoglobulin IgG (Beyotime Biotechnology, China), coupled with G-Sepharose beads (Beyotime Biotechnology, China), and incubated overnight at 4 °C. Cross-linked DNA-protein complexes were immunoprecipitated by beads and were reversed by heating at 65 °C for 4 h. DNA was extracted and purified. A standard PCR reaction was performed with primer sequences specific to the *NSUN2* or BCL2L1 promoter. Fold enrichment was calculated using the $2^{-\Delta\Delta Ct}$ method: ΔCt = Ct of the ChIP DNA - Ct of the input DNA, and ΔΔCt = ΔCt of the sample (immunoprecipitated DNA of NSUN2 or BCL2L1) - ΔCt of the IgG control.

For ChIP-Seq, MOLM-13 and MV4-11 cells were overexpressed with Flag-tagged FOSB, which were cross-linked with 1% formaldehyde for 10 min. DNA-protein complexes were immunoprecipitated using specific antibodies against Flag (Anti-DYKDDDDK Affinity Beads, Smart-Lifesciences, Nanjing, Jiangsu, China), or non-relevant mouse immunoglobulin IgG (Beyotime Biotechnology, China) coupled with G-Sepharose beads (Beyotime Biotechnology,

China). DNA was extracted, purified, and subjected for sequence. The occupancy of FOSB at *NUSN2* or *BCL2L1* promoter was visualized by IGV software.

Luciferase (Luc) activity

For the Luc reporter assay, 293T cells were transfected with various concentrations of pLVX-FOSB, as well as wild-type pGL3-NSUN2-P (WT), pGL3-NSUN2-P (Mut), pGL3-BCL2L1-P (WT), pGL3-BCL2L1-P (Mut), or empty control (Vec) using polyethylenimine (PEI, Sigma-Aldrich) according to the manufacturer's instructions. The cells were also co-transfected with the pRL-TK control vector (Promega) encoding Renilla Luc for normalization of transfection efficiency. The Firefly and Renilla Luc activities were measured 48 h post-transfection using the Dual-Luciferase Reporter Assay System (Promega, Madison, WI), according to the manufacturer's guidelines. The results were expressed as the relative Luc units of the Firefly/Renilla Luc ratio.

RNA immunoprecipitation (RIP)

Anti-m^5C antibody (ab10805, Abcam), anti-m^6A antibody (ab151230, Abcam), anti-NSUN2 antibody (ab259941, Abcam), and mouse IgG (ab190475, Abcam) were incubated with protein G-Sepharose beads (ab193259, Abcam) overnight at 4 °C with rotation. AML cells were exposed to UVC (400 mJ/cm^2), and cellular extracts were incubated with conjugated m^5C, m^6A, NSUN2, or IgG antibody at 4 °C for IP for 2 h. Methylated RNAs were immunoprecipitated (IPed) by beads, and RNA was extracted and purified using the RNeasy kit (QIAGEN). Fragmented RNA (1/10) was used as an input control. qPCR was performed using IPed RNA or input RNA with primers (Table S2). The amplification cycle (Cq) value for the m^5C, m^6A, or NSUN2-IP was normalized to the Cq of the corresponding input to calculate relative enrichment.

RNA sequencing (RNA-seq) analysis

Total RNA was extracted by TRIzol reagent (Invitrogen) according to the manufacturer's protocol. RNA concentration and quality were measured using DS-11 spectrophotometer (DeNovix). The cDNA library was constructed using the KAPA Stranded RNA-Seq Library Preparation Kit (Illumina) as follows: Oligo (dT) magnetic beads were used to isolate poly (A) mRNA. The mRNA was then fragmented into small pieces by the fragmentation buffer. cDNA libraries were constructed by PCR amplification of suitable fragments. Sequencing was performed on the Illumina HiSeq 4000 platform, and image analysis, base calling, and error estimation were obtained by Illumina/Solexa Pipeline. StringTie (version 1.2.3) was used to reconstruct the transcriptome after the trimmed reads were mapped to the corresponding reference genome (hg38 from UCSC) by HISAT2 (version 2.0.4) using default parameters[3]. The software Integrative Genomics Viewer and the R packages ggplot2, pheatmap, and ggpubr were used for data visualization and analysis of differentially expressed genes (DEGs). DEGs were identified based on a Log_2fold change (FC) > 0.5 and $P < 0.05$. Gene ontology (GO) and pathway enrichment analyses were performed on DEG. Downregulated genes ($P < 0.05$, $\log_2 FC \leq -0.5$) were subjected to GO enrichment analysis.

Methylated RNA immunoprecipitation sequencing (MeRIP-seq) analysis

MeRIP-seq was performed by Cloudseq Biotech Inc. (Shanghai, China) following the reported procedure with some modifications.[4] Briefly, total RNA was collected, fragmented, and incubated with an anti-m^5C monoclonal antibody (ab10805, Abcam) for 2 h at 4 °C in an IPP buffer. The mixture was subsequently incubated with protein A beads (Thermo Fisher) at 4 °C for an additional 2 h. The bound RNA was eluted from the beads in the IPP buffer and extracted by TRIzol reagent (Thermo Fisher). Purified RNA was used for RNA-seq library generation. The input sample (without immunoprecipitation) and the m^5C IP samples were subjected to 150 bp paired-end

sequencing on an Illumina HiSeq sequencer. For m^5C-seq analysis, raw reads for both IP and input samples were trimmed by Cutadapt (version 4.8). Spliced Transcripts Alignment to a Reference (STAR, version 2.7.11b) was used to compare the reads to the human genome (hg38 from UCSC) using default parameters.[3] GO and pathway enrichment analyses were performed on the differentially methylated genes (DMG) identified by $Log_2FC > 0.5$ and $P < 0.05$. MeRIP-Seq, RNA-seq, and the subsequent bioinformatics analysis were provided by Cloud-Seq Biotech Ltd. Co. (Shanghai, China).

Mice housing

Nsun2$^{fl/fl}$ inducible knockout mice were purchased from GemPharmatech Co., Ltd (Nanjing, Jiangsu, China) by Cas9-knockout technology.[5] Cre^{ERT2} mice (strain 129S/SvEvx57BL/6) with a background of C57BL/6J were obtained from the Shanghai Model Organisms Center (Shanghai, China) and were crossed with wide-type C57/B6 for at least 10 generations.[6] *Nsun2*$^{fl/fl}$ and Cre^{ERT2} mice were crossed to produce *Nsun2*$^{fl/fl}$ Cre^{ERT2}. Mice were housed under pathogen-free conditions in standard housing conditions at the animal core of the First Affiliated Hospital of Wenzhou Medical University. All procedures involving mice follow the ARRIVE guidelines and were approved by the Animal Care and Use Committee of the First Affiliated Hospital of Wenzhou Medical University (WYYY-AEC-2021-298).

MLL-AF9 (MA9) and AML1-ETO9a (AE9a)-induced murine AML model

BM lineage-negative (Lin$^-$) cells, collected from BM of 8-week-old *Nsun2*$^{fl/fl}$ Cre^{ERT} mice five days after 5-fluorouracil (TargetMol) treatment, were cultured overnight in StemSpan SFEM (Stemcell Technologies) supplemented with murine SCF (50 ng/mL, PeproTech), TPO (50 ng/mL, PeproTech), and FLT3-L (50 ng/mL, PeproTech). Lin$^-$ cells were transduced with MSCV-GFP-IRES-MA9 or

AE9a (Addgene, Watertown, MA, USA) via two rounds of "spinoculation" as previously described.[7, 8] For primary BMT in the MA9-induced murine model, GFP^+ cells (5×10^5 for every recipient mouse) were sorted by flow cytometry 48 h after transduction. They were intravenously injected into lethally irradiated (8.0 Gy) C57BL/6J mice (Shanghai Model Organisms Center, Shanghai, China). TAM (Sigma–Aldrich) was dissolved in corn oil (Sigma–Aldrich) at 10 mg/mL. It was aliquoted and stored at -20 ℃ in the dark until use. The required aliquots of TAM were thawed by shaking at room temperature 2 h before injection. To induce *Nsun2* depletion in primary BMT, recipient mice were intraperitoneally injected with either corn oil or TAM (75 mg/kg body weight) once daily from days 15 to 20 after transplantation. For secondary or tertiary BMT, sorted fl/fl GFP^+ cells (5×10^3 for every recipient mouse) from primary or secondary BMT recipients were collected and injected via tail vein into lethally irradiated (8.0 Gy) recipient mice along with normal BM cells (5×10^5 for every recipient mouse). TAM (75 mg/kg body weight) was injected once daily from days 10 to 15 after transplantation. The mice were euthanized by CO_2 inhalation when typical leukemic symptoms, i.e., hunched posture, labored breathing, and decreased activity, had been observed. BM cells, spleen, and liver were isolated for various tests. All mice were randomly assigned. Responses were then scored by an experimenter blinded to the injection condition and experimental cohort.

For primary BMT in the AE9a-induced model, TAM (75 mg/kg body weight) was injected once daily from days 41 to 46 after transplantation to induce the depletion of *Nsun2*. For secondary BMT in the AE9a-induced model, TAM (75 mg/kg body weight) was injected once daily from days 21 to 26 after transplantation to deplete *Nsun2*.

Colony formation assay

BM GFP^+ cells were sorted from Nsun2-depleted or WT MA9-transduced AML mice. Murine LSK

(Lin$^-$Sca-1$^+$cKit$^+$) cells were sorted from the BM of Nsun2-depleted or WT mice. BM GFP$^+$ and LSK cells were plated in murine methylcellulose medium (MethoCult™ GF M3434, Stemcell Technologies) for 14 days to observe colony formation. Human AML cells with or without *NSUN2* knockdown (KD) were seeded in human methylcellulose medium (MethoCult^{TM} H4434 Classic, Stemcell Technologies). Colony (> 40 cells) was counted 14 days after plating according to the manufacturer's protocol.

Plasmid production

The wild-type coding sequence (CDS) of *NSUN2* was amplified from mononuclear cells of a healthy donor and inserted into the retroviral vector MSCV-puro (Clontech, Palo Alto, CA, USA) between Bgl II/EcoRI (Takara Bio). The wild-type CDS of *FOSB* or *BCL2L1* was amplified from mononuclear cells of a healthy donor and inserted into the vector LVX-puro (Sigma-Aldrich) between EcoRI/NotI (Takara Bio). *NSUN2* mutants (C271A and C321A) were constructed using the site-directed mutagenesis kit (Vazyme Biotech). Gene-specific short hairpin RNAs (shRNAs) for *NSUN2*, *FOSB*, and *YBX1* were designed and cloned into vector pLKO.1-Puro (Sigma-Aldrich). A nonfunctional shRNA construct was also prepared. FOSB-5'-untranslated region (UTR), CDS, and 3'-UTR-1, -2, and -3 were amplified and cloned into the vector pGL-3-basic between MluI/HindIII (Takara Bio). The FOSB-3'-UTR-3 mutant (C3656T) was generated using the site-directed mutagenesis kit (Vazyme Biotech). Potential FOSB-binding motifs at the *NSUN2* or BCL2L1 promoter were amplified and cloned into pGL-3-basic. Mutations on FOSB-binding motifs at the *NSUN2* or BCL2L1 promoter were constructed by the site-directed mutagenesis kit (Vazyme Biotech). All constructs were verified by DNA sequencing.

Supplemental References

1. Song MG, Gao SM, Du KM, et al. Nanomolar concentration of NSC606985, a camptothecin analog, induces leukemic-cell apoptosis through protein kinase Cdelta-dependent mechanisms. Blood. 2005;105(9):3714-3721.
2. Weng H, Huang H, Wu H, et al. METTL14 Inhibits Hematopoietic Stem/Progenitor Differentiation and Promotes Leukemogenesis via mRNA m(6)A Modification. Cell Stem Cell. 2018;22(2):191-205 e199.
3. Dobin A, Davis CA, Schlesinger F, et al. STAR: ultrafast universal RNA-seq aligner. Bioinformatics. 2013;29(1):15-21.
4. Meyer KD, Saletore Y, Zumbo P, Elemento O, Mason CE, Jaffrey SR. Comprehensive analysis of mRNA methylation reveals enrichment in 3' UTRs and near stop codons. Cell. 2012;149(7):1635-1646.
5. Feng J, Xu T, He M, et al. NSUN2-mediated m5C modification of HBV RNA positively regulates HBV replication. PLoS Pathog. 2023;19(12):e1011808.
6. Feil S, Valtcheva N, Feil R. Inducible Cre mice. Methods Mol Biol. 2009;530:343-363.
7. Li Z, Chen P, Su R, et al. Overexpression and knockout of miR-126 both promote leukemogenesis. Blood. 2015;126(17):2005-2015.
8. Zhou B, Jin X, Jin W, et al. WT1 facilitates the self-renewal of leukemia-initiating cells through the upregulation of BCL2L2: WT1-BCL2L2 axis as a new acute myeloid leukemia therapy target. J Transl Med. 2020;18(1):254.

Supplemental Table 1. The clinical characteristics of 102 AML patients for qRT-PCR

Characteristic	All patients N (%)	Relative expression of NSUN2
Overall	102	
Gender		
Male	57 (55.8)	0.69–26.53
Female	45 (44.2)	0.39–15.34
Age (range)	51 (17-75)	
FAB subtype		
M0-M1	11 (10.8)	0.92–8.66
M2	14 (13.8)	2.44–9.32
M3	7 (6.9)	0.39–5.38
M4	34 (33.3)	0.69–26.53
M5	36 (35.3)	0.72–20.35
Cytogenetics		
Normal karyotype	38 (37.2)	0.72–15.34
Complex karyotype	18 (17.6)	0.98–19.91
t(15;17)	7 (6.9)	0.39–5.38
t(8;21)	15 (14.7)	2.44–13.32
Inv(16)	11 (10.8)	1.99–26.53
t(11q23)	11 (10.8)	1.25–20.35
Not available	2 (1.9)	4.45–4.84
Genetic mutation		
WT1 mutation	12 (11.7)	1.29–20.35
FLT3 mutation	13 (12.7)	0.92–14.88
CEBPA mutation	18 (17.6)	0.39–19.91
MLL-PTD mutation	4 (3.9)	1.40–6.36
TET2 mutation	14 (13.7)	1.29–26.53
NPM1 mutation	6 (5.9)	0.72–9.32
c-KIT mutation	9 (8.8)	0.69–11.37

Supplemental Table 2. The sequences of primers

Genes	Sequences
NSUN2-F	5′-CAA GCT GTT CGA GCA CTA CTA C-3′
NSUN2-R	5′-CTC CCT GAG AGC GTC CAT GA-3′
FOSB-F	5′-TGC GCC GGG AAC GAA ATA A-3′
FOSB-R	5′-CTG AGC CCG GCA AAT CTC TC-3′
YBX1-F	5′-TGC AGC AGA CCG TAA CCA TT-3′
YBX1-R	5′-TGG TAA TTG CGT GGA GGA CC-3′
SEMA3A-F	5′-GTG CCA AGG CTG AAA TTA TCC T-3′
SEMA3A-R	5′-CCC ACT TGC ATT CAT CTC TTC T-3′
RYR1-F	5′-TGG CTC ACC TAT GCT GCT C-3′
RYR1-R	5′-GAC AGT GCG TCG TCC ATG T-3′
PDE11A-F	5′-CAC TGC TGG GTT TCA AGA CAT-3′
PDE11A-R	5′-GAA GGC ATT GTT GGT TCC CC-3′
FHAD1-F	5′-TAA AGA GCG CAG AAG GCT TTT-3′
FHAD1-R	5′-GAG TGC ATG GTG GTT GTC GAT-3′
ANKDD1A-F	5′-AGA GGC ACG TCT GTG TTT TGG-3′
ANKDD1A-R	5′-ATC TTG GCC CCT GAG TTT ACC-3′
DNAJC12-F	5′-AGC ATC CTG AAA ACC CCA AAG-3′
DNAJC12-R	5′-GGC TCG ACT CTC TTC ATT GGT-3′
INPP5A-F	5′-ACT CGG ATA CCT TAG AGA GCA C-3′
INPP5A-R	5′-TTC TTG ACC ATT TGC ACT CGG-3′
PHC2-F	5′-ACG CAT GTT ATC GAA GGG TTT-3′
PHC2-R	5′-ACC CCT GTG CAT ACT TCT TCT-3′
TMEM67-F	5′-CTT GGC TGT TTT ATG GAG ACC A-3′
TMEM67-R	5′-ACC TCC TTC TAA AGT TTG CCA C-3′
NT5DC3-F	5′-GGA GGA CTG GTG CAA TCA TCC-3′
NT5DC3-R	5′-GGT CAT TTC TCG CAT CTC CTT C-3′
DCAF4-F	5′-ACC TGC AAA GTC TGA AGA CCC-3′
DCAF4-R	5′-GGC ATA GCA GAA TGT GGG AAT C-3′
Pre-FOSB-F	5′-GGG TAA TGC GCT GCT CAA TG-3′
Pre-FOSB-R	5′-AAA GTT CTC AGC CCC GCT AC-3′
BCL2L1-F	5′-GAG CTG GTG GTT GAC TTT CTC-3′
BCL2L1-R	5′-TCC ATC TCC GAT TCA GTC CCT-3′
GAPDH-F	5′-CCG GGA AAC TGT GGC GTG ATG G-3′
GAPDH-R	5′-AGG TGG AGG AGT GGG TGT CGC TGT T-3′
β-actin-F (mouse)	5′-GGC TGT ATT CCC CTC CAT CG-3′
β-actin-R (mouse)	5′-CCA GTT GGT AAC AAT GCC ATG T-3′
Nsun2-F (mouse)	5′-TAC CAT GTT CCC ACC AAC GG-3′
Nsun2-R (mouse)	5′-GGA TTC GAA GGC ATC GCT CT-3′
Fosb-F (mouse)	5′-CGA GAA GAG ACA CTT ACC CCA-3′
Fosb-R (mouse)	5′-GTT TCC GCC TGA AGT CGA TCT-3′

Firefly-luciferase-F	5′-CAC TCT GGC GAC ATT GCC TA-3′
Firefly-luciferase-R	5′-GCT GCA GCA GGA TAG ACT CC-3′
Renilla-luciferase-F	5′-GAG AAG GGC GAG GTT AGA CG-3′
Renilla-luciferase-R	5′-TGG AAA AGA ACC CAG GGT CG-3′
m^5C-RIP-F (FOSB-3'-UTR)	5′-TTT TCT CCT CCG CCT GTG TC-3′
m^5C-RIP-R (FOSB-3'-UTR)	5′-TCA CAC TCT CAC ACT CGC AC-3′
*sh-NSUN2#1	5′-TGC AGT GTC CCA TCG TCT TAT-3′
*sh-NSUN2#2	5′-CAG TGG AAG GTA ATG ACG AAA -3′
*sh-NSUN2#3 (3'-UTR)	5′-GTG AGG CAA GAC CGA AGT AAA-3′
*sh-FOSB#1	5′-GCC AAC CAC AAT TCA ATG AAT-3′
*sh-FOSB#2	5′-CCT TCG TAC ACT TCT TCG TTT-3′
*sh-YBX1#1	5′-GCA GAC CGT AAC CAT TAT A-3′
*sh-YBX1#2	5′-GGT TCC CAC CTT ACT ACA T-3′
*sh-NC (Scramble)	5′-CAA ATC ACA GAA TCG TCG TAT-3′
*sh-Fosb (mouse)#1	5′-CAA CGG TCA CCG CAA TCA CAA-3′
*sh-Fosb (mouse)#2	5′-CTC TTT ACA CAC AGT GAA GTT-3′
*MSCV-NSUN2-F	5′-CCG CTC GAG ATG GGG CGG CGG TCG CGG GG-3′
*MSCV-NSUN2-R	5′-GGA ATT CTC ACC GGG GTG GAT GGA CCC-3′
*LVX-FOSB-F	5′-GGA TCT ATT TCC GGT GAA TTC ATG TTT CAG GCT TTC CCC GG-3′
*LVX-FOSB-R	5′-AGA GGG GCG GGA TCC GCG GCC GCT CAC AGA GCG AGG AGG GAG G-3′
*LVX-BCL2L1-F	5′-CAT TCT AGA ACT AGT CTC GAG ATG TCT CAG AGC AAC CGG GA-3′
*LVX-BCL2L1-R	5′-GGA TCT ATT TCC GGT GAA TTC TCA TTT CCG ACT GAA GAG TGA GC-3′
*NSUN2-P(WT)-F	5′-AGG TAC CGA GCT CTT ACG CGT GTT TCA GCA TGT TGG TCA GGA CG-3′
*NSUN2-P(WT)-R	5′-CAG TAC CGG AAT GCC AAG CTT CAA ATC GCA AAT CGC ATG AA-3′
*NSUN2-P(WT1)-F	5′-AGG TAC CGA GCT CTT ACG CGT TGG CCA CCA 5′-GTC CTA ACA AAG-3′
*NSUN2-P(WT1)-R	5′-CAG TAC CGG AAT GCC AAG CTT TGG GGG GCT TTG CAG ACT-3′
*NSUN2-P(WT2)-F	5′-AGG TAC CGA GCT CTT ACG CGT GAA TAC TCT GAC CTG AGA TTG CTT TT-3′
*NSUN2-P(WT2)-R	5′-CAG TAC CGG AAT GCC AAG CTT GCA GTC TGT GTC CTC AGT GTG C-3′
*NSUN2-P(WT3)-F	5′-AGG TAC CGA GCT CTT ACG CGT ACG GTA GGA TAT GCT TAG GAG AGA A-3′
*NSUN2-P(WT3)-R	5′-CAG TAC CGG AAT GCC AAG CTT TTT AAG CAA TGG AGA ATC TCT TTT GC-3′

*BCL2L1-P(WT)-F	5′-CTA GCT AGC CTC AGA GCA ACC GGG AGC TG-3′
*BCL2L1-P(WT)-R	5′-GAA GAT CTT CGA CAG ATG GAG AGG TCT GT-3′
*BCL2L1-P(WT1)-F	5′-CTA GCT AGC GGC CAC AGC AGC AGT TTG GA-3′
*BCL2L1-P(WT1)-R	5′-GAA GAT CTC TCA CCA ATA CCT GCA TCT-3′
*BCL2L1-P(WT2)-F	5′-CTA GCT AGC ATA CAA ATG ACC CTG TGC TT-3′
*BCL2L1-P(WT2)-R	5′-GAA GAT CTT ATA AGG TAA GGG AAA CAC C-3′
*FOSB-5'UTR-F	5′-AGG TAC CGA GCT CTT ACG CGT ATT CAT AAG ACT CAG AGC TAC GGC C-3′
*FOSB-5'UTR-R	5′-CAG TAC CGG AAT GCC AAG CTT TTC CCT GGG CAC AGG GGG C-3′
*FOSB-CDS-F	5′-AGG TAC CGA GCT CTT ACG CGT ATG TTT CAG GCT TTC CCC GG-3′
*FOSB-CDS-R	5′-CAG TAC CGG AAT GCC AAG CTT TCA CAG AGC GAG GAG GGA GG-3′
*FOSB-3'UTR-1-F	5′-AGG TAC CGA GCT CTT ACG CGT CTC TGT GAA CTC TTT AGA CAC ACA AAA C-3′
*FOSB-3'UTR-1-R	5′-CAG TAC CGG AAT GCC AAG CTT GGG ATC AAT AAG CTA AGG TCG G-3′
*FOSB-3'UTR-2-F	5′-AGG TAC CGA GCT CTT ACG CGT CCC ACA TTT CCA TGG TGT GAG-3′
*FOSB-3'UTR-2-R	5′-CAG TAC CGG AAT GCC AAG CTT GCC CCT TGA GTC TGC CAG TC-3′
*FOSB-3'UTR-3-F	5′-AGG TAC CGA GCT CTT ACG CGT GGG CTG GAA TCT CAT GAT TCC-3′
*FOSB-3'UTR-3-R	5′-CAG TAC CGG AAT GCC AAG CTT TGC GTT TTT AAG AGC TTT TTA TTG G-3′
ChIP-1F for NSUN2	5′-GGC ATC TGA CTG TGC ACT CT-3′
ChIP-1R for NSUN2	5′-AGG CTG CTT TGC TCA TGG AT-3′
ChIP-2F for NSUN2	5′-GCA CCG AAT ACT CTG ACC TGA-3′
ChIP-2R for NSUN2	5′-AGT GAG TAC TGT GTG CCT GA-3′
ChIP-3F for NSUN2	5′-GCA GTG TTG CTC TTA GGG CT-3′
ChIP-3R for NSUN2	5′-ACC AAC TTT TGC ATG GAG AGT-3′
ChIP-4F for NSUN2	5′-GGC TCA AAC AGT GTG GAT TGC-3′
ChIP-4R for NSUN2	5′-TCT CTT TTG CGT GGC TAT TGA-3′
ChIP-1F for BCL2L1	5′-TCC CCA TGG CAG CAG TAA AG-3′
ChIP-1R for BCL2L1	5′-AAA AAG GCC ACA ATG CGA CC-3′
ChIP-2F for BCL2L1	5′-GGC ATC TTT CAC CCT GGT CA-3′
ChIP-2R for BCL2L1	5′-CCT ACC CTC ACA GGT TTG GG-3′
NSUN2-RIP-F1 (FOSB-3'-UTR)	5′-GTG CGA GTG TGA GAG TGT GA-3′
NSUN2-RIP-R1 (FOSB-3'-UTR)	5′-CCA CAA GTA CAG CAT GGG GT-3′

NSUN2-RIP-F2 (FOSB-3'-UTR)	5′-TTT TCT CCT CCG CCT GTG TC-3′
NSUN2-RIP-R2 (FOSB-3'-UTR)	5′-TCA CAC TCT CAC ACT CGC AC-3′

*Primers for construction of plasmids.

RIP: RNA immunoprecipitation.

ChIP: Chromatin immunoprecipitation.

Supplemental Table 3. Limiting dilution assay of MLL-AF9-transduced *Nsun2*$^{fl/fl}$ and *Nsun2*$^{\Delta/\Delta}$ AML mice

Dose	fl/fl (response/total)	Δ/Δ (response/total)	*P* value
50	4/6	1/6	
100	5/6	3/6	
200	6/6	5/6	
LSC frequency	1 in 49	1 in 144	0.021

The numbers of response mice mean that the recipient mice develop full-blown leukemia and die within six months after transplantation.

Supplemental Figures and legend

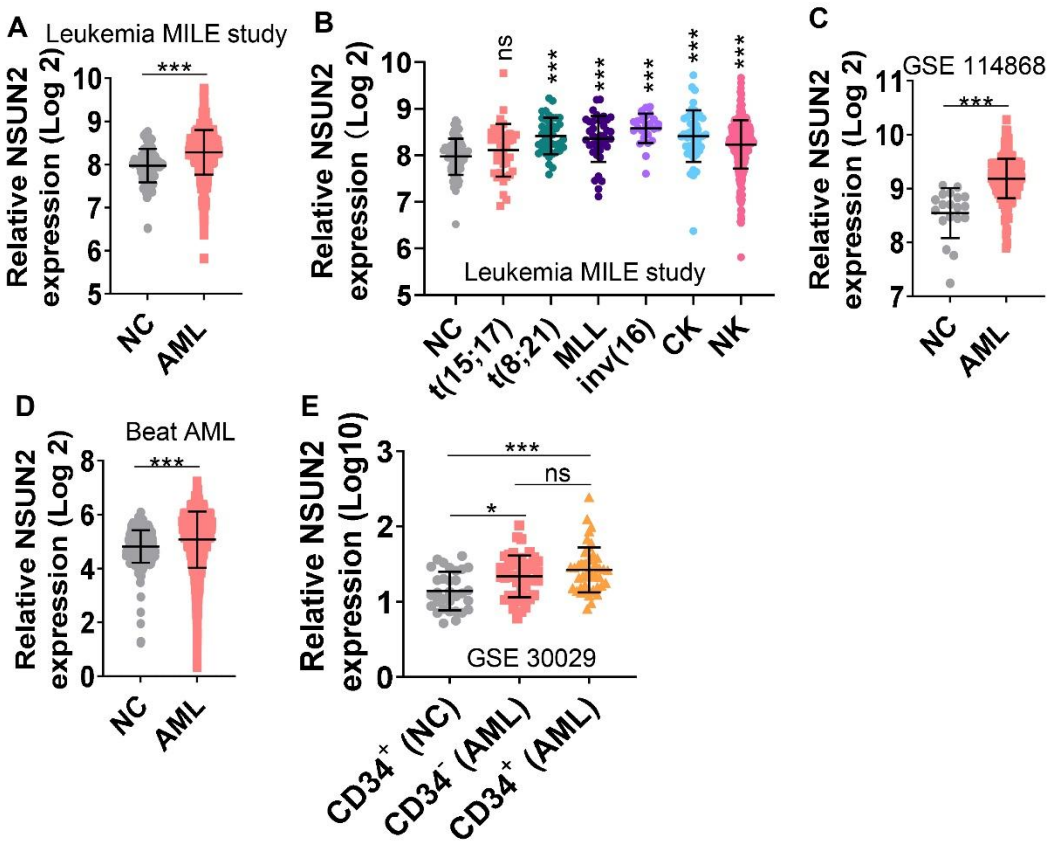

Supplemental Figure 1: NSUN2 expressions are higher in primary AML samples compared with normal controls (NC). (A and B) *NSUN2* expressions were analyzed using the BloodSpot database. (C and D) *NSUN2* expressions were assessed in NC and primary AML samples using the GSE 114868 (C) and Beat AML database (D). (E) *NSUN2* expressions were determined in $CD34^+$ HSPCs, $CD34^-$ AML, and $CD34^+$ AML cells according to GSE 30029 database. $^*P < 0.05$; $^{**}P < 0.01$; $^{***}P < 0.001$ compared with NC; ns = not significant.

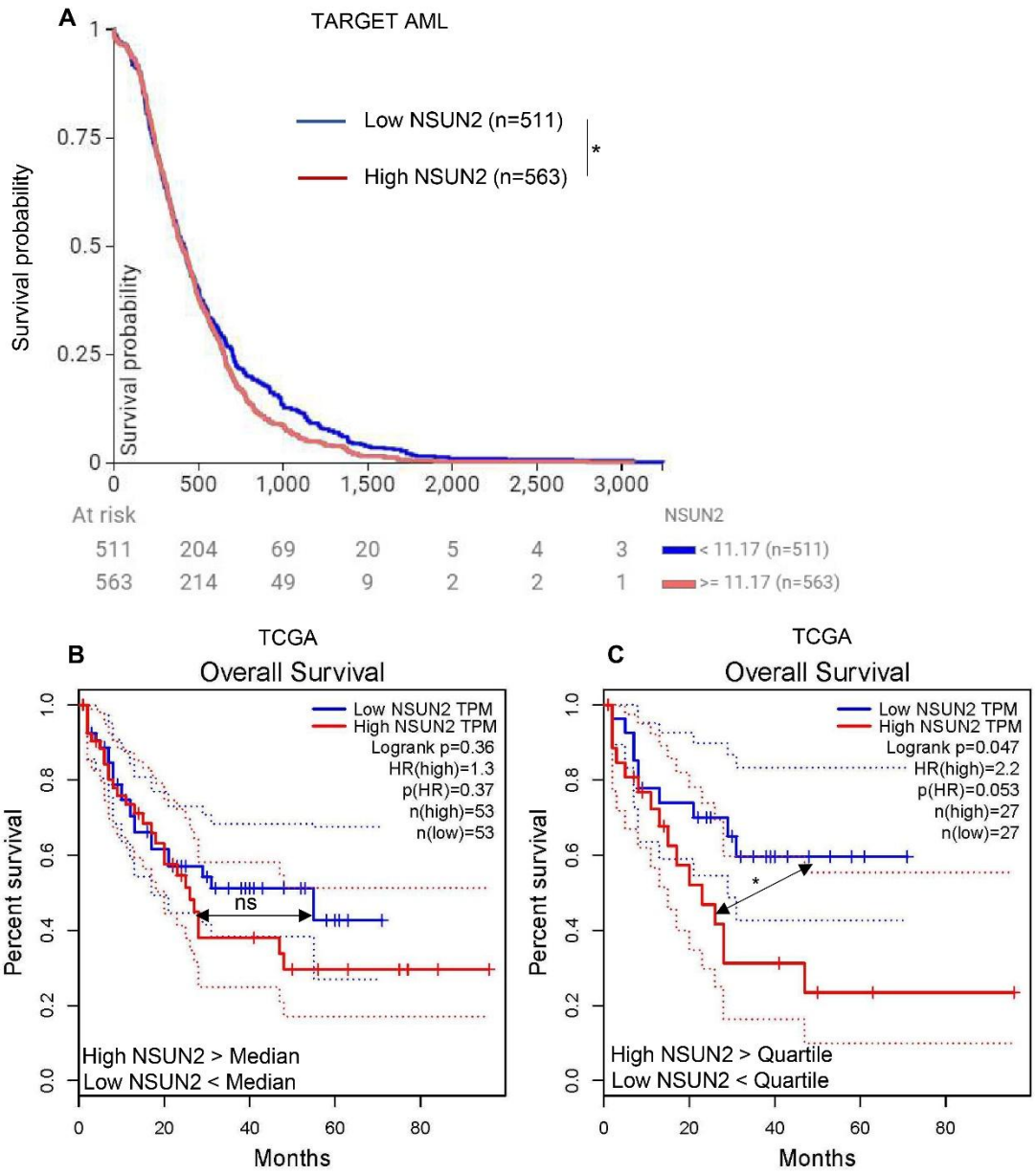

Supplemental Figure 2. Analyzing the outcome in AML patients according to different NSUN2 expressions. (A) Overall survival (OS) was evaluated in AML patients with higher (above the median) versus lower (below the median) expression of *NSUN2* in the Therapeutically Applicable Research to Generate Effective Treatments (TARGET) AML database (https://target.nci.nih.gov/dataMatrix/ TARGET_DataMatrix.html). (B) OS was evaluated in AML patients with higher (above the median) versus lower (below the median) expression of *NSUN2* in the TCGA database. (C) OS was assessed in AML patients with higher (above the quartile) versus

lower (below the quartile) expression of *NSUN2* in the TCGA database. *$P < 0.05$; ns = not significant.

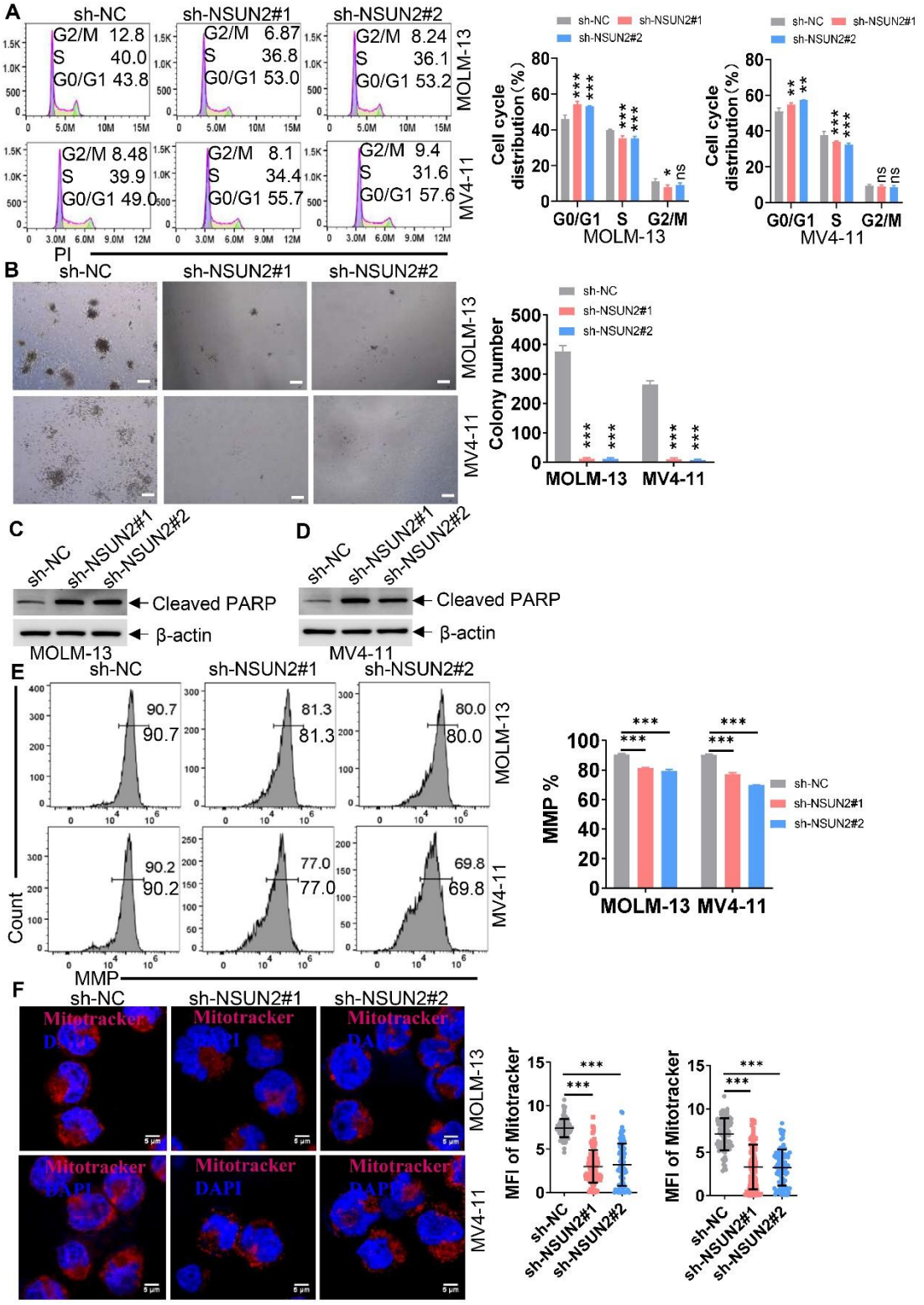

Supplemental Figure 3. NSUN2 knockdown (KD) inhibits survival and affects mitochondrial function in AML cells. (A) AML cells were transduced with sh-NSUN2 or sh-NC for 48 h. Cells were stained with PI solution, and cell cycle distribution was assessed using flow cytometry.

Representative plots (left) and statistical analysis of G0/G1, S, and G2/M phases (right) are shown. (B) AML cells transduced with sh-NSUN2 (2×10^3/dish) or sh-NC (2×10^3/dish) were plated in methylcellulose medium with puromycin (1 μg/mL) for 14 days to count colony formation. Representative plots (left) and statistical analysis of colonies (right) are shown. Bar scales represent 100 μm. (C and D) Cleaved PARP protein levels were measured in AML cells transduced with sh-NSUN2 or sh-NC for 48 h, followed by puromycin (1 μg/mL) treatment for an additional 48 h. n = 3 technical replicates. (E) Mitochondrial membrane potential (MMP) assay was measured by JC-1 probe staining in leukemic cells transduced with sh-NSUN2 or sh-NC. Statistical analysis of MMP (left) and the representative plots (right) are shown. (F) The mitochondria were stained by MitoTracker Red CMXRos in red. Relative mitochondrial mass was calculated by MFI of MitoTracker staining. The representative images (left) and statistical analysis of MFI of MitoTracker staining (right, n = 50 per group) are shown. *$P < 0.05$; **$P < 0.01$; ***$P < 0.001$ versus sh-NC. ns = not significant.

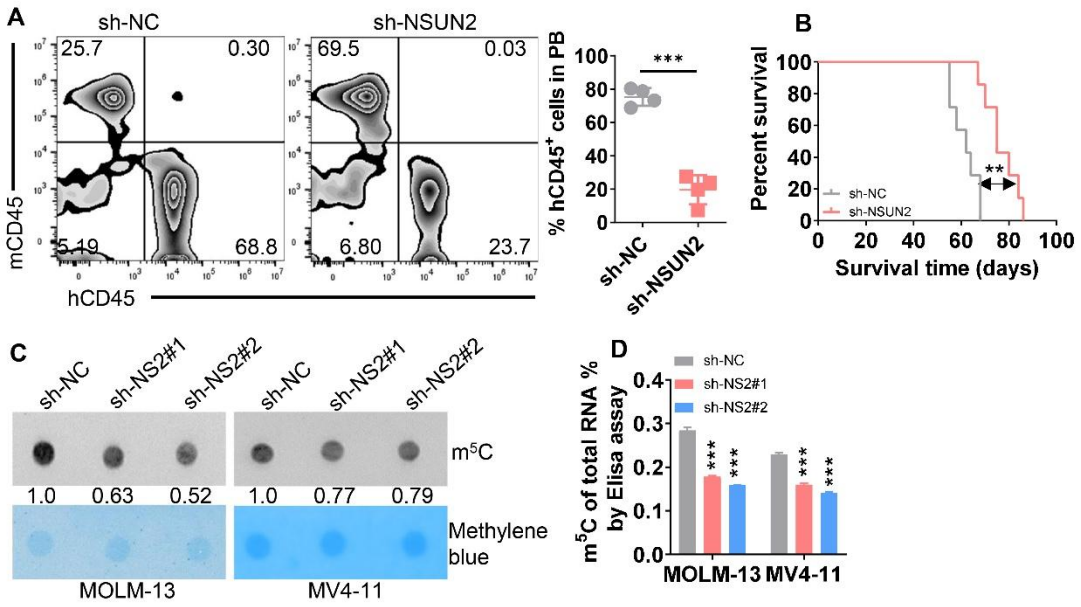

Supplemental Figure 4. NSUN2 KD inhibits survival in NSG mice and decreases m^{5}C levels.

(A) The frequency of human CD45/murine CD45 (hCD45/mCD45) was measured in PB from MOLM-13-sh-NC (n = 4) and MOLM-13-sh-NSUN2#1 (n = 4)-xenografted NSG mice. Representative plots (left) of hCD45 and mCD45 staining and statistical analysis of hCD45/hCD45+mCD45 cells (right) are shown. (B) OS was determined in MOLM-13-sh-NC (n = 7) and MOLM-13-sh-NSUN2#1 (n = 7)-transplanted NSG mice. (C and D) m^{5}C levels in total RNA were measured by m^{5}C blot (C) and ELISA assay (D) in AML cells transduced with sh-NC or sh-NS2 for 48 h, followed by puromycin (1 μg/mL) treatment for an additional 48 h. $^{**}P < 0.01$; $^{***}P < 0.001$ versus sh-NC.

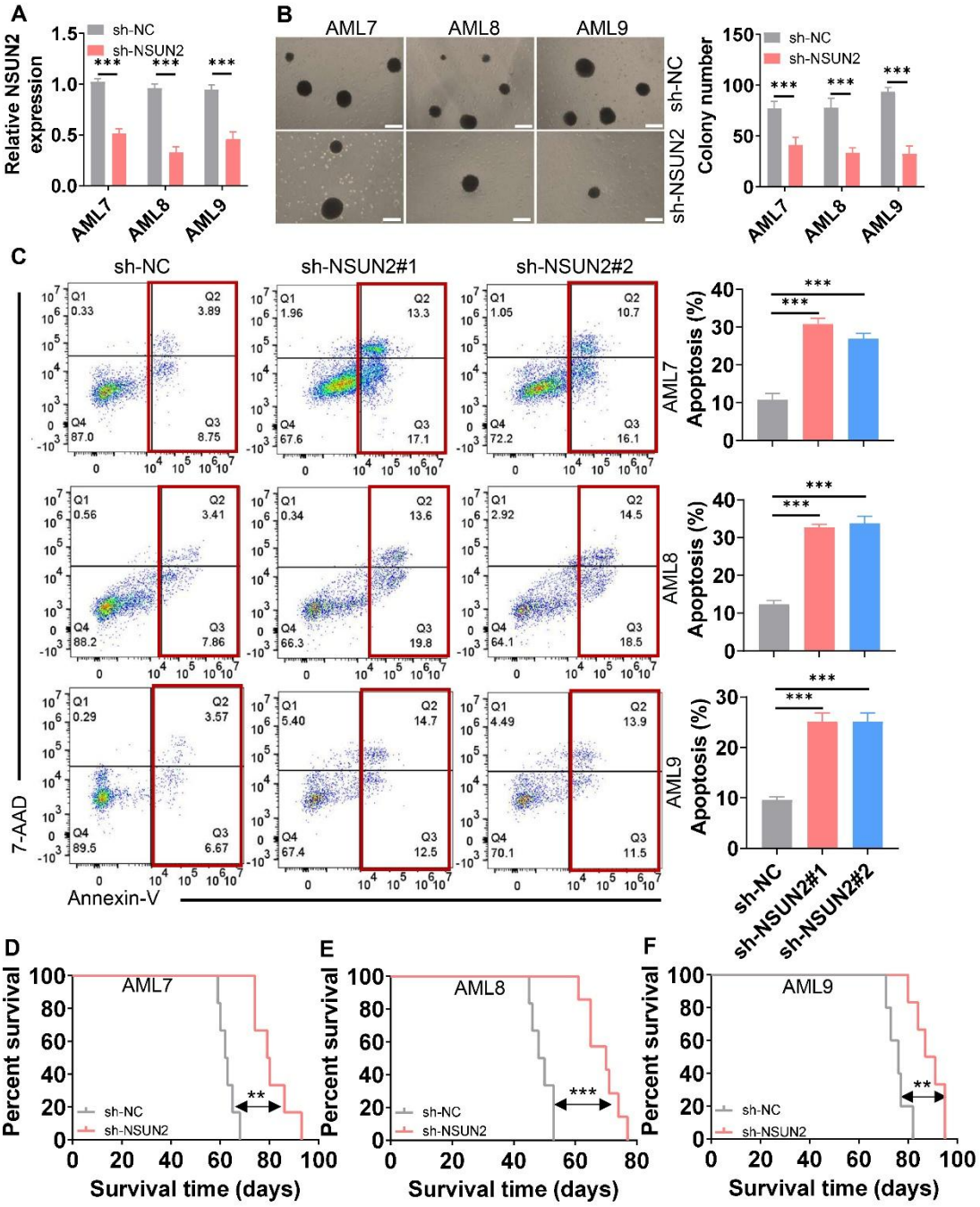

Supplemental Figure 5. NSUN2 KD inhibits survival and induces apoptosis in AML patient specimens. (A) *NSUN2* transcript levels were measured in CD34$^+$cells from three AML patients after transduction with sh-NC or sh-NSUN2#1 for 48 h. (B) Primary CD34$^+$ cells after transduction with sh-NC or sh-NSUN2#1 were plated in methylcellulose medium for 14 days for colony formation (2×10^3/dish). Representative plots (left) and statistical analysis of colony counts (right) are shown. Bar scales represent 200 μm. (C) BM cells from three AML patients were transduced

with sh-NC or sh-NSUN2#1 for 48 h. Apoptosis was measured by Annexin V/7-AAD staining. Representative plots (left) and statistical analysis of Annexin V^+/7-AAD^+ + Annexin V^+/7-AAD^- cells (right) are shown. (D–F) OS was assessed in NSG mice transplanted with primary cells transduced with sh-NC or sh-NSUN2#1 from AML#7 (n = 6 for sh-NC and n = 6 for sh-NSUN2#1), AML#8 (n = 6 for sh-NC and n = 7 for sh-NSUN2#1), and AML#9 (n = 5 for sh-NC and n = 6 for sh-NSUN2#1). $^{**}P < 0.01$; $^{***}P < 0.001$ versus sh-NC.

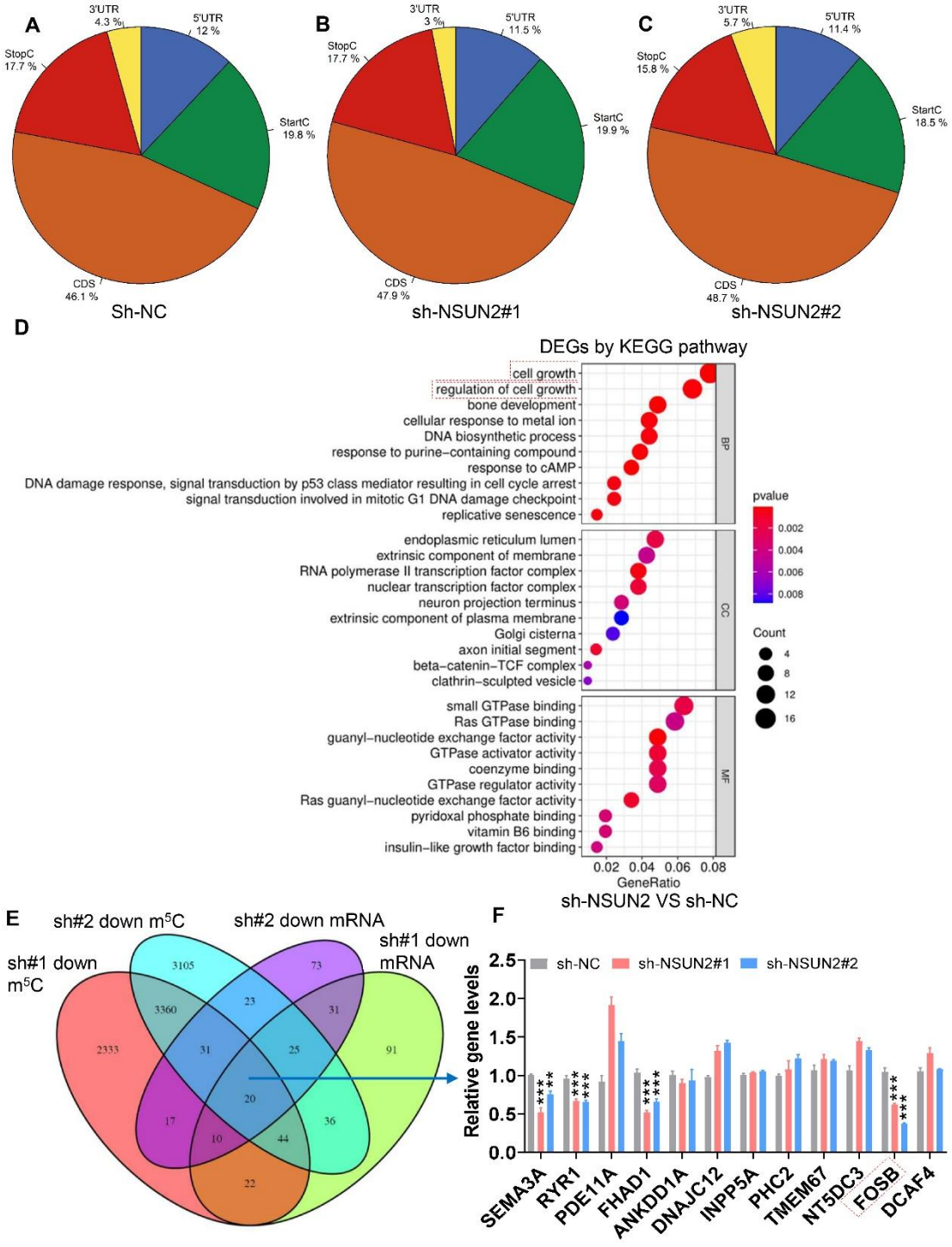

Supplemental Figure 6. Methylated RNA immunoprecipitation sequencing (MeRIP-seq) and RNA-seq analysis identify potential NSUN2 targets. MeRIP-seq and RNA-seq were performed in MOLM-13 cells transduced with sh-NC or sh-NSUN2. (A–C) Distribution of different m^5C sites across the indicated transcript regions. (D) Kyoto Encyclopedia of Genes and Genomes (KEGG)

pathway analysis revealed enriched signal pathways. (E) Venn diagram showing the overlap between differentially methylated genes (DMGs) and differentially expressed genes (DEGs), as determined by MeRIP-seq and RNA-seq. (F) The transcript levels of potential NSUN2 targets were measured by qRT-PCR. $^{**}P < 0.01$; $^{***}P < 0.001$ versus sh-NC.

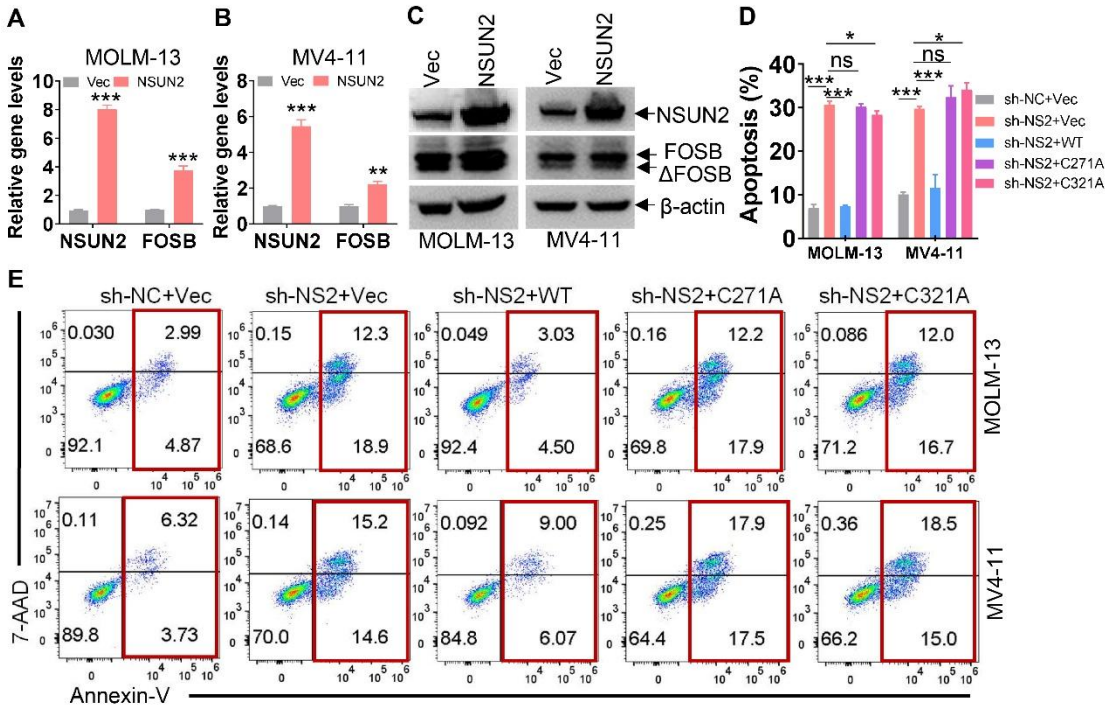

Supplemental Figure 7. NSUN2 positively regulates FOSB expression and promotes leukemogenesis in an m^{5}C-dependent manner. (A–C) NSUN2 and FOSB transcript and protein levels were measured in leukemic cells overexpressing blank control (Vec) or NSUN2. (D and E) AML cells transduced with sh-NC were overexpressed with Vec, and AML cells transduced with sh-NSUN2#3 (3'-UTR) were overexpressed with Vec, wild-type (WT) NSUN2, or its two catalytically inactive mutants (C271A or C321A). Apoptosis was measured by Annexin V/7-AAD staining. n = 3 or more independent biological replicates. *$P < 0.05$; **$P < 0.01$; ***$P < 0.001$; ns = not significant.

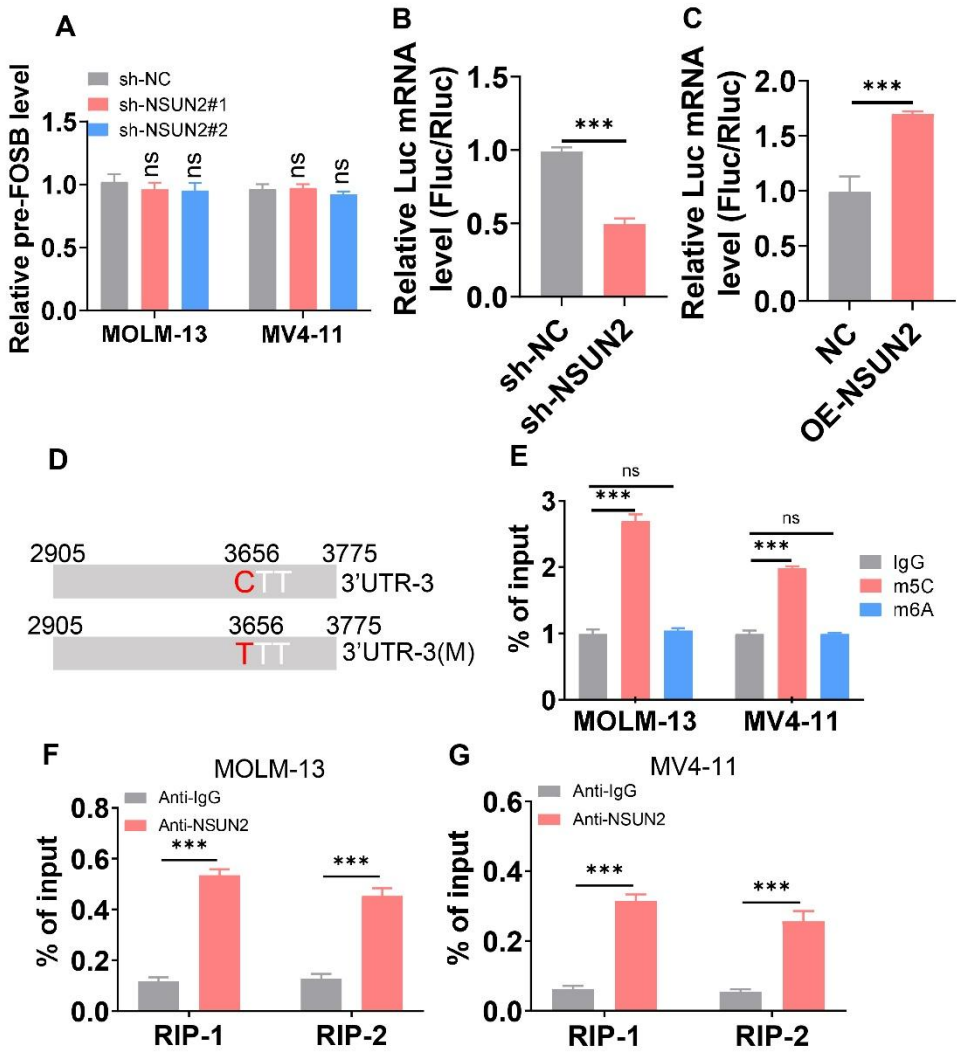

Supplemental Figure 8. NSUN2 stabilizes *FOSB* mRNA by methylating its 3'UTR. (A) Pre-*FOSB* transcript levels were measured in AML cells transduced with sh-NSUN2 or sh-NC. (B and C) pGL3-FOSB-3'UTR-3 was transfected into 293T cells with KD of NSUN2 or OE of NSUN2. Relative Luc mRNA levels (Firefly/Renilla) were measured in each cell lysate. (D) Schematic presentation of m^5C methylation at position 3656 of *FOSB*-3'UTR-3, where C at position 3656 was mutated to T. (E) Enrichment of endogenous m^5C or m^6A modification in *FOSB* mRNA in AML cells. (F and G) Enrichment of endogenous *FOSB* mRNA when RIP was performed by anti-NSUN2 or anti-IgG antibody in AML cells. ***$P < 0.001$. ns = not significant.

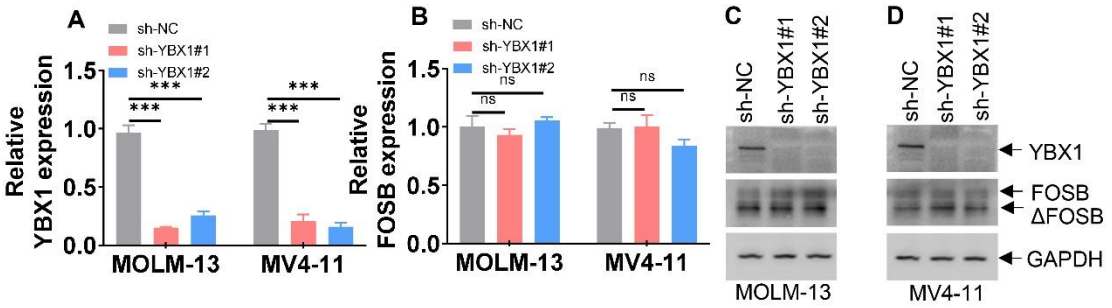

Supplemental Figure 9. KD of *YBX1* does not affect FOSB expression in leukemic cells. (A–D) The transcript (A and B) and protein (C and D) expressions of YBX1 and FOSB were measured in MOLM-13 and MV4-11 cells, which were transduced with sh-NC or sh-YBX1 for 48 h, followed by puromycin (1 μg/mL) treatment for an additional 48 h. *** $P < 0.001$ versus sh-NC. ns = not significant.

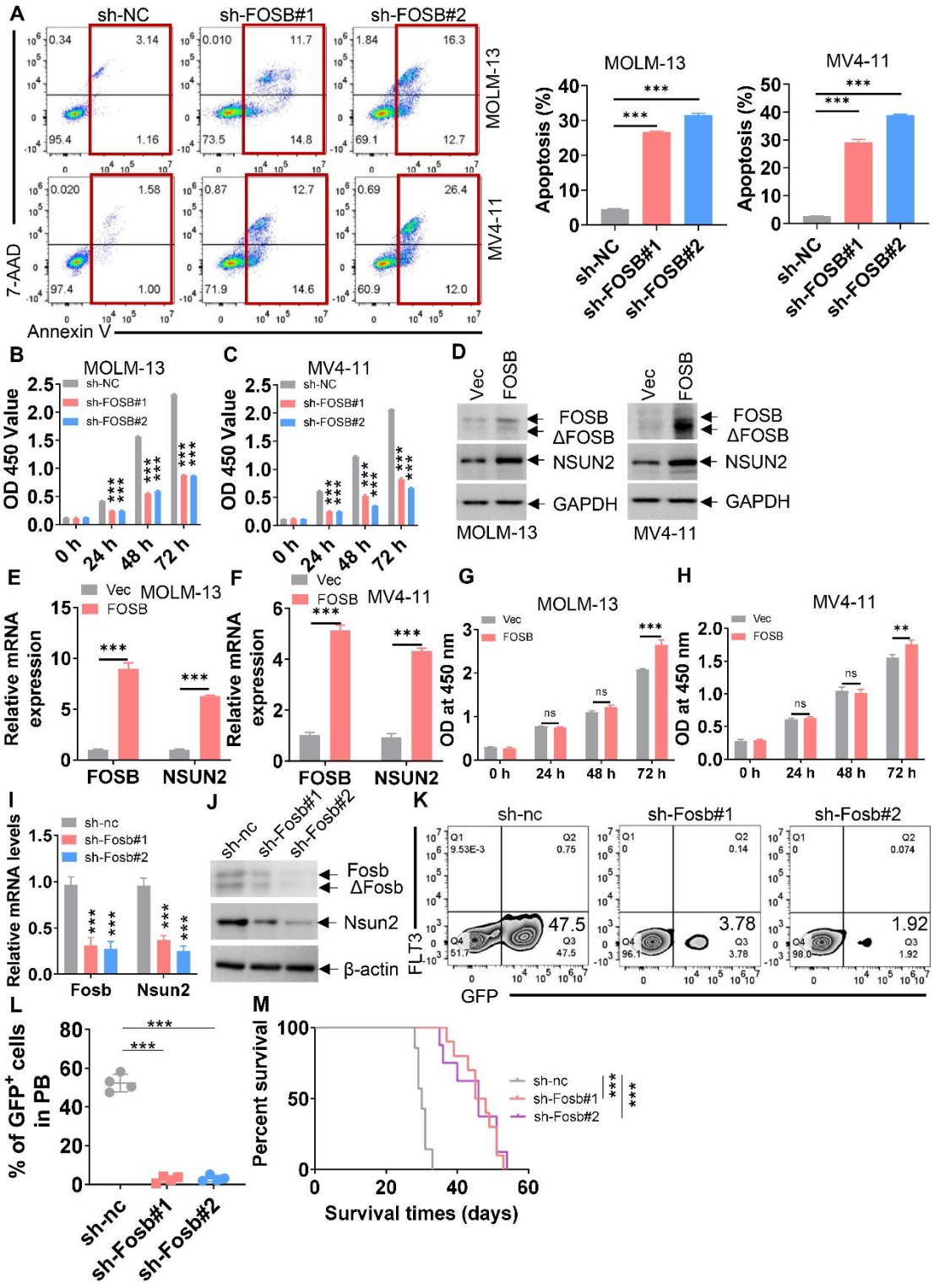

Supplemental Figure 10. FOSB facilitates leukemogenesis. (A) Apoptosis was measured in AML cells after transduction with sh-FOSB or sh-NC for 48 h, followed by puromycin (1 μg/mL) treatment for an additional 48 h. (B and C) Cell proliferation was measured by CCK-8 assay in MOLM-13 and MV4-11 cells at the indicated times after transduction with sh-FOSB or sh-NC for

48 h. (D–F) The protein and transcript levels of FOSB and NSUN2 were measured in AML cells, which were overexpressed with FOSB or negative control (Vec) for 48 h. (G and H) Cell proliferation was measured by CCK-8 assay in MOLM-13 and MV4-11 cells at indicated times after overexpressing FOSB or Vec for 48 h. (I and J) BM GFP^+ cells isolated from MA9-transformed leukemic mice were transduced with sh-nc or sh-Fosb for 48 h. The transcript (I) and protein expressions (J) of Fosb and Nsun2 were measured in GFP^+ cells with sh-nc or sh-Fosb. (K and L) Equal GFP^+ cells transduced with sh-nc or sh-Fosb (1×10^4 GFP^+ cells per mouse) were xenografted into recipient mice. GFP^+ cells were measured in PB from mice transplanted with GFP^+ cells with sh-nc (n = 4), sh-Fosb#1 (n = 4), or sh-Fosb#2 (n = 4). Representative flow cytometry plots (K) and statistical analysis (L) are shown. (M) OS was assessed in recipient mice xenografted with GFP^+ cells with sh-nc (n = 7), sh-Fosb#1 (n = 10), or sh-Fosb#2 (n = 9). $^{**}P < 0.01$; $^{***}P < 0.001$. ns = not significant.

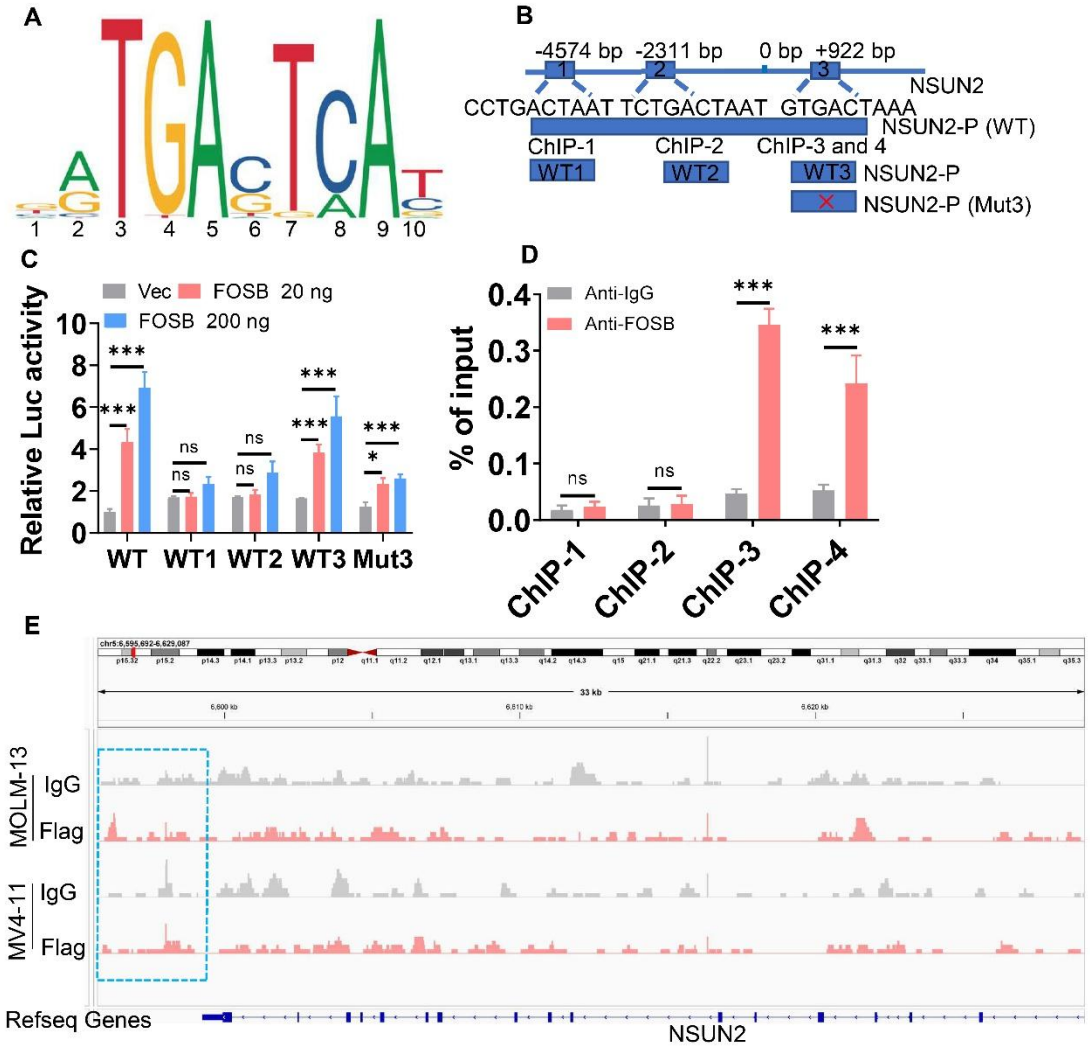

Supplemental Figure 11. FOSB activates NSUN2 expression by directly binding to *NSUN2* promoter. (A) Predicted FOSB-binding motif in *NSUN2* promoter using JASPAR (https://jaspar.elixir.no/). (B) Three potential FOSB-binding sequences in the *NSUN2* promoter are shown. The potential binding motif (GTGACTAA) in WT3 was mutated to Mut3. (C) Luc activity was measured in 293T cells, which were transfected with blank vector or different doses of vector overexpressing FOSB, along with co-transfection of pGL3-NSUN2-P (WT1-3) or Mut3 for 48 h. (D) Soluble chromatin from MOLM-13 cells was immunoprecipitated (IPed) with anti-FOSB or anti-IgG. IPed DNA was analyzed by qPCR using four different primers for ChIP assays. (E) MOLM-13 and MV4-11 cells overexpressing Flag-tagged FOSB were IPed by anti-IgG or anti-Flag

antibody. IPed DNA were subjected to sequence. A FOSB-binding peak was identified in *NSUN2* promoter. n = 3 or more independent biological replicates. *$P < 0.05$; ***$P < 0.001$. ns = not significant.

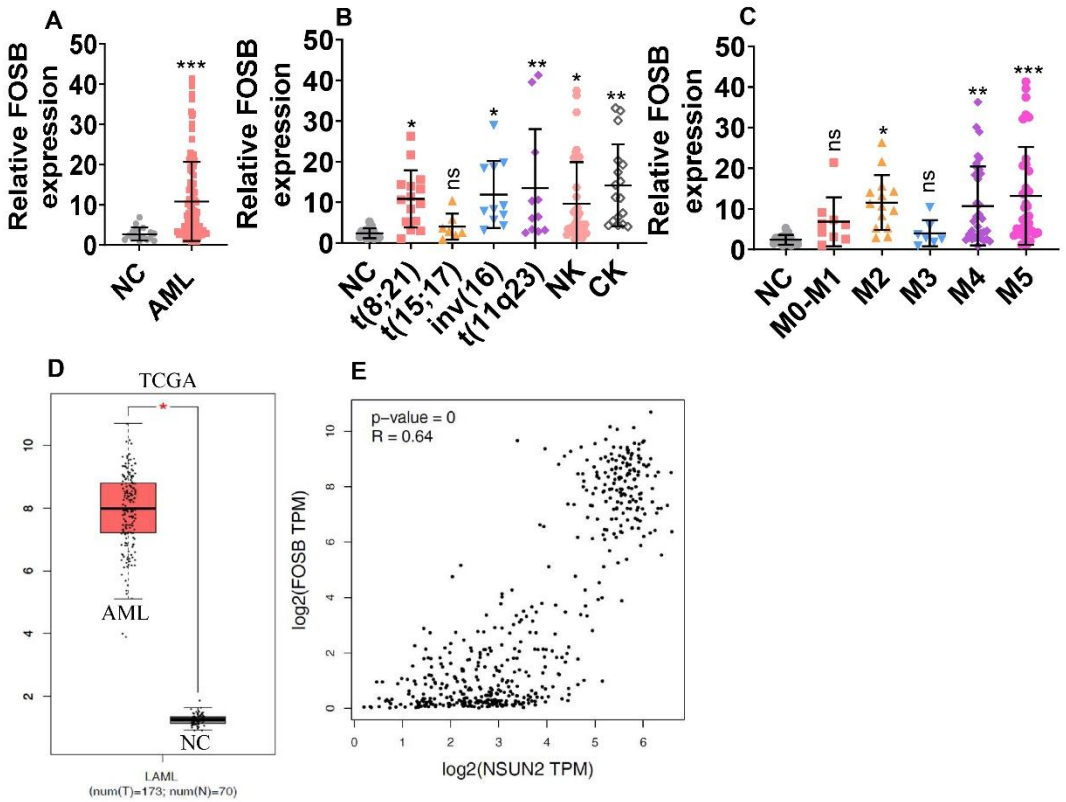

Supplemental Figure 12. *FOSB* expression is higher in AML patient samples compared with NC samples. (A) The transcript expression of *FOSB* was measured in BM cells from 102 untreated AML patients and 18 NC samples by qRT-PCR. (B) The expression of *FOSB* was analyzed in 102 untreated AML patients with different chromosomal translocations compared with 18 NC samples. (C) The expression of FOSB was analyzed in 102 untreated AML patients according to FAB subtypes (M0–M5) compared with 18 NC samples. (D) *FOSB* expression was assessed in the TCGA database. (E) The relationship between *NSUN2* and *FOSB* mRNA expressions was analyzed using GEPIA (Gene Expression Profiling Interactive Analysis). **P* < 0.05; ***P* < 0.01; ****P* < 0.001 versus NC samples. ns = not significant.

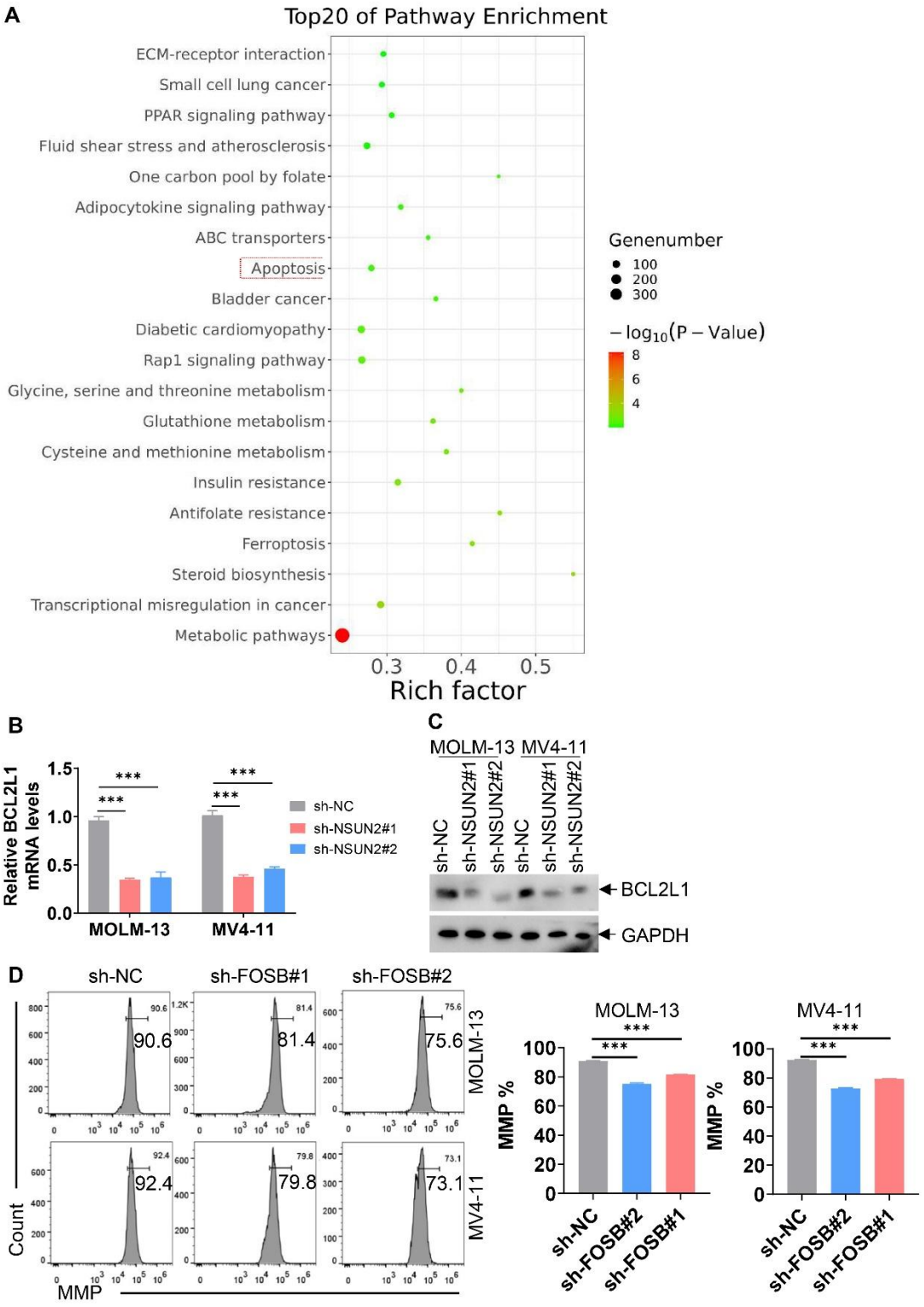

Supplemental Figure 13. NSUN2 KD inhibits BCL2L1 expression and FOSB KD affects mitochondrial function in AML cells. (A) MOLM-13 cells transduced with sh-NC or sh-FOSB#1 (sh-FOSB) were subjected for RNA-seq. Apoptosis-associated genes were significantly enriched by

pathway enrichment analysis. (B and C) BCL2L1 transcript and protein levels were measured in MOLM-13 and MV4-11 cells after sh-NSUN2 or sh-NC transduction for 48 h, followed by puromycin (1 μg/mL) treatment for an additional 48 h. (D) MMP assay was measured by JC-1 probe staining in leukemic cells transduced with sh-FOSB or sh-NC. The representative images (left) and statistical analysis of MMP (right) are shown. ***$P < 0.001$.

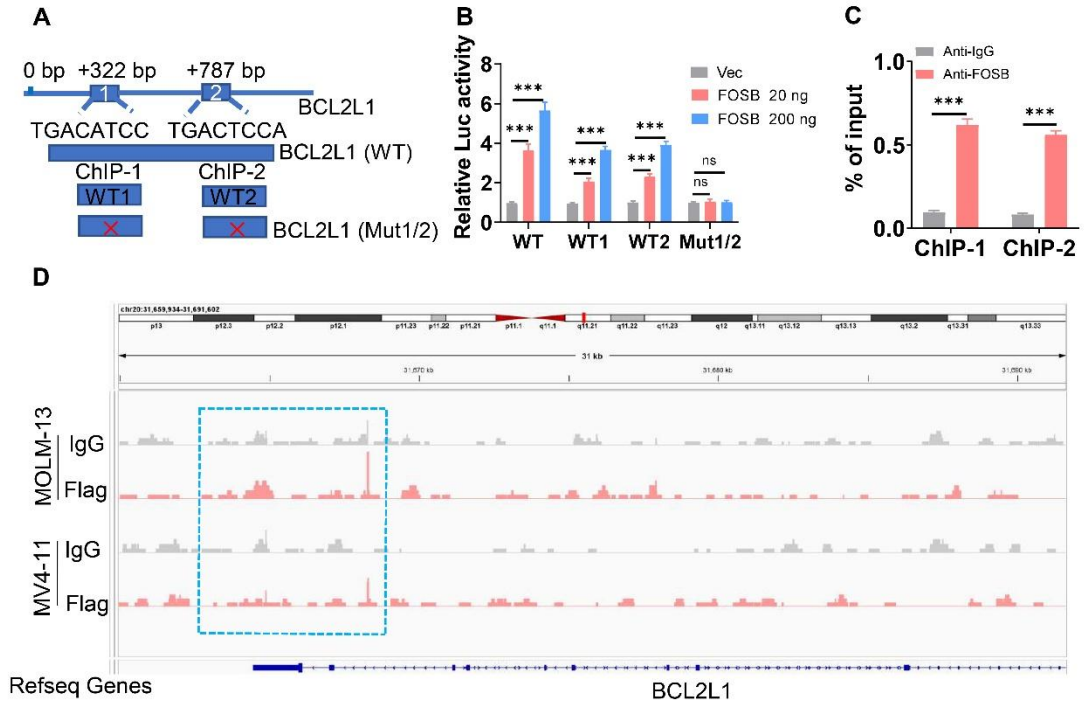

Supplemental Figure 14. FOSB activates BCL2L1 expression by direct binding to *BCL2L1* promoter. (A) Two potential FOSB-binding sequences in the *BCL2L1* promoter. The potential binding motifs in WT1 and WT2 were mutated to Mut1/2. (B) Luc activity was measured in 293T cells, which were transfected with blank vector or different doses of vector overexpressing FOSB, along with co-transfection of pGL3-BCL2L1-WT, WT1, WT2, or Mut1/2 for 48 h. (C) ChIP-qPCR showing FOSB binding to the *BCL2L1* promoter in MOLM-13 cells. (D) MOLM-13 and MV4-11 cells overexpressing Flag-tagged FOSB were IPed by anti-IgG or anti-Flag antibody. IPed DNA were subjected to sequence. A FOSB-binding peak was identified in the *BCL2L1* promoter. n = 3 or more independent biological replicates. ***$P < 0.001$. ns = not significant.

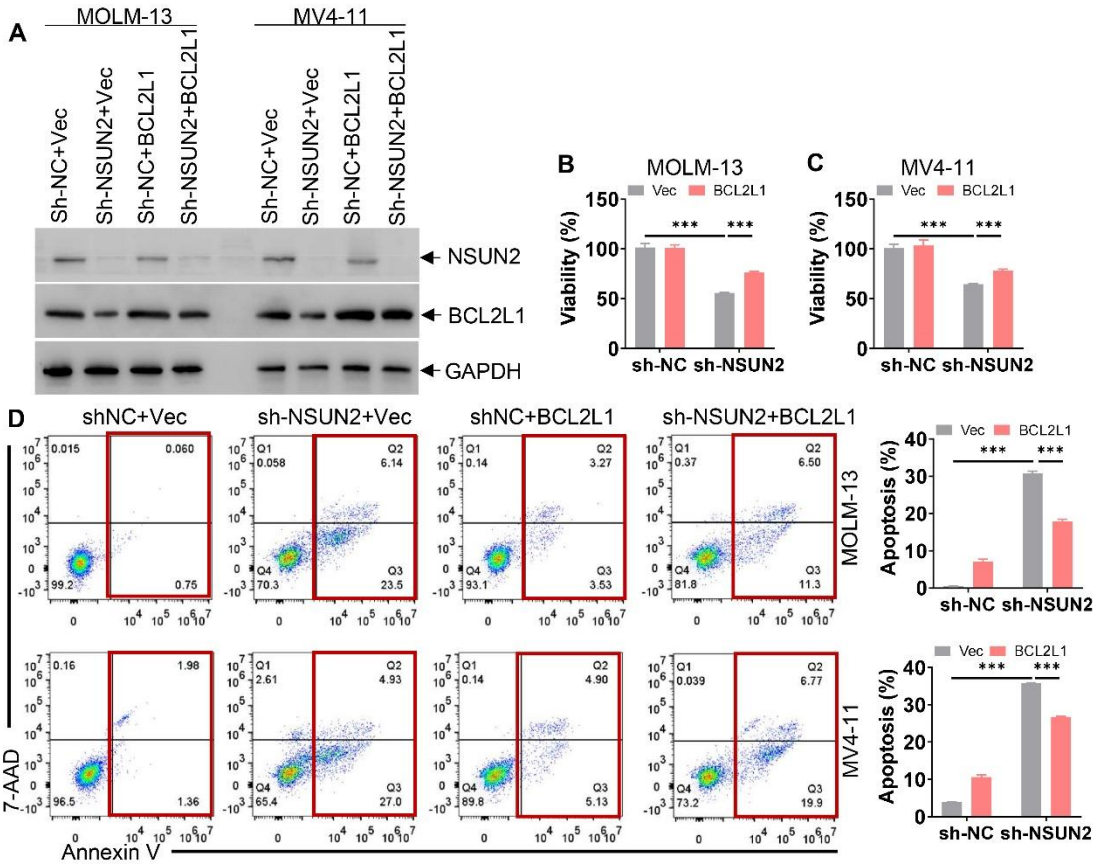

Supplemental Figure 15. BCL2L1 overexpression rescues the NSUN2 KD-induced phenotype.

Leukemic cells were transduced with sh-NC or sh-NSUN2 for 48 h and overexpressed with blank vector (Vec) or vector overexpressing BCL2L1 for another 48 h. NSUN2 and BCL2L1 protein levels (A), viability (B and C), and apoptosis (D) were measured. ***$P < 0.001$.

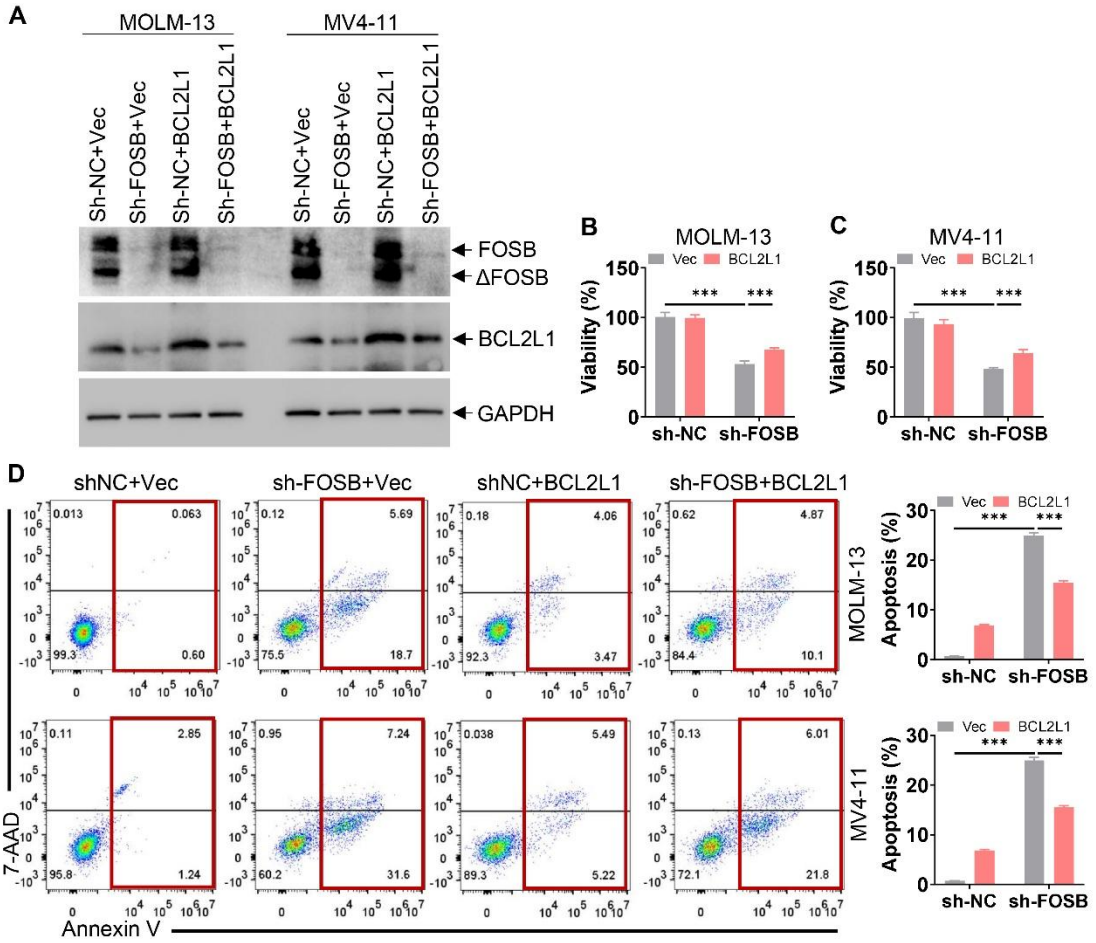

Supplemental Figure 16. BCL2L1 overexpression rescues the FOSB KD-induced phenotype.

Leukemic cells were transduced with sh-NC or sh-FOSB for 48 h and overexpressed with blank vector (Vec) or vector overexpressing BCL2L1 for another 48 h. FOSB and BCL2L1 protein levels (A), viability (B and C), and apoptosis (D) were measured. ***$P < 0.001$.

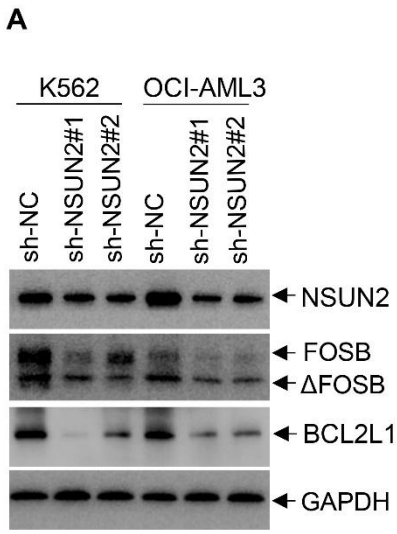

Supplemental Figure 17. NSUN2 KD decreases FOSB and BCL2L1 protein levels in K562 and OCI-AML3 cells. (A) NSUN2, FOSB, and BCL2L1 protein levels were measured in K562 and OCI-AML3 cells after transduction with sh-NSUN2 or sh-NC for 48 h, followed by puromycin (1 μg/mL) treatment for an additional 48 h.

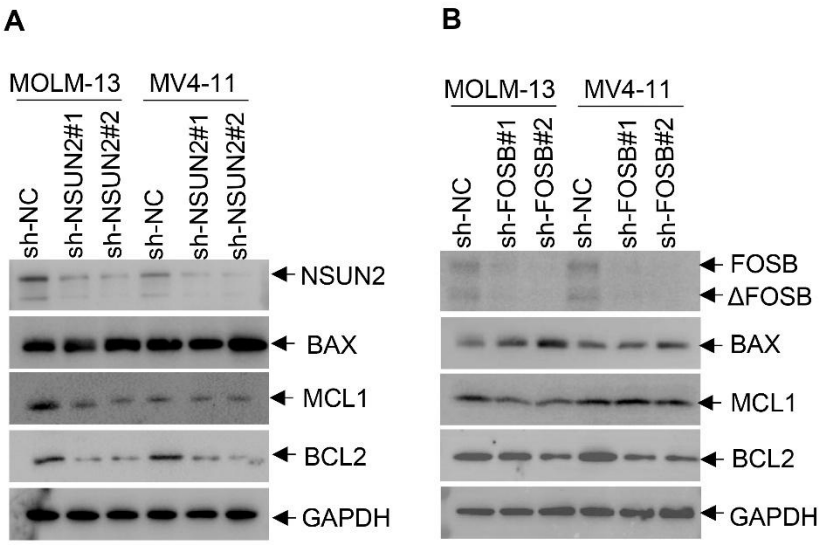

Supplemental Figure 18. NSUN2-FOSB axis regulates BCL-2 family members. (A) The indicated protein levels were measured in MOLM-13 and MV4-11 cells after transduction with sh-NSUN2 or sh-NC for 48 h, followed by puromycin (1 μg/mL) treatment for an additional 48 h. (B) The indicated protein levels were measured in MOLM-13 and MV4-11 cells after transduction with sh-FOSB or sh-NC for 48 h, followed by puromycin (1 μg/mL) treatment for an additional 48 h.

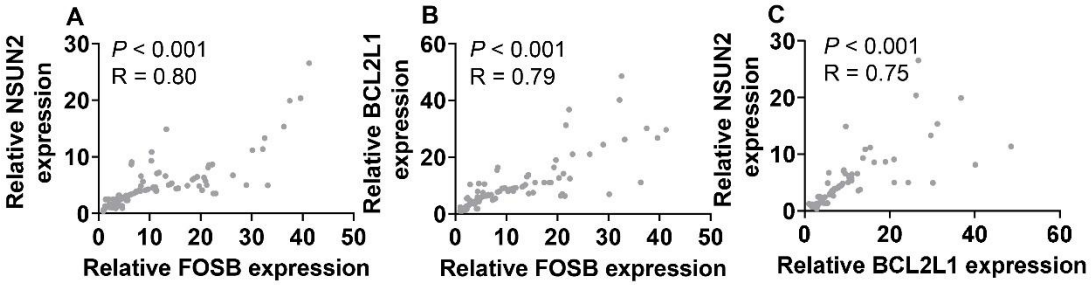

Supplemental Figure 19. The relationship between *NSUN2*, *FOSB*, and *BCL2L1* mRNA levels in primary AML patient samples. (A–C) *NSUN2* vs *FOSB* (A), *NSUN2* vs *BCL2L1* (B), and *FOSB* vs *BCL2L1* mRNA levels (C) were measured and analyzed in 102 untreated AML patients in-house.

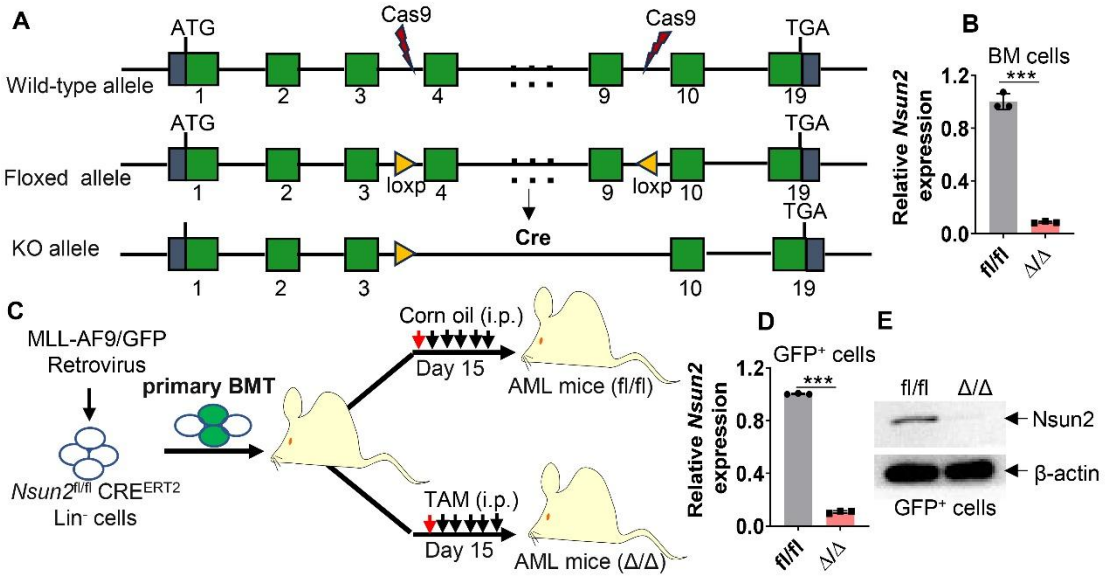

Supplemental Figure 20. TAM treatment depletes *Nsun2* in *Nsun2*$^{fl/fl}$ Cre^{ERT2} mice. (A) Schematic representation of the *Nsun2*$^{flox/flox}$ mice produced by the Cas9 system. (B) Six-week-old *Nsun2*$^{fl/fl}$ Cre^{ERT2} mice were treated with TAM to deplete *Nsun2* expression (referred to as Δ/Δ) or with corn oil as a vehicle control (referred to as fl/fl). Mice were sacrificed one month after the last TAM injection, and BM cells from fl/fl (n = 3) and Δ/Δ (n = 3) mice were isolated to measure *Nsun2* transcript levels by qRT-PCR. (C) Experimental scheme for the MA9-transformed leukemic mouse model. Corn oil or TAM was injected on days 15 – 20 during primary BM transplantation (BMT). (D and E) Nsun2 transcript and protein expressions were measured by qRT-PCR (D, n = 3 for fl/fl and n = 3 for Δ/Δ) and Western blot (E) in BM GFP$^+$ fl/fl and Δ/Δ leukemic cells, respectively. A two-tailed Student's t-test was used to compare differences between two groups. ***$P < 0.001$.

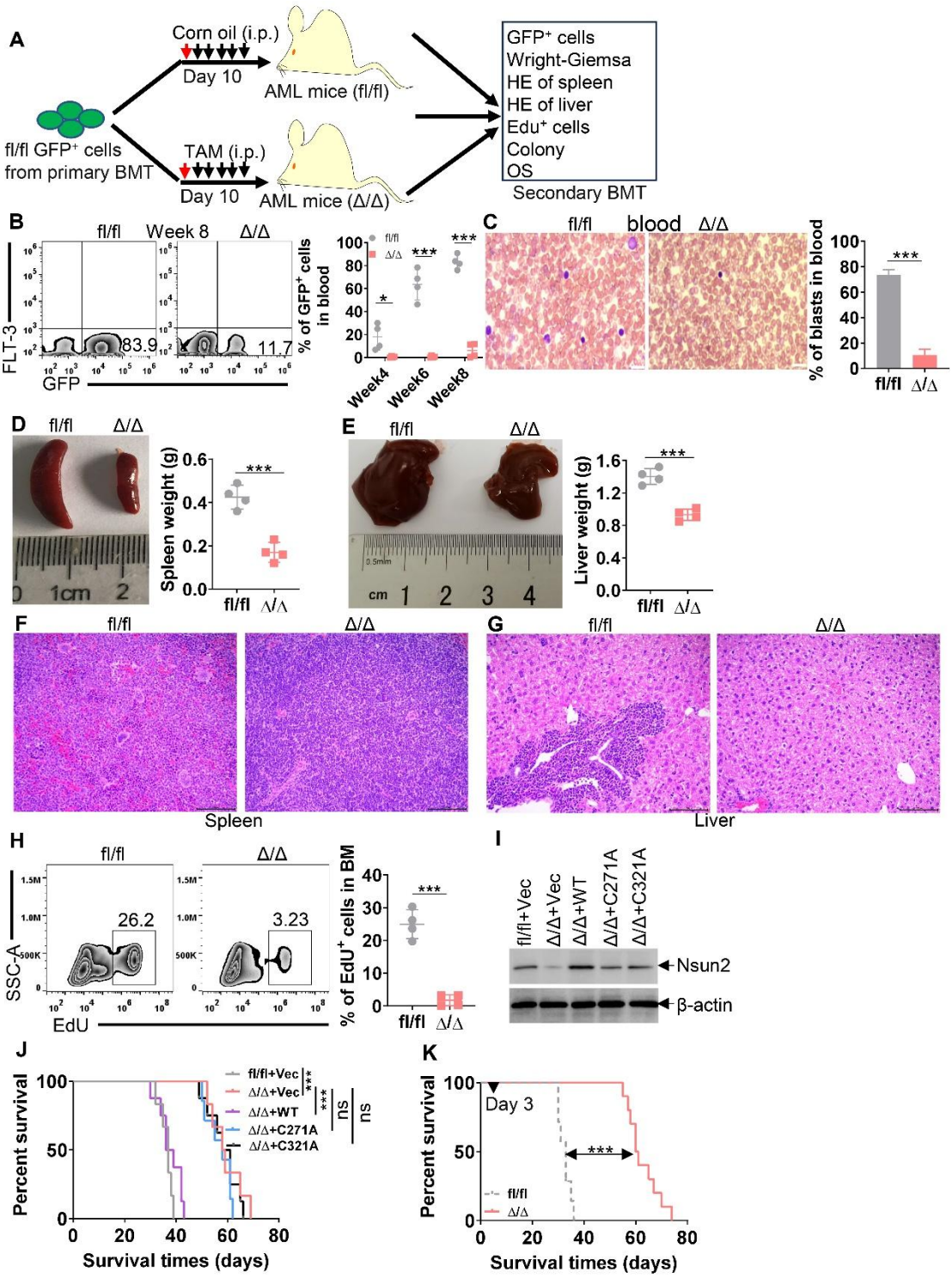

Supplemental Figure 21. The anti-leukemogenesis effects of *Nsun2* knockout in the MA9-transformed murine AML model. (A) Experimental scheme for the MA9-transformed murine AML model. Corn oil or TAM was injected in secondary BMT on days 10–15. (B) The frequency of GFP$^+$ cells was measured in peripheral blood (PB) from fl/fl (n = 4) and Δ/Δ (n = 4) leukemic

mice at 4, 6, and 8 weeks after BMT. Representative flow cytometry plots (left) and statistical analysis (right) are shown. (C) Representative images of PB smears from fl/fl (n = 3) and Δ/Δ (n = 3) mice (left). Statistical analysis of the average percentage of leukemic cells in PB is shown (right). Scale bar represents 20 μm for PB. (D and E) The representative images of the spleen (left, D) and liver (left, E), and statistical analysis of the spleen (right, D) and liver (right, E) weights from fl/fl (n = 4) and Δ/Δ (n = 4) leukemic mice. (F and G) H&E staining of the spleen (E) and liver (F) tissues from fl/fl and Δ/Δ leukemic mice. Scale bars = 100 μm. (H) EdU staining was performed in BM GFP^+ cells from fl/fl (n = 4) and Δ/Δ (n = 4) leukemic mice. Representative flow cytometry plots (left) and statistical analysis are shown (right). A two-tailed Student's t-test was used to compare differences between two groups. (I and J) Fl/fl cells were overexpressed with Vec, and Δ/Δ cells were overexpressed with Vec, wild-type (WT) Nsun2, or its two mutants. The protein levels of Nsun2 were measured by Western blot (I). All these groups of cells were xenografted in mice (n = 6 for fl/fl+Vec; n = 6 for Δ/Δ+Vec; n = 8 for Δ/Δ+WT; n = 7 for Δ/Δ+C271A; n = 8 for Δ/Δ+C271A), and OS was calculated (J). (K) GFP^+ cells from primary BMT were transplanted into recipient mice. Corn oil or TAM was injected on days 3–8 in recipient mice. OS was calculated in fl/fl (n = 7) and Δ/Δ (n = 10) leukemic mice. Kaplan-Meier survival curves were generated to analyze OS time. *P < 0.05; ***P < 0.001. ns = not significant.

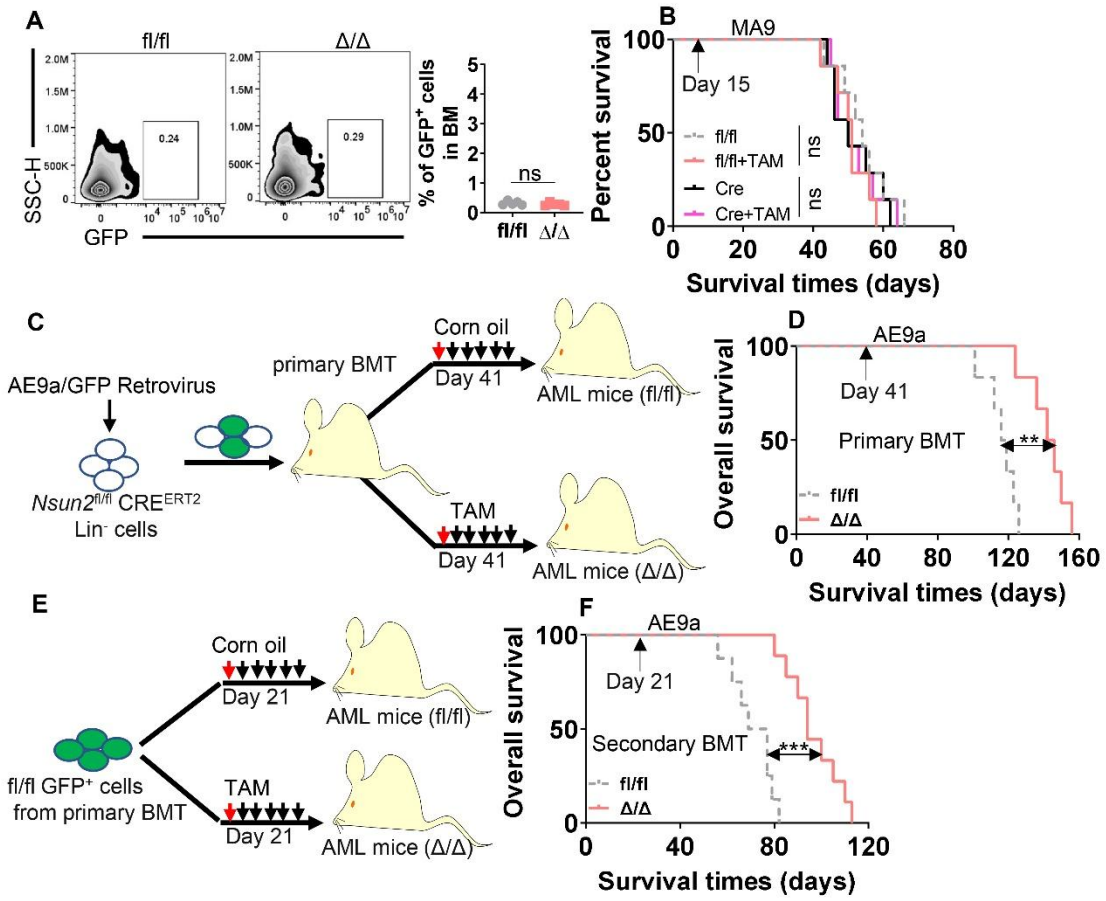

Supplemental Figure 22. The effect of homing ability, flox/flox, or Cre^{ERT2} on the survival of the MA9-induced model and the anti-leukemia effect of *Nsun2* knockout in AML1-ETO9a (AE9a)-induced murine AML model. (A) BM GFP$^+$ cells from secondary BMT of mice receiving fl/fl or Δ/Δ cells were injected into the lethally irradiated mice. Homed cells (GFP$^+$) were measured in BM at 16 h after transplantation. Representative plots (left) and statistical analysis of GFP$^+$ cells are shown (right). (B) BM Lin$^-$ cells from *Nsun2*$^{fl/fl}$ or Cre^{ERT2} mice were transduced with MA9 and transplanted into lethally irradiated mice treated with or without TAM (days 15 – 20). OS was calculated in four groups (n = 7 for fl/fl; n = 7 for fl/fl+TAM; n = 8 for Cre; n = 8 for Cre+TAM). (C and D) Experimental scheme for the AE9a-transformed mouse model in primary BMT. Corn oil or TAM was injected on days 41–46 after transplantation (C). Kaplan-Meier curve showing the effect of *Nsun2* depletion in the primary BMT (n = 6 for fl/fl; n = 6 for Δ/Δ) (D). (E and F)

Experimental scheme for the AE9a-transformed mouse model in secondary BMT. Corn oil or TAM was injected on days 21–26 after transplantation (E). Kaplan-Meier curve showing the effect of *Nsun2* depletion in secondary BMT (n = 8 for fl/fl; n = 10 for Δ/Δ) (F). Kaplan-Meier survival curves were generated to analyze OS time. $^{**}P < 0.01$; $^{***}P < 0.001$. ns = not significant.

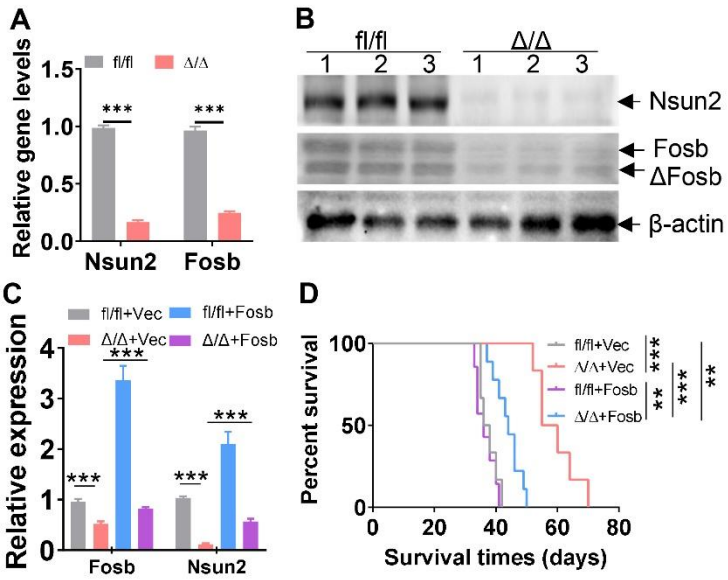

Supplemental Figure S23. Fosb expression is lower in Δ/Δ than fl/fl cells, and overexpression of Fosb rescues the extended OS induced by *Nsun2* knockout. (A and B) Murine Nsun2 and Fosb transcript (A) and protein (B) levels were measured in BM fl/fl (n = 3) and Δ/Δ (n = 3) GFP^+ cells from MA9-transduced leukemic mice. (C and D) GFP^+ fl/fl and Δ/Δ cells were isolated from MA9-transformed mice and transduced with blank Vec or vector overexpressing Fosb. Transcript levels of *Fosb* and *Nsun2* were measured (C). Equal numbers of cells (1×10^4 GFP^+ cells for per mouse) from the four groups were xenografted into recipient mice for calculating OS (n = 6 for fl/fl+Vec; n = 6 for Δ/Δ+Vec; n = 7 for fl/fl+Fosb; n =9 for Δ/Δ+Fosb) (D). $^{**}P < 0.01$; $^{***}P < 0.001$.

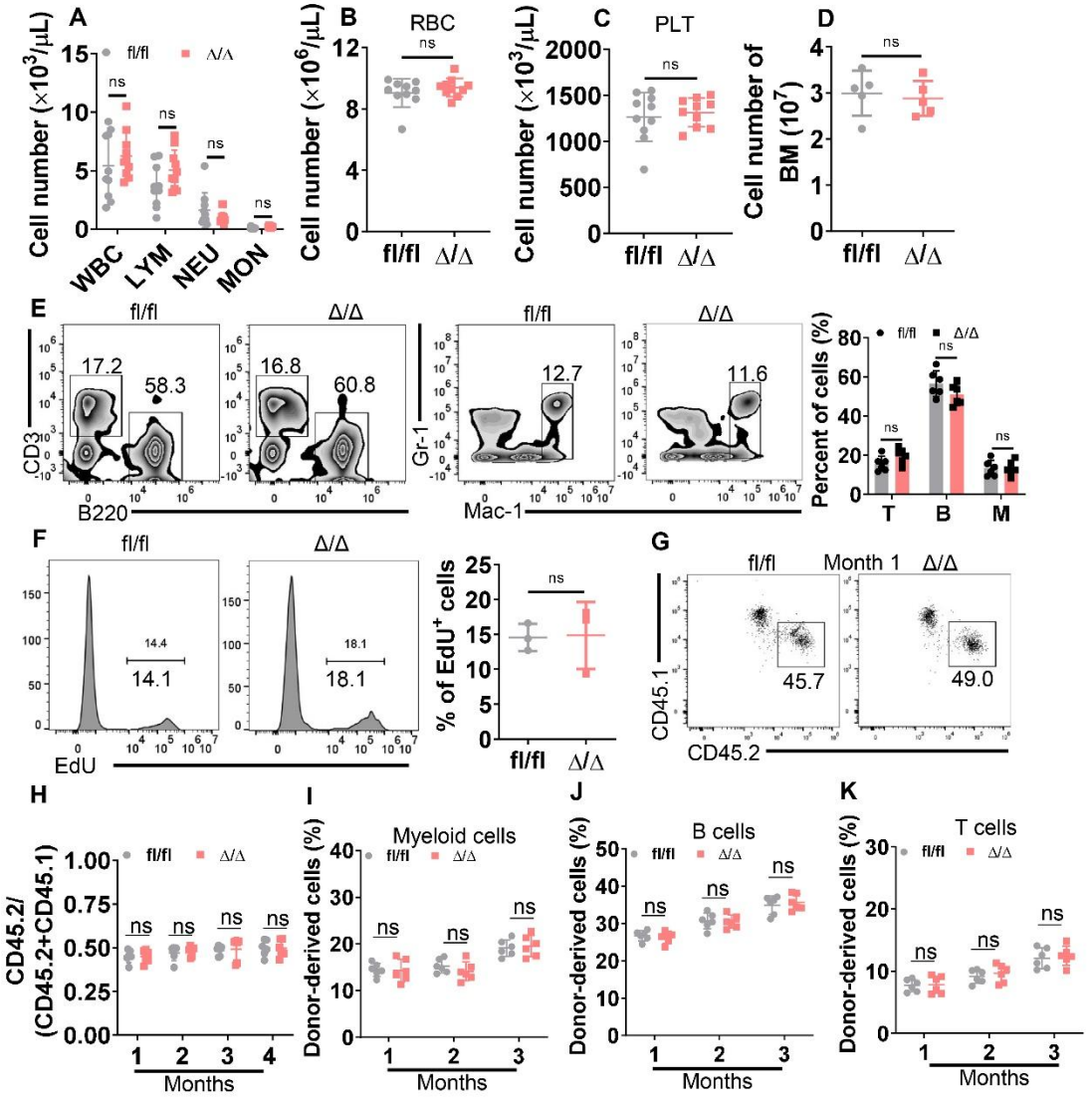

Supplemental Figure 24. *Nsun2* depletion does not affect normal hematopoiesis. Six-week-old *Nsun2*$^{fl/fl}$ Cre^{ERT2} mice were treated with TAM to deplete *Nsun2* expression (Δ/Δ) or corn oil as a vehicle control (fl/fl). Mice were sacrificed one month after the last TAM injection. (A–C) Blood count analysis was performed in the PB from fl/fl (n = 10) and Δ/Δ (n = 10) mice. A for WBC, LYM, NEU, and MON; B for RBC; C for PLT. (D) Total BM cell numbers were counted in fl/fl (n = 5) and Δ/Δ (n = 5) mice. (E) Mature lineage cells were analyzed in the PB from fl/fl (n = 5) and Δ/Δ (n = 5) mice. T cells (CD3$^+$B220$^-$); B cells (CD3$^-$B220$^+$); M cells (Mac-1$^+$Gr-1$^+$ or Mac-1$^+$Gr-1$^-$). (F) EdU staining was performed in BM cells from fl/fl (n = 3) and Δ/Δ (n = 3) mice.

Representative flow cytometry plots (left) and statistical analysis of EdU^+ cells (right) are shown. (G–K) Total BM cells from fl/fl or Δ/Δ mice (CD45.2) mixed with an equal number of CD45.1 BM cells were transplanted into CD45.1 mice. Representative plots (G) and statistical analysis of CD45.2/(CD45.2+CD45.1) populations at different months after BMT (n = 6 for fl/fl and Δ/Δ) (H). Mature lineage cells including myeloid cells (I), B cells (J), and T cells (K) were analyzed in the PB from CD45.1 mice (n = 6 for fl/fl and Δ/Δ). ns = not significant.

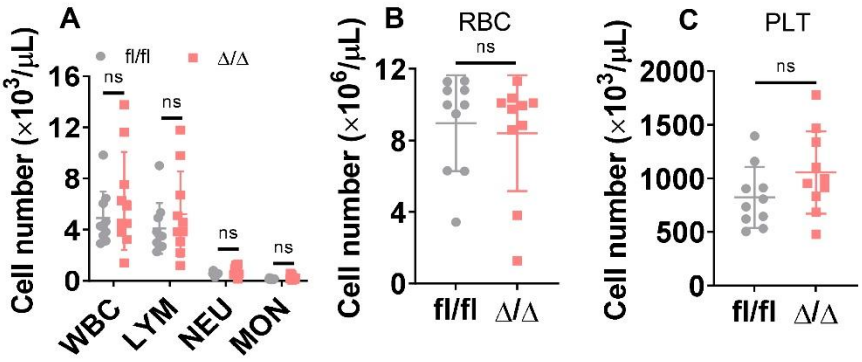

Supplemental Figure 25. *Nsun2* depletion does not affect normal hematopoiesis in elderly mice.

Elderly *Nsun2*$^{fl/fl}$ Cre^{ERT2} mice (> 12 months) were treated with TAM to deplete *Nsun2* expression (Δ/Δ) or corn oil as a vehicle control (fl/fl). Mice were sacrificed one month after the last TAM injection. (A–C) Blood count analysis was performed in the PB from fl/fl (n = 10) and Δ/Δ (n = 10) mice. A for WBC, LYM, NEU, and MON; B for RBC; C for PLT. ns = not significant.

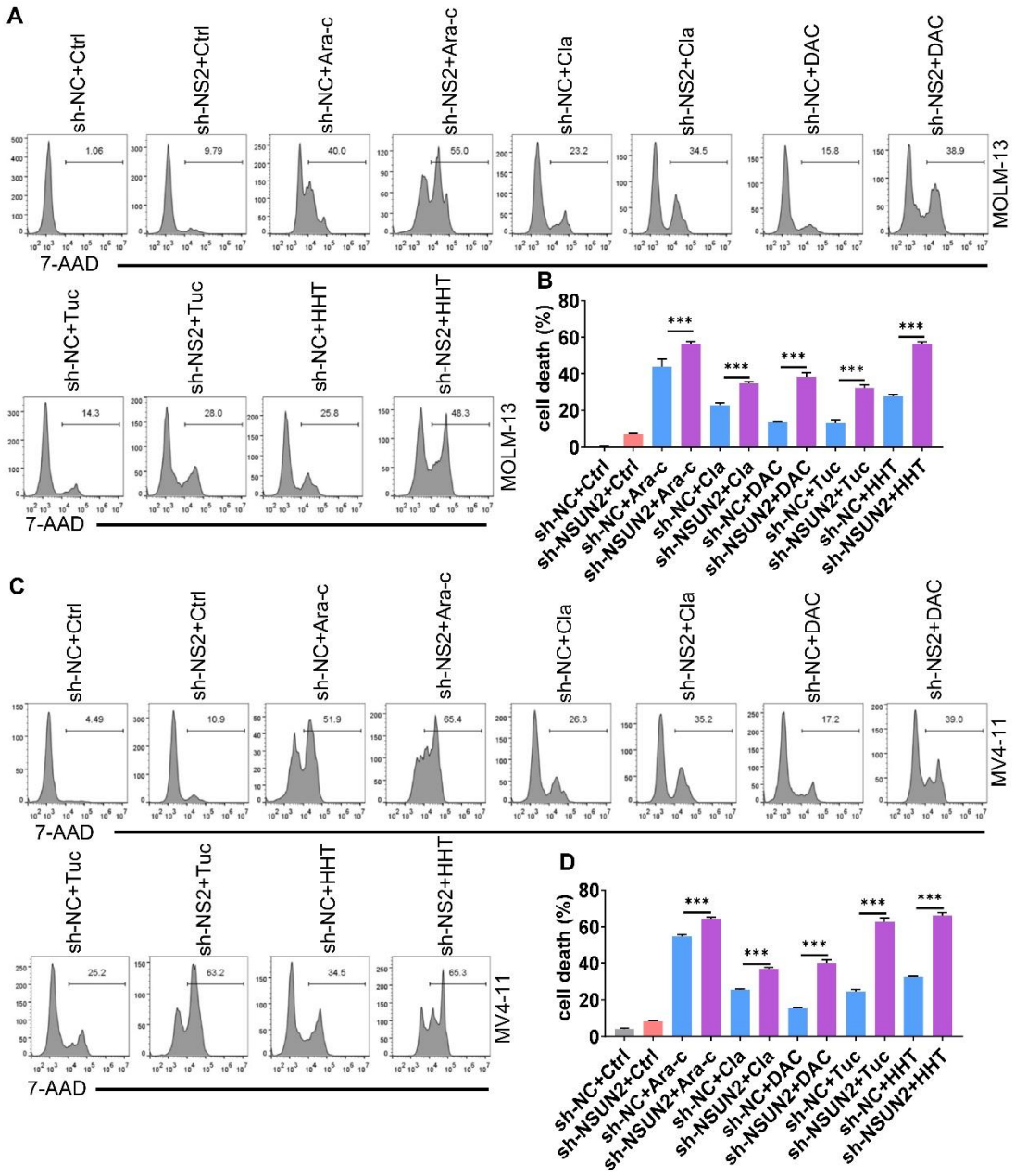

Supplemental Figure 26. NSUN2 KD facilitates cytotoxicity of chemotherapeutic drugs. (A–D) Cell death was measured by 7-AAD staining using flow cytometry in MOLM-13 and MV4-11 cells, which were transduced with sh-NC or sh-NSUN2 for 48 h, followed by treatment with cytarabine (1 μM, Ara-C), cladribine (0.5 μM, Cla), decitabine (1 μM, DAC), tucidinostat (1 μM, Tuc), and homoharringtonine (0.002 μM, HHT) for 24 h. Representative plots (A and C) and statistical analysis of 7-AAD$^+$ cells (B and D) are shown. ***$P < 0.001$.

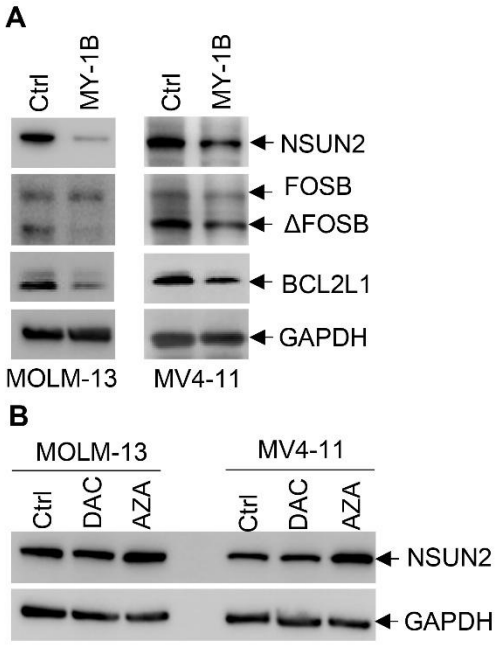

Supplemental Figure 27. NSUN2 inhibitor MY-1B regulates FOSB-BCL2L1 axis and hypomethylation agents do not regulate NSUN2 protein level. (A) The protein levels of NSUN2, FOSB, and BCL2L1 were measured in MOLM-13 and MV4-11 cells, which were treated with or without MY-1B (5 μM) for 48 h. (B) The protein level of NSUN2 was measured in MOLM-13 and MV4-11 cells, which were treated with or without DAC (1 μM) or AZA (1 μM) for 72 h.